Tailoring Porous Silicon for Biomedical Applications : From Drug Delivery to Cancer Immunotherapy

Li, Wei

2018-06-13

Advanced Materials

Tailoring porous silicon for biomedical applications: from drug delivery to cancer immunotherapy
--Manuscript Draft--

	Helsinki Institute of Life Science (HiLIFE), University of Helsinki, Finland @ email: helder.santos@helsinki.fi http://www.helsinki.fi/~hsantos/ https://scholar.google.com/citations?hl=en-EN&user=K3Pj_gwAAAAJ
Do you or any of your co-authors have a conflict of interest to declare?	No. The authors declare no conflict of interest.
Corresponding Author Secondary Information:	
Corresponding Author's Institution:	University of Helsinki
Corresponding Author's Secondary Institution:	
First Author:	Wei Li
First Author Secondary Information:	
Order of Authors:	Wei Li
	Zehua Liu
	Flavia Fontana
	Yaping Ding
	Dongfei Liu
	Jouni Hirvonen
	Helder Santos, D.Sc. (Chem. Eng.)
Order of Authors Secondary Information:	
Abstract:	In the past two decades, porous silicon (PSi) has attracted increasing attention for its potential biomedical applications. With its controllable geometry, tunable nanoporous structure, large pore volume/high specific surface area and versatile surface chemistry, PSi shows significant advantages over conventional drug carriers. In this review, we overview the recent progresses of PSi in drug delivery and cancer immunotherapy. First, we provide an overview of the fabrication of PSi with various geometric structures and highlight how the unique geometry of PSi facilitates its biomedical applications, especially for drug delivery. Second, surface chemistry and modification of PSi are discussed in relation to strengthen its performance in drug delivery and bioimaging. Then, emerging technologies for engineering PSi-based composites are summarized. This review also highlights the emerging advances of PSi in the context of cancer immunotherapy. Overall, the very promising research results encourage further exploration of PSi for biomedical applications, particularly in drug delivery and cancer immunotherapy, and future translation of PSi into clinical applications.

WILEY-VCH

Title Tailoring porous silicon for biomedical applications: from drug delivery to cancer immunotherapy

Wei Li, Zehua Liu, Flavia Fontana, Yaping Ding, Dongfei Liu, Jouni T. Hirvonen* and Hélder A. Santos*

Dr. W. Li, Z. Liu, F. Fontana, Dr. Y. Ding, Prof. J. T. Hirvonen, Dr. D. Liu, Prof. H. A. Santos

Drug Research Program, Division of Pharmaceutical Chemistry and Technology

Faculty of Pharmacy

University of Helsinki

FI-00014 Helsinki, Finland

E-mail: jouni.hirvonen@helsinki.fi; helder.santos@helsinki.fi; Tel. +358 2941 59661

Dr. D. Liu, Prof. H. A. Santos

Helsinki Institute of Life Science (HiLIFE)

University of Helsinki

FI-00014 Helsinki, Finland

Abstract

In the past two decades, porous silicon (PSi) has attracted increasing attention for its potential biomedical applications. With its controllable geometry, tunable nanoporous structure, large pore volume/high specific surface area and versatile surface chemistry, PSi shows significant advantages over conventional drug carriers. In this review, we overview the recent progresses of PSi in drug delivery and cancer immunotherapy. First, we provide an overview of the fabrication of PSi with various geometric structures and highlight how the unique geometry of PSi facilitates its biomedical applications, especially for drug delivery. Second, surface chemistry and modification of PSi are discussed in relation to strengthen its performance in drug delivery and bioimaging. Then, emerging technologies for engineering PSi-based composites are summarized. This review also highlights the emerging advances of PSi in the context of cancer immunotherapy. Overall, the very promising research results encourage further exploration of PSi for biomedical applications, particularly in drug delivery and cancer immunotherapy, and future translation of PSi into clinical applications.

1. Introduction

Porous silicon (PSi) was accidentally discovered by the Ulhirs at the Bell Labs in 1956 when they were searching for a technique to shape the surface of silicon.[1] However, scientists did not show much interest in PSi until Canham discovered that PSi had quantum confinement effects with efficient visible photoluminescence in 1989.[2] Since then, the non-linear optical and electrical properties of PSi have been intensively studied. In 1995, Canham demonstrated that PSi is biocompatible and biodegradable,[3] and consequently, a new era was opened for the biomedical applications of PSi. The last two decades have witnessed the increasing application of PSi in drug delivery, bioimaging, biosensing, tissue engineering and

2

immunotherapy.[4] In addition, PSi has also been investigated as battery anode[5] and hydrogen-generating materials.[6] In this review, we will mainly focus on the fabrication and application of PSi for both drug delivery and cancer immunotherapy.

The most common method to produce PSi is the electrochemical anodization of monocrystalline silicon wafers in a hydrofluoric acid electrolyte solution.[7] The pore size and porosity/pore volume of PSi can be precisely controlled by manipulating the fabrication parameters, and its biodegradability can be adjusted by porosity and pore size.[8] Importantly, PSi possesses several particularly appealing tunable properties for designing drug delivery systems: (1) high porosity/large pore volume (~50–80%/~0.5–2.0 cm^3 g^{-1}) for achieving high loading degree of payloads;[9] (2) tunable pore size (~5–150 nm) for loading a broad range of small molecules, macromolecules and nanoparticles;[9-10] (3) versatile surface chemistry and high specific surface area (up to 580 m^2 g^{-1}) that can be surface functionalized for controlled drug release and (multiple) biological functions;[7,11] (4) excellent biocompatibility and the ability to completely degrade into non-toxic orthosilicic acid [Si(OH)$_4$] which is naturally present in the human body.[3,8,12] The PSi for constructing drug delivery systems are mostly (quasi-) spherical shaped micro- and nano-particles due to their wide applicability and easiness of fabrication. For example, (quasi-) spherical PSi micro- and nano-particles were either applied directly or formulated into micro- or nano-composites to enhance the intestinal absorption of oral delivered small molecules (indomethacin and 5-Flurorouracil), peptides (glucagon-like peptide-1 (GLP-1), peptide tyrosine tyrosine 3-36) and proteins (insulin),[4g,13] and they were also constructed into nanocomposites for the intravenous delivery of chemotherapeutics (methotrexate (MTX) and sorafenib (SFN)) for cancer therapy.[14] In the last decade, several novel "top-down" and "bottom-up" approaches have been developed to fabricate spherical PSi particles. For example, comminution of PSi films obtained from "top-

down" approach by microfluidization shows a great potential for mass production of spherical PSi particles,[15] and the "bottom-up" approach using silicon tetrachloride for synthesizing spherical PSi particles avoids the use of hydrofluoric acid.[11b] Furthermore, the introduction of silicon microfabrication techniques into the fabrication process of PSi provides the possibility to precisely fabricate PSi in geometry other than common (quasi-) spherical shape. For example, quasi-hemispherical/discoidal PSi particles and PSi needles have been developed in the last decade for the delivery of therapeutics and imaging agents.[4i,4k,16]

Before the successful accumulation of therapeutics specifically at diseased sites, biological barriers need to be overcome.[17] In the case of topical administration, needles can directly reach the desirable drug delivery sites by physically and straightforwardly crossing the barriers such as skin or cell membrane.[4i,16b] While upon intravenous administration, drug carriers encounter a complex series of biological barriers that prevent the achievement of satisfactory therapeutic effects. These hurdles include opsonization and subsequent sequestration of the drug carriers by the mononuclear phagocyte system (MPS), nonspecific distribution, pressure gradients, cellular internalization, escape from endosomal and lysosomal compartments and drug efflux pumps.[18] Substantial research efforts have been made to incorporate multiple functionalities and moieties within the overall design of PSi-based composites/hybrids for crossing these frustrating barriers, utilizing the combined power of particle geometry control, surface modification and emerging technologies for physical encapsulation of particles, and many promising advances in fields, such as cancer therapy,[4j,13d,14a,19] have been reported during the last years. For example, the unique geometry of discoidal PSi microparticles enabled them to sequentially overcome the biological barriers that particles encountering from the intravenous administration site to the disease site, *i.e.*, tumors;[4j] the surface modification of PSi nanoparticles with polyethylenimine (PEI)

contributed to the sustained delivery of small interfering RNA (siRNA) to human breast cancer cells;[20] and the physical encapsulation of PSi nanoparticles in acid-degradable acetalated dextran (AcDX) facilitated the simultaneously loading of multiple chemotherapeutics into the nanocomposites for combination cancer therapy.[14b]

However, every coin has two sides. The opened and interconnected nanopores of PSi facilitate the straightforward loading of a broad range of payloads including small molecules,[14b,21] peptides,[4g,13a-c,22] proteins,[16b,23] nucleic acids[4i,20,24] and nanoparticles.[4k,19a,25] The easy accessed pores of PSi are likely to lead to premature and uncontrolled release of the payloads and deactivation of loaded fragile therapeutics, especially when the therapeutics loaded in PSi need to be transported from the administration sites to the diseased sites. In order to overcome these limitations, many strategies have been developed in recent years in terms of controlled drug release for PSi using surface modification and/or physical encapsulation.[13b,13d,14a,23c,26] For example, the surface modification of PSi nanoparticles with temperature responsive polymer enabled the controlled drug release in response to the heating induced by infrared or radiofrequency radiation,[27] and the physical encapsulation of PSi nanoparticles in pH-responsive polymers protected GLP-1 and insulin from the harsh conditions of the gastrointestinal tract, and provided site specific drug release in small intestines for enhanced absorption.[4g,28]

Recently, cancer immunotherapy has also attracted tremendous attention as a new paradigm in cancer treatment given the significant increase in patient survival that has been achieved in clinical trials.[29] The emerging multidisciplinary research in cancer biology, immunology, bioengineering and biomaterials shows great potential to further enhance the therapeutic effects and reduce the side effects of cancer immunotherapy.[30] Among the biomaterials, PSi is being increasingly explored for its potential as an adjuvant,[4b,31] and the excellent loading

5

capacity and versatile surface chemistry of PSi also make it a unique candidate for combined chemoimmunotherapy.[32] Exciting progress has also been made in the last few years.[4a,4c]

To provide an overview of the latest research advances and future developments of PSi in drug delivery and cancer immunotherapy, this review is organized as follows. We firstly outline the fabrication and application of PSi in different geometry. Subsequently, the strategies to boost PSi for drug delivery applications by using the versatile surface chemistry of PSi for surface modification and by employing emerging technologies to engineer PSi-based composites are discussed. Then, the recent advances in using PSi for cancer immunotherapy are highlighted and discussed. The conclusions and outlook of the role of PSi for drug delivery and cancer immunotherapy are finally presented.

2. PSi with controllable geometry

The size and geometry of the particles play an important role in their *in vitro* and *in vivo* behavior.[33] For example, upon intravenous administration of the particles, size and geometry affect circulation time, hemorheological dynamics, extravasation through leaky vasculature, cellular uptake and *in vivo* distribution. In addition, the geometry also drives the initial cellular internalization of the particles.[18] PSi particles can now be produced with precise and uniform size, and the utilization of silicon microfabrication techniques also makes it possible to fabricate PSi in geometries other than spherical shape, such as quasi-hemispherical, discoidal and needle shape. In this section, we present and discuss the recent advances in the fabrication and application of PSi characterized by various geometric features.

2.1. Spherical PSi particles

PSi is a nanostructured material most commonly prepared by the electrochemical etching of single-crystal silicon wafers. Recent developments in engineering micro/nano-sized particles of PSi have attracted much attention. After anodization, the PSi layer is detached from the silicon wafer as intact membranes or large flakes (**Figure 1a**). The production of particles from anodized silicon wafers requires a "top-down" approach. Comminution of PSi can be achieved by ultrasonication,[34] milling,[35] or high-pressure microfluidization,[15] and the obtained PSi particles are in (quasi-) spherical shape. The spherical shape is the dominant shape of PSi particles due to its wide applicability, easiness of fabrication and wide range of fabrication methods available.[36]

Ultrasonication is the first comminution method developed to prepare small particles of PSi.[34b] In a liquid, such as ethanol, the sonication radiation fractures the PSi film into small particles. Depending on the liquid used and the duration of sonication, the average size of obtained PSi particles can be tuned from a few microns to hundreds of nanometers.[34a] The engineering of PSi nanoparticles smaller than 300 nm is challenging by ultrasonication, which typically proceeds for several hours (**Figure 1b**). In such a long ultrasonication duration, the dissolution of PSi in the ultrasonication medium can be excessive.[15] The dissolution process is also accompanied by the oxidation of PSi particles.[15] With the help of high power ultrasonication, the particle size of PSi could be reduced to as low as around 50 nm (**Figure 1d**).[37] The size distribution of PSi particles prepared by ultrasonication is relatively broad. To achieve a specific size cut, the PSi particles can be centrifuged or filtered,[38] which however reduces the final yield. Qin *et al.*[34c] applied periodical high-current density pulses during the etching process, and therefore a porous multilayer was obtained, in which porous layers were separated by thin layers of much higher porosity. Ultrasonication selectively

fractured the porous film along these high-porosity perforations, providing better size control and 5 times higher yield of the resulting PSi nanoparticles.

PSi layers can also be milled into powders. The milling comminution techniques include rotor milling, ball milling and jet milling,[39] among which rotor milling and ball milling are energy intensive processes. The choice of milling technique and condition governs the average particle size, size distribution, and crystallinity of the obtained PSi particles. For example, ball milling can even render the crystalline structure of bulk silicon into amorphous.[40] Mechanochemical processes based on ball milling have been used to produce functionalized powders from PSi.[41] Since PSi feedstock is highly reactive with high surface area, great care must be taken to minimize pressure and temperature buildup. Both milling techniques and conditions are important considerations for the comminution of PSi layers. After milling, the size distribution of PSi particles can be narrowed to a specific range by incorporating a classifier or using graded sieves.[35b]

The high-shear microfluidization, also called high pressure homogenization, is a rapid, reproducible, and high-yield method to prepare nanoparticles with a narrow size distribution.[42] Roberts *et al.*[15] compared the features of PSi nanoparticles prepared by microfluidization and ultrasonication (**Figure 1c**). Without a filtration step, PSi nanoparticles fabricated by microfluidization showed a narrower size distribution (polydispersity index (PDI) = 0.263 *vs.* 0.47) than those prepared by ultrasonication. Toward microfluidization, the average size of PSi particles can be adjusted between 150 and 350 nm by tuning the process parameters. In comparison to ultrasonication, microfluidization is a more rapid method for PSi particle engineering (20 min *vs.* 16 h). By introducing a silicon oxidant (*e.g.*, sodium tetraborate) in the carrying fluid, a core/shell structured nanoparticle with a silicon core and a silicon oxide shell was obtained. The photoluminescent core/shell PSi nanoparticles with a

quantum yield around 19% were obtained by microfluidization in a single step. Overall, microfluidization is an approach with a great potential for large-scale production of PSi nanoparticles.[15]

In addition to the top-down approach, PSi nanoparticles can be synthesized from silicon tetrachloride by a bottom-up strategy.[11b] Rather than chemical corrosion of silicon, the self-forming salt byproducts served as the templates for pore formation (**Figure 1d**). Simple water rinse removed the salt templates easily. In comparison to the top-down strategy, the bottom-up approach avoided the use of harsh etchants, such as hydrofluoric acid. By simply changing the treatment temperature, the average particle size, pore diameter and specific surface area of PSi nanoparticles can be tuned. For example, three heat treatment temperatures, 600, 700 and 820 °C, were employed to prepare PSi materials, PSi-600 (**Figure 1f**), PSi-700 (**Figure 1g**) and PSi-820 (**Figure 1h**). The transmission electron microscopy (TEM) images of all three PSi particles presented similar disordered mesoporous structures. The high resolution-TEM (HR-TEM) images show that the crystallite sizes of PSi-600, PSi-700 and PSi-820 are 3–5, 7–10 and 10–20 nm, respectively. The resulting PSi materials show high surface areas, up to 580 m^2/g, a value much higher than those of the PSi prepared by electrochemical etching.
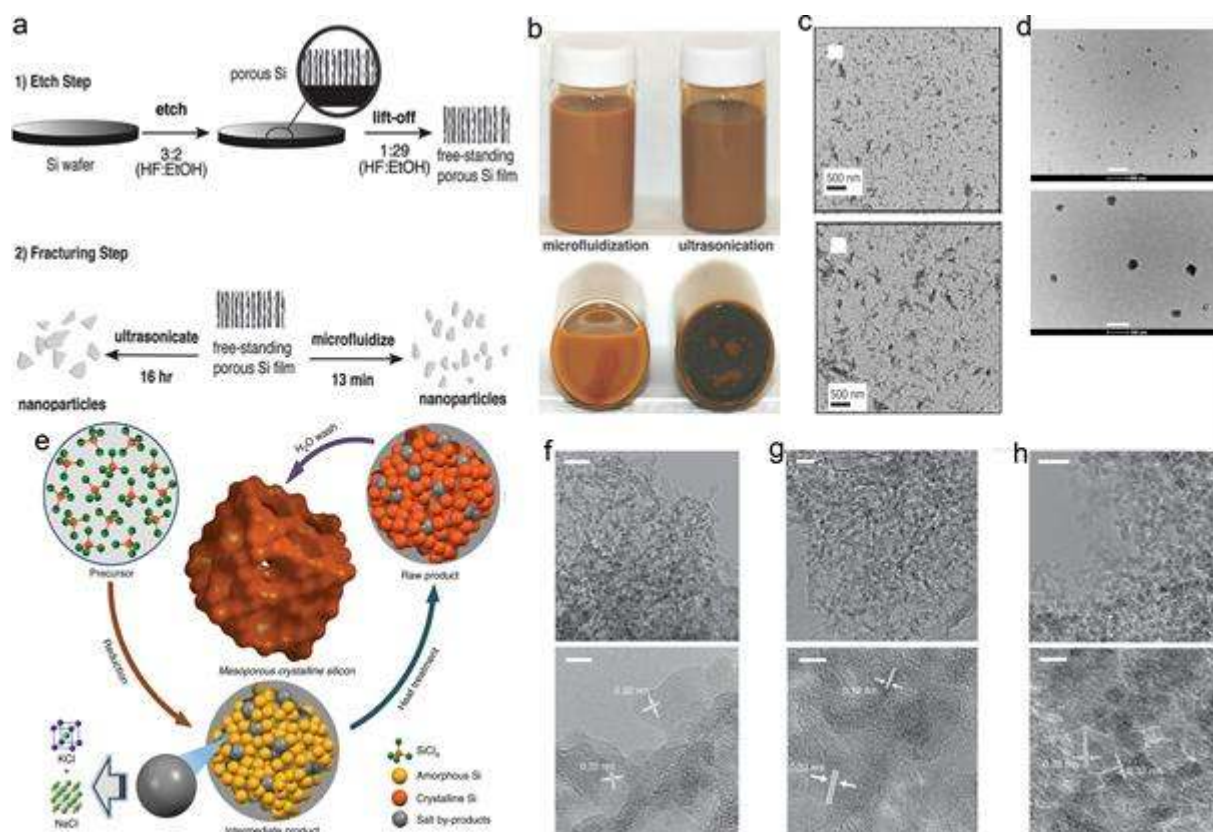
Figure 1. Engineering (quasi-) spherical PSi particles. **(a)** Comparing the ultrasonication and high-shear microfluidization methods for preparing PSi nanoparticles. **(b)** Photographs of vials containing PSi nanoparticles prepared by microfluidization (left) and ultrasonication (right). **(c)** Transmission electron microscopy (TEM) images of PSi nanoparticles fractured by microfluidization (upper) and ultrasonication (bottom). **(d)** TEM images of PSi nanoparticles fractured by high power ultrasonication. Scale bars, 500 (upper) and 100 (bottom) nm, respectively. **(e)** Scheme of the bottom-up synthesis route for PSi particles. **(f-h)** TEM (upper) and HR-TEM (bottom) images of PSi particles, which were fabricated at **(f)** 600, **(g)** 700 and **(h)** 820 ℃, respectively. Scale bars, 20 (upper) and 5 (bottom) nm, respectively. Figures are reproduced with permissions: **(a-c)** from ref. [15], Copyright 2017, WILEY-VCH; **(d) from ref. [37], Copyright 2011, MDPI AG;** and **(e-h)** from ref. [11b], Copyright 2014, Macmillan.

A production rate of particles of kilograms or more per day is desirable both for clinical studies and for industrial scale production.[43] The comminution of PSi wafer is the easiest method to prepare (quasi-) spherical PSi particles. Among all the abovementioned comminution methods, microfluidization can rapidly and high throughput prepare PSi particles with a narrow size distribution, therefore showing a great potential for the mass production of PSi particles.[44]

Much work has also been focused on PSi-based particulate drug delivery systems, which can be ascribed to their wide applicability and relative ease of fabrication as well as administration.[44] PSi particles are being assessed for biomedical applications,[4c,4g,13b,26a,45] and some of them have already been tested in clinical trials by pSiMedica Ltd, UK (pSivida Corp, USA).[46] The loading of small drug molecules, peptides, proteins, genetic materials and even nanoparticles in PSi has already been successfully demonstrated,[44-45,47] and they showed promising therapeutic effects in the therapy of diseases such as cancer,[13d,48] diabetes,[13b,49] heart diseases,[50] wound healing[51] and immunotherapy.[4a,4c,4d,31-32] The applications of spherical PSi particles will also be discussed more in detail in Sections 3–5.

2.2. Quasi-hemispherical and discoidal PSi particles

Quasi-hemispherical and discoidal PSi particles, usually in the micrometer range, have been developed as a key component to construct multistage vectors (MSVs),[4k] which are designed with the aim of overcoming multiple biological barriers to improve the accumulation of payloads in disease sites such as tumors. MSVs are typically composed of three components with different sizes: quasi-hemispherical or discoidal PSi microparticles are the first stage vector for loading the second stage vector, which is usually nanoparticles; and the third stage vector is the therapeutic which is encapsulated by the second stage vector.

11

PSi was selected as the material for the first stage vector due to its complete biodegradability, excellent biocompatibility, and controllable geometry, pore size and porosity during fabrication.[4k,9b,9c] Rather than spherical geometry, PSi was designed and fabricated in a non-spherical geometry, specifically quasi-hemispherical or discoidal shape, to obtain superior blood tumbling and margination dynamics and to preferentially adhere to disease sites for delivering the successive staged vectors.[52]

2.2.1. Fabrication and properties of quasi-hemispherical and discoidal PSi particles

To precisely control the geometry, pore size and porosity, quasi-hemispherical and discoidal PSi micro- and nano-particles are produced by a combination of photolithography/colloidal lithography and electrochemical etching.[9b,9c,16a] The geometry of the PSi particles is precisely controlled by photolithography[9b,9c] or colloidal lithography,[16a] while the nanoporous structure is determined by the electrochemical etching. The fabrication methods for quasi-hemispherical and discoidal PSi micro- and nano-particles were reported in detail by Chiappini *et al*.[9b], Godin *et al*.[9c] and Alhmound *et al*.[16a], and are briefly described in **Figure 2**. Quasi-hemispherical PSi particles can be tailored to diameters of 0.97–3.2 μm, porosities of 47–80% and pore sizes of 5–50 nm.[9b] Discoidal PSi microparticles are typically with diameters ranging from 0.5–2.6 μm, heights from 200–700 nm, porosities from 40–90% and pore sizes from 5–150 nm.[9c,16a] The tunable pore size of these PSi particles makes them flexible to load nanoparticles of different sizes within their nanoporous structure.

Both quasi-hemispherical and discoidal PSi micro- and nano-particles showed excellent *in vitro* and *in vivo* biocompatibility.[16a,53] For example, they were non-toxic towards cell types, including macrophages, human umbilical vein endothelial cells (HUVEC), mouse adipose-derived mesenchymal stromal cells (ADMSC) and erythrocytes.[16a,53a,53b] Both acute single

dose (10^7, 10^8, 5×10^8 particles/mice) and subchronic multiple dose (10^8 particles/mice/week for 4 weeks) of negatively charged oxidized or positively charged (3-aminopropyl)triethoxysilane (APTES) modified quasi-hemispherical PSi microparticles were intravenously injected into mice, and these particles did not change plasma levels of blood urea nitrogen, creatinine and lactate dehydrogenase (LDH), as well as 23 plasma cytokines. Also, they did not change LDH levels in liver and spleen, nor lead to infiltration of leukocytes into the liver, spleen, kidney, lung, brain, heart and thyroid.[53c] In addition, quasi-hemispherical PSi microparticles did not cause any significant acute or chronic effects on tissues in a long term (up to six months) *in vivo* study.[53b]

Moreover, quasi-hemispherical and discoidal PSi micro- and nano-particles are biodegradable in physiological conditions, and their degradation rates can be tuned by pore size, porosity and surface modifications.[9c,16a,54] For example, discoidal PSi nanoparticles (diameter of 600 nm and thickness of 400 nm) fully degraded in Tris buffer (pH 7.2) after 2 h at a degradation rate of 2.3 mM h^{-1}, while surface modification with semicarbazide and undecylenic acid decreased the degradation rate to 18×10^{-3} mM h^{-1} and 27×10^{-3} mM h^{-1}, respectively.[9c] Quasi-hemispherical PSi microparticles (diameter of 3.2 μm and thickness of 900 nm) were also completely degradable in PBS (pH 7.4), cell culture medium, serum and blood within 24 h.[54e] The timely degradation of quasi-hemispherical and discoidal PSi microparticles is crucial for MSVs as it guarantees the delivering of second stage vector to the target sites.
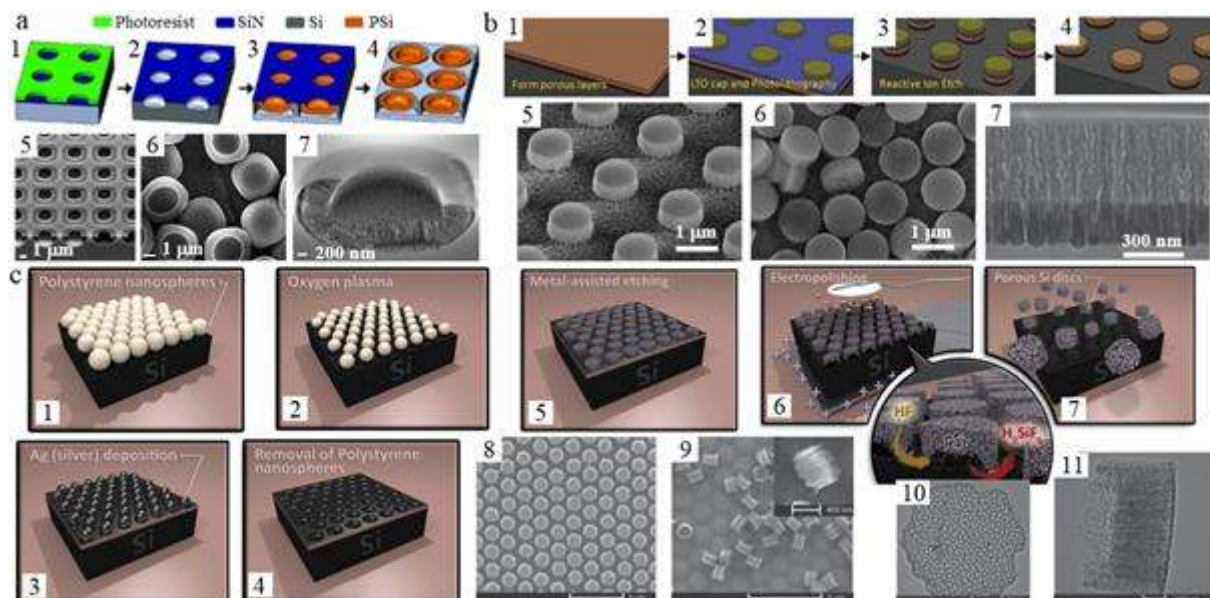
Figure 2. (a) Fabrication process of quasi-hemispherical PSi microparticles using the combination of photolithography and electrochemical etching.[9b] **a1)** Pattern transfer to the photoresist layer on top of the sacrificial SiN layer. **a2)** Trench formation in the silicon substrate through a combination of dry and wet etching. **a3)** Formation of the PSi microparticles and release layer following anodic etching. **a4)** PSi microparticles ready to be released by ultrasonication following stripping of the SiN mask. Scanning electron microscope (SEM) images of **a5)** particle array on wafer, **a6)** released particles and **a7)** cross-section of particles. **(b)** Fabrication process of discoidal PSi microparticles using the combination of photolithography and electrochemical etching.[9c] **b1–b4)** Process flow. SEM images of **b5)** particle array on wafer, **b6)** released particles and **b7)** cross-section of particles. **(c)** Fabrication process of discoidal PSi nanoparticles using the combination of colloidal lithography and electrochemical etching.[16a] **c1)** Self-assembly of polystyrene nanospheres (PSNS) onto a silicon wafer, **c2)** Size reduction of PSNS by O$_2$ plasma treatment, **c3)** Ag deposition and **c4)** removal of the PSNS layer, **c5)** Discoidal nanoparticles array on the silicon wafer after metal-assisted chemical etching (MACE) in HF/H$_2$O$_2$, **c6)** Removal of the Ag layer and the subsequent electropolishing step done to lift off the discoidal nanoparticles from

the silicon wafer using electropolishing, **c7)** Discoidal nanoparticles after removal from the silicon wafer. SEM images of **c8)** discoidal nanoparticles array on the silicon wafer and **c9)** Released discoidal nanoparticles. TEM images of **c10)** top view and **c11)** side view of an individual discoidal nanoparticle. Figures are reproduced with permissions: **(a)** from ref. [9b], Copyright 2010, WILEY-VCH; **(b)** from ref. [9c], Copyright 2012, WILEY-VCH; and **(c)** from ref. [16a], Copyright 2015, WILEY-VCH.

2.2.2. *Quasi-hemispherical and discoidal PSi microparticles for carrying therapeutics or nanoparticles*

Quasi-hemispherical and discoidal PSi microparticles, as the first stage vector, transport payloads that are loaded in their nanopores and protect them during the transportation from the administration sites to the target sites. The first stage vector can be directly loaded with therapeutics. For example, small molecule drugs,[21a,55] peptides,[56] proteins,[23a] siRNAs,[19a,20,24a,57] and micro RNAs (miRNAs)[24a] have been successfully encapsulated in quasi-hemispherical or discoidal PSi microparticles through electrostatic attraction or covalent bonding. Therapeutics can also be pre-loaded in nanoparticles, which are then entrapped in quasi-hemispherical or discoidal PSi microparticles. Depending on the application, the second stage vector can be any currently available nanoparticles, such as liposomes,[19a,24b,57-58] micelles,[25c,55,59] polyplexes,[60] polymer nanoparticles,[24b,25d] and imaging agents.[4m,25b] At the lesion sites, nanoparticles released from the quasi-hemispherical or discoidal PSi microparticles address the biological barriers in extracellular and intracellular compartments, delivering the third stage vector, such as chemotherapeutic agents like paclitaxel (PTX),[25c,25d] doxorubicin (DOX),[55] and docetaxel,[24b] nonsteroidal anti-inflammatory drug,[59] and siRNAs,[19a,24b,57,58b,60] for the treatment of diseases. For example, clinically used nanoparticle

albumin-bound paclitaxel (nAb-PTX) was loaded into discoidal PSi microparticles (diameter

of 1 μm and thickness of 400 nm), which enabled the cross of the drug through the tumor

vessel wall and enhanced its interaction with liver macrophages, and eventually increased the

efficacy of nAb-PTX and survival in mouse models of breast and lung liver metastasis.[25d]

2.2.3. Discoidal PSi microparticles for generating nanoparticles

Instead of directly loading nanoparticles, Xu *et al.*[4j] developed an alternative approach to

load discoidal PSi microparticles with nanoparticles by triggering the formation of

nanoparticles inside the nanopores of the microparticles (**Figure 3a**). In detail, DOX was

conjugated to poly(L-glutamic acid) through a pH-sensitive cleavable hydrazine linker to

form a polymeric drug (pDox), which was then loaded into the discoidal PSi microparticles

(diameter of 2.5 μm and thickness of 700 nm) with pore size of 40 or 80 nm to assemble PSi-

pDox with a loading degree of 25 wt% for pDOX. Intravenously injected PSi-pDox

accumulated in metastatic MDA-MB-231 tumors and consequently released the pDox

molecules which assembled *in situ* into pDox nanoparticles with a diameter in the range of

30–80 nm (**Figure 3a**). The particle size of the formed pDox nanoparticles was influenced by

the pores of the PSi. The pDox nanoparticles were released for up to 2 weeks at pH 7.4 in a

sustained manner and were internalized by tumor cells. Intracellularly, pDox nanoparticles

underwent trafficking to the perinuclear regions of the cells. The pH-sensitive linker was

cleaved in the acidic environment of the endosomes, yielding high intracellular concentrations

of activated Dox and avoiding the excretion by drug efflux pumps. Compared to the

individual components of PSi-pDox, including PSi, pDox nanoparticles and Dox, or Doxil

(FDA-approved nanodrug), PSi-pDox showed enhanced therapeutic effects in mouse models

of metastatic breast cancer, including functional cures in 40–50% of the treated mice. The

distinct biological barriers that each component of PSi-pDox can overcome following systemic administration are presented in **Figure 3a**. Compared to other MSVs, this PSi-pDox construct has the unique capability to *in situ* generate nanoparticles for a sustained site-specific drug release, which acts as an intravascular drug depot for prolonged drug exposure at therapeutically relevant levels.

2.2.4. Quasi-hemispherical and discoidal PSi microparticles for enhancing imaging

Owing to the relatively large overall size and tunable pore size, quasi-hemispherical and discoidal PSi microparticles have great potential to be flexibly used for the simultaneously delivery of multiple therapeutics for combination therapy[24b] or simultaneously delivery of therapeutics and imaging agents for theranostics.[4k] When quasi-hemispherical or discoidal PSi microparticles are applied as carriers of imaging agents only, like other types of PSi particles, their surface has the possibility to be used for the electrostatic attraction or covalent bonding of numerous kinds of dyes, fluorophores, fluorescent/radioactive molecules and other imaging agents.[16a,25b,26b,54e,59,61] The most unique characteristic of quasi-hemispherical and discoidal PSi microparticles is that they do not only act as carriers for magnetic resonance imaging (MRI) contrast agents, but also enhance the imaging capability of the MRI contrast agents.[4m] [25b] MRI is one of the most powerful and non-invasive diagnostic imaging technique, and contrast agents are widely used to improve its sensitivity and specificity. The most commonly used MRI contrast agents in clinic are based on Gd^{3+} ions, which are toxic as solubilized aqueous ions. Chelation can significantly reduce the toxicity of Gd^{3+} ions, which however also lowers the relaxivities in a large extend, *i.e.*, weakens the ability of Gd^{3+} to perform as an MRI contrast agent.

Ananta *et al.*[4m] designed a new class of MRI contrast enhancing agents through the loading of Gd-based contrast agents into the nanopores of quasi-hemispherical or discoidal PSi microparticles. Enhanced efficiency was obtained on three different Gd-based contrast agents, namely Magnevist (MAG) ($r_1 \approx 14$ mM^{-1} s^{-1}/Gd^{3+} ion), a clinically used chelate, and two carbon nanostructure-based lipophilic agents, gadofullerenes (GFs) ($r_1 \approx 200$ mM^{-1} s^{-1}/Gd^{3+} ion) and gadonanotubes (GNTs) ($r_1 \approx 150$ mM^{-1} s^{-1}/Gd^{3+} ion). The longitudinal relaxivity values of the resulting new MRI constructs were ~4–50 times larger than that of the clinically used MAG ($r_1 \approx 4$ mM^{-1} s^{-1}/Gd^{3+} ion). The enhancement in the MRI contrast is due to the geometrical confinement of the Gd-based contrast agents within the nanopores of PSi, which influences the paramagnetic behavior of the Gd^{3+} ions.

Besides Gd-based contrast agents, SPIONs represent another popular contrast agent.[62] Serda *et al.*[25b] found that the loading of SPIONs into the discoidal PSi microparticles (**Figure 3b**) led to shorter relaxation times in a SPIONs concentration dependent manner. The differences in signal intensity were more obviously at lower echo times in gradient-echo images. The entrapment of a large amount of SPIONs inside the protective nanopores of PSi microparticles also facilitated the delivery of an abundance of contrast agent to the target sites which boosted the ability for biological imaging (**Figure 3b**).[25a,25b]
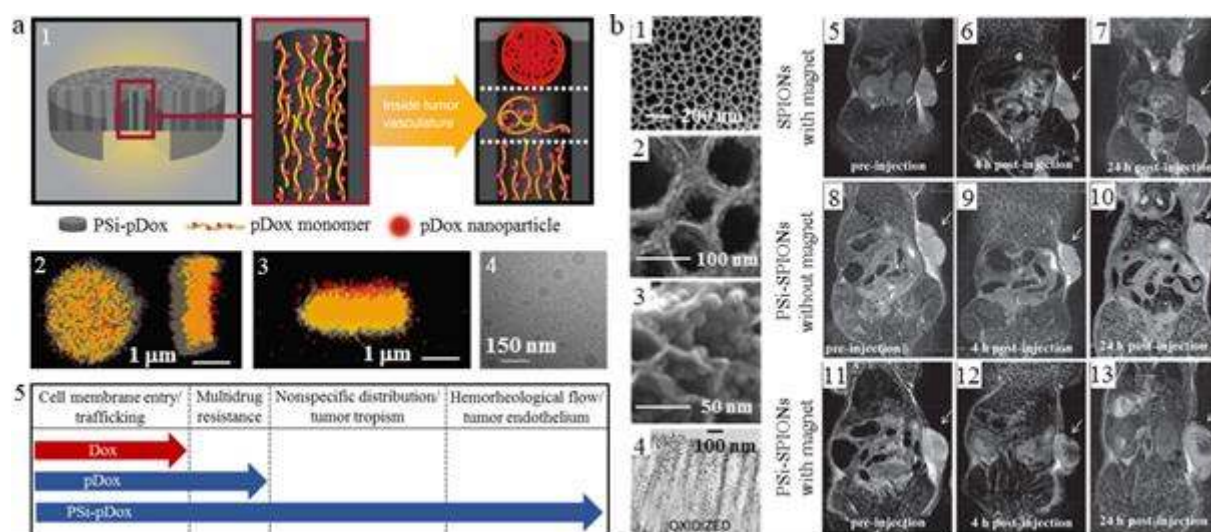
Figure 3. **(a)** Discoidal PSi microparticles for generating nanoparticle.[4j] **a1)** Schematic diagram depicting PSi-pDox composition, pDox prodrug encapsulation, and pDox nanoparticle assembly and release from nanopores. **a2)** Z-series confocal microscopy images of the PSi-pDox particles, highlighting the presence of pDox (red) within the nanopores of the PSi particle (gray). **a3)** 3D reconstruction following sagittal cross-sectioning of the PSi-pDox particles, depicting pDox (red) within the nanopores of the PSi particle (gray), as well as the presence of pDox nanoparticles (red) released from the microparticles. **a4)** Cryogenic TEM of pDox nanoparticles released from PSi-pDox. **a5)** Schematic diagram demonstrating the individual components of the PSi-pDox construct and the distinct biological barriers that each component is capable of overcoming following systemic administration. **(b)** Discoidal PSi microparticles for enhancing MRI imaging.[25a,25b] **b1)** and **b2)–b3)** SEM of the surface of PSi microparticles before and after loading with SPIONs. **b4)** TEM of the cross-section of SPIONs loaded PSi. **b5–b13)** MRI images of a melanoma tumor growing in the right flank of a mouse before, 4 h, and 24 h post injection of free SPIONs with a static magnet applied over the tumor, and injection of PSi-SPIONs with and without a static magnet applied over the tumor.[25a] Figures are reproduced with permissions: **(a)** from ref. [4j], Copyright 2016, Springer Nature; and **(b)** from ref. [25a,25b], Copyright 2010 and 2014, WILEY-VCH.

2.3. PSi needles

2.3.1. Evolution of silicon needles: from solid to porous

Injection using a hypodermic needle provides a rapid and direct way to deliver almost any type of molecule into the body. However, hypodermic needles cannot be easily used by patients themselves, and the injection pain leads to poor patient compliance. In order to improve the patient compliance and safety while making full use of its powerful delivery

capability, needles are envisaged to be miniaturized to micron size for painlessness and minimal invasiveness.[63] In this review, needle is used in its broad meaning referring to conical needle, cylindrical wire and pillar. With the development of silicon microfabrication techniques in semiconductor industry, the first microneedle was fabricated out of silicon in 1990s for biomedical applications.[64] Silicon microneedle is also the first microneedle used for drug delivery.[65] The details of the fabrication methods, functions and applications of conventional silicon micro/nano-needles can be found in some review papers.[66]

The conventional silicon needles are non-porous, *i.e.*, either solid [64-65,67] or hollow.[68] These silicon needles can directly interface with tissues or cells for therapeutics delivery. However, they have limited loading capacity of payloads due to their non-porous structure with low specific surface area, which limits their therapeutic efficacy. In addition, the miniaturization of silicon needles to micro/nano-meter size increases the risk of mechanical failure during insertion of needles into tissues or cells. The non-porous silicon needles are poorly biodegradable, which raises concern that the broken silicon needle tips might cause biological complications. Therefore, the mechanical failure of non-porous silicon needles must be prevented in clinical applications. Unfortunately, it is not possible to completely avoid the mechanical failure of silicon needles because of the brittle characteristic of silicon. Thereby, the development of biodegradable silicon needles becomes strongly necessary.

2.3.2. Fabrication and properties of PSi needles

In order to increase the loading capacity of therapeutics and biodegradation rate that ultimately maximize the biological benefits of silicon needles, PSi needles were developed.[4i,16b] The fabrication method of PSi needles, in several variations, combines the

arrangement of the needle array by lithography with the porosification of the silicon substrate by (electro-) chemical etching.[4i,16b,69]

At the early development stage of PSi needles, silicon needles were porous only at the tips level. Chen *et al.*[70] fabricated pyramidal silicon microneedles with porous tips by selective electrochemical etching of pyramidal silicon microneedles, which were obtained by deep reactive ion etching (RIE), using the photoresist reflow effect and RIE notching effect. The porous tip had a height of ~30 µm (**Figure 4a**). The *in vitro* transdermal drug delivery experiments showed that the skin permeability of calcein and bovine serum albumin (BSA) was enhanced to 5–6 and ~7 times with these microneedles, respectively, compared to the passive transdermal delivery without microneedles.[70-71] However, the potential of the PSi tip for drug delivery was not fully exploited in this study, because these needles were used as a pretreatment for pore formation in the skin rather than employed as carriers of payloads. In another study conducted by Gentile *et al.*,[69b] cylindrical silicon microneedles with porous tips (**Figure 4b**) were fabricated by deep RIE of UV photolithography patterned disks to form silicon microneedles and followed by electrochemical etching of the microneedle tips for porosification. The drug delivery capability of the developed needles, however, was not investigated.

Ideal porous needles should be a single unit drug delivery system, whereby the whole needle is porous and loaded with therapeutics.[66c,72] Several methods have been developed to fabricate silicon needles with fully porous structure, and the typical ones combine the methods of nanosphere lithography and templated MACE (**Figure 4c**),[16b] or standard microfabrication and MACE (**Figure 4d**).[4i,69c] By the later method, conical PSi nanoneedles with variable sizes (**Figure 4d3**) were fabricated, and the one that had 5 µm length, 50 nm apical width and 600 nm base diameter provided an over 300-fold increased surface area for

drug adsorption compared to a solid cylindrical nanoneedles of equivalent apical width. The porosity of the PSi nanoneedles could be tailored between 45% and 70%, enabling the adjustment of mechanical properties, degradation rate and drug loading capacity. Chiappini *et al.*[4i,69c] confirmed the excellent biodegradability of PSi needles (**Figure 4d4**). PSi nanoneedles completely dissolved within 72 h, which enable the PSi nanoneedles to temporarily interface with cells or tissues, *i.e.*, completely degrade after delivering the payloads. Moreover, in addition to porosity, the degradation rate of PSi needles can be adjusted by surface treatments.[4i,69c]
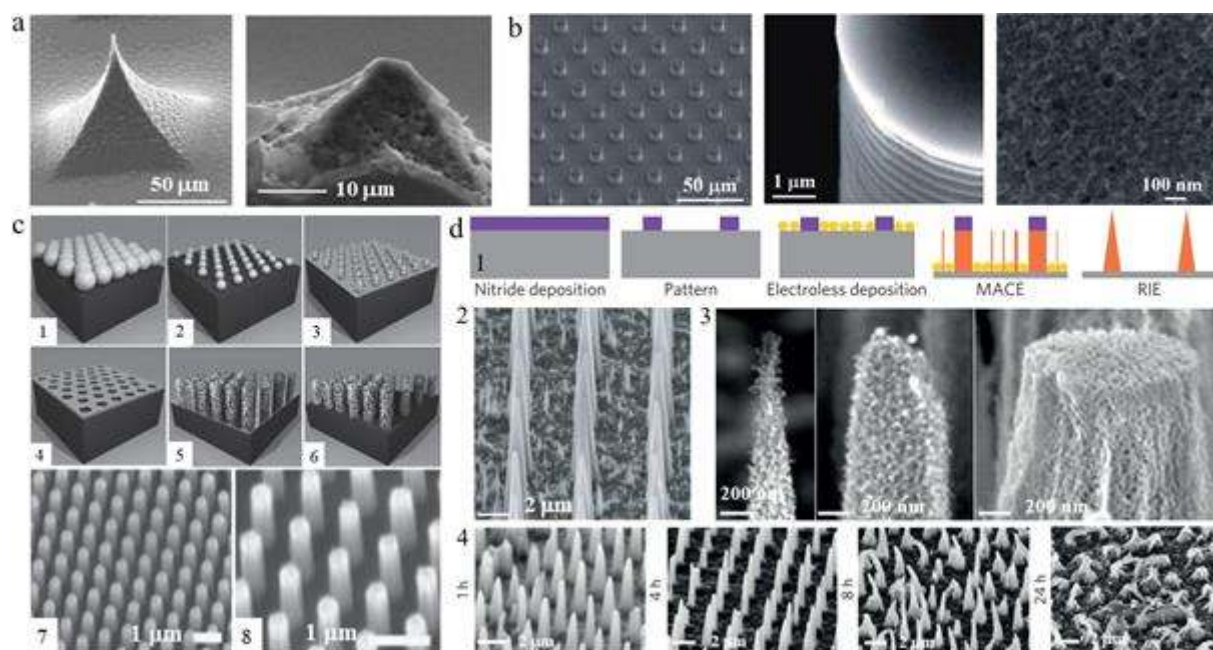
Figure 4. **(a)** SEM images of pyramidal silicon microneedles with porous tips.[70] **(b)** SEM images of cylindrical silicon microneedles with porous tips.[69b] **(c)** Fabrication of cylindrical PSi nanoneedles using nanosphere lithography and tMACE method.[16b] **c1)** A hexagonal close-packed (hcp) monolayer of monodisperse PSNS was assembled on a silicon wafer via convective assembly and then **c2)** transferred into a nonclose-packed (ncp) PSNS array via O$_2$ plasma etching. **c3)** The array was used as a mask for Ag metal layer deposition by sputter coating. **c4)** After removing the PSNS by lift off, an ordered array of holes was produced in

the Ag film. Subsequently, the metal layer served as a catalyst for the wet etching of silicon by MACE. **c5)** Using this method, arrays of vertically aligned PSi nanoneedle arrays were fabricated with different aspect ratios. **c6)** The Ag layer was finally removed with nitric acid. **c7–c8)** SEM images of PSi nanoneedles with different diameters. **(d)** Conical PSi nanoneedles.[4i] **d1)** Schematic of the PSi nanoneedle fabrication process combining conventional microfabrication and MACE. **d2–d3)** SEM images of PSi nanoneedles showing the nanoneedles' porous structure and the tunable tip diameter. **d4)** Progressive biodegradation of PSi nanoneedles in cell culture medium at 37 °C. Figures are reproduced with permissions: **(a)** from ref. [69a], Copyright 2006, IOP Publishing; **(b)** from ref. [69b], Copyright 2014, RSC; **(c)** from ref. [16b], Copyright 2015, WILEY-VCH; and **(d)** from ref. [4i], Copyright 2015, Springer Nature.

2.3.3. PSi needles for the delivery of therapeutics

The first study that used PSi needles for drug delivery, consisting of completely porous needles with 10–40 nm in diameter and 1–3 μm in length, was reported by Brammer *et al.*.[73] These PSi needles were able to provide a sustained release of penicillin and streptomycin for 42 days. Loading capacity of therapeutics is another important evaluation index for porous carriers including PSi needles. Peng *et al.*[21b] demonstrated that PSi nanoneedles had an ultrahigh DOX loading capacity of 20,800 mg g^{-1}.

Chiappini *et al.*[4i] performed intracellular delivery of nucleic acids by PSi nanoneedles, which also represents the first use of nanoneedles in an *in vivo* study. These PSi nanoneedles (tip diameter 50 nm and pitch 2 μm) were shown to be robust: they could penetrate the cells for nanoinjection (**Figure 5a**), and their structure was substantially maintained after pressing against skin or muscle. Nanoinjection through PSi nanoneedles was completed by either

cellular activity (**Figure 5a**) or application of an external force,[4i] and the cells impaled by the former approach exhibited a higher transfection efficiency.[16b] Furthermore, nanoinjection did not induce neither significant toxicity nor leakage of intracellular material.[4i]

Nucleic acids were also effectively loaded in PSi nanoneedles and were released over 12–18 h in a sustained manner. Nanoneedles were able to overcome biological barriers (such as cell membrane or the endolysosomal system), and intracellularly co-deliver nucleic acids with a transfection efficiency over 90% to the same cell via nanoinjection process, and the delivered nucleic acids were able to simultaneously regulate gene expression.[4i] Nanoinjection can mediate *in vivo* delivery (**Figure 5b**) and it showed *in vivo* safety. Furthermore, the nanoinjection of vascular endothelial growth factor (VEGF) modulated the local gene expression, heightened the tissue neovascularization, and increased the local blood perfusion for six times when compared to direct injection of VEGF.[4i]

Compared to microneedles, nanoneedles provide a more uniform delivery owing to the higher density of nanoneedles per surface area. They further reduced the invasiveness of the injection, limited the impact on the overall structure of the tissues, and confined the treatment to a localized region (**Figure 5c–d**). However, due to the limited penetration depth of nanoneedles, they can only deliver the payloads to the cells in a localized superficial area of tissue and require a surgical incision to access the non-exposed tissues. In addition to drug delivery application, PSi nanoneedles have also been used for intracellular delivery of nanoparticles[25e] and intracellular sensing of protease/small molecule.[74]
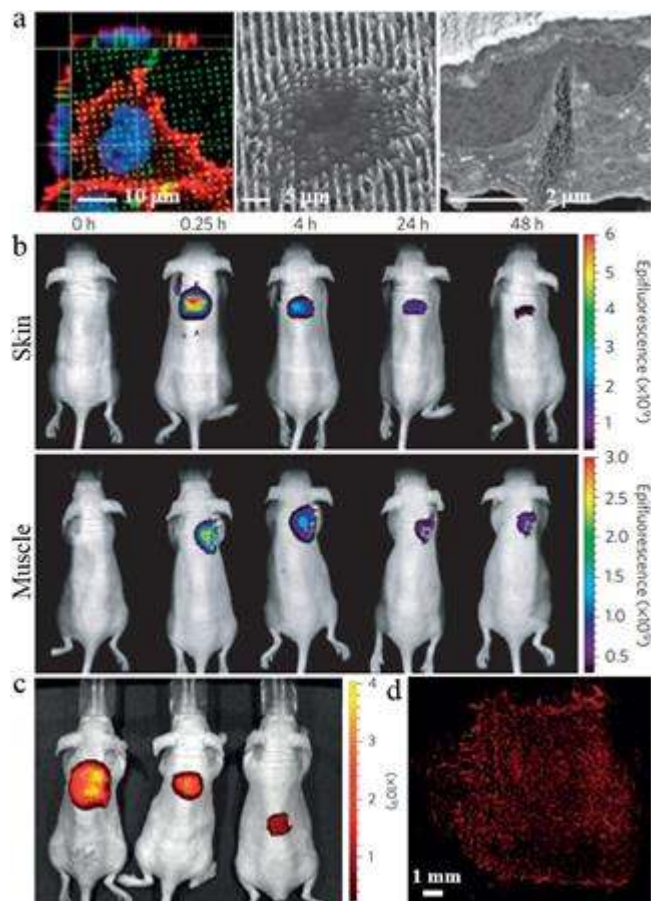
Figure 5. (a) Confocal microscopy, SEM and FIB-SEM cross-sections of cells over PSi nanoneedles at 4 h show cell spreading, adhesion and nanoneedle interfacing. **(b)** PSi nanoneedles mediate *in vivo* delivery. Longitudinal imaging of mice treated with nanoneedles on top of the skin or underneath the skin on the back muscle and loaded with a near-infrared fluorescent dye. The distribution and diffusion of the delivered fluorescent dye was monitored. **(c)** Near-infrared fluorescent imaging on the skin of mice, comparing the delivery of DyLight 800 using a drop (left), flat Si wafer (middle), or nanoneedles (right). **(d)** Intravital confocal image, showing the delivery pattern of dye-loaded nanoneedles. Reproduced with permission from ref.[4i], Copyright 2015, Springer Nature.

3. Surface chemistry and modification of PSi

Despite the bottom-up methods developed to produce PSi, the biomedical applications of these PSi are not widely investigated yet. The most commonly used PSi for biomedical applications is still produced by electrochemical etching. Eventhough freshly etched PSi may be feasible for the development of drug delivery systems,[49,75] there are several undesirable characteristics that may mitigate its further applications. Freshly etched PSi is highly reactive because of its hydride terminated (Si_ySiH_x, $x+y=4$) surface.[76] Such a reactive surface is not stable due to the slow oxidation upon its exposure to atmospheric conditions, which may further lead to changes in structural and optoelectronic properties.[76] In addition, the reactivity may also result in some undesirable chemical reactions with payloads.[77] Furthermore, previous studies demonstrated singlet oxygen generation from non-treated PSi under certain condition whereas reactive oxygen species (ROS) generation on oxidized PSi surfaces was no longer evident.[78] To better apply PSi for biomedical usage, more specifically, as drug delivery systems, further surface chemical modification should be performed.

The first step towards the surface chemical modification of PSi is through direct oxidation to stabilize its surface (**Figure 6**). The back-bond oxidation of PSi takes place at 300–400 °C where the oxygen bridges are formed between the surface Si atoms and the second atomic Si layer (O_ySiH). A further increase of the temperature leads to an increase of the oxidation degree: oxidation at 600 °C and above removes all SiH_x species.[79] Besides of thermal oxidation, other oxidation methods have also been proposed including aqueous oxidation,[39] anodic oxidation,[80] photo-oxidation[81] and chemical oxidation.[82] Despite different methods, all these oxidations are characterized with the disappearance of Si_xSiH_y bond and the generation of O_ySi-OH and Si-O-Si species. Along with the increased stability, this oxidation process also changes the surface of PSi from hydrophobic to hydrophilic,[83] which is

beneficial for many drug delivery applications under physiological conditions, as discussed in the following sections.

In addition to oxidation, thermal carbonization is an alternative method to modify the surface chemistry of PSi (**Figure 6**), which was firstly proposed by Salonen *et al.*[84] via the thermal decomposition of acetylene, which starts at 400–900 °C. According to the processing temperature, it can be divided into two distinct categories, namely, thermally hydrocarbonized PSi (THCPSi) and thermally carbonized PSi (TCPSi) which are yielded at lower and higher temperatures, respectively.[7,84-85] Carbonized films show improved stability against thermal oxidation due to the almost complete coverage of the original silicon hydride surface.[86] Another main advantage of this process is that after this treatment there is not a significantly reduction in the specific surface area of PSi.[87] A drawback of thermally carbonized PSi is that the characteristic luminescence of PSi disappears.[88] An interesting feature of carbonized PSi is manifested after its immersion into HF solution, since a Si–OH termination is formed.[85] The appearance of silanol groups facilitates the use of silane coupling chemistry, typically utilized for the functionalization of silica based or oxidized silicon materials.

Other methods used for the stabilization and the functionalization of PSi are hydrosilylation and silanization chemistry (**Figure 6**).[89] Upon the exposure to Lewis acids, thermal treatment, UV-irradiation and ultrasound sonication, surface silicon hydride can undergo a series of hydrosilylation reactions with the existence of unsaturated compound such as alkenes, alkynes and aldehydes.[11a,90] One of the main advantages of this method is the relatively mild reaction condition: some of the surface modifications can take place even at room temperature.[90b,90e] Other advantages include the versatile possibility to provide different functional groups.[11a] Ligand containing unsaturated groups can simultaneously have specific functional groups on the opposite end of the chain. In this way, various PSi with functional terminations including

carboxylic groups, amine groups, alkenes and hylohydrocarbons are formed.[91] Silanization is

also a suitable method for PSi functionalization. However, it is more commonly used with

porous silica materials, as the silane coupling reactions usually proceed on oxide surfaces

requiring a pre-oxidation of the PSi.[92] After the primary surface stabilization, secondary

surface modification can take place, owing to the appearance of the functional groups such as

amine, carboxyl, alkynyl and aldehyde, for further achieving multiple functions.
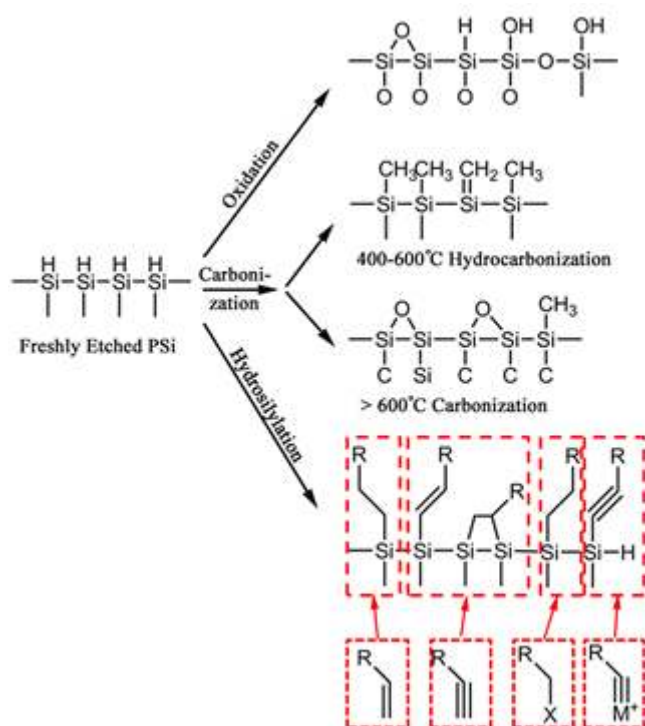
Figure 6. Basic graphic illustration of primary surface modification for freshly etched PSi.

3.1. Surface modification of PSi for controlled drug loading and release

From the chemical point of view, PSi is a favorable carrier for developing drug delivery

systems, because its relative stability enables further surface chemical modifications. A

variety of chemical modifications have been realized on the surface of PSi and on the surface

of its pores.[44,93] **Table 1** summarizes typical examples applying PSi with various geometries

as carriers for therapeutics/imaging agents. In the following sections, we will discuss about

the recent advances focusing on the improvement of the drug loading and release behavior of

PSi, and relative aspects which may need further investigation.

Table 1. Typical examples of using PSi as carriers for therapeutics and imaging agents.

Geometry of PSi	Application	Average size (nm)	Primary modification	Secondary modification	Targeting Moieties	Loaded Cargos	Loading Degree (%)	Imaging	Strategies for Controlled Release	Ref.
Spherical PSi particles	Cancer	16000	THCPSi	NA	NA	Fenofibrate, furosemide methotrexate, ranitidine	25	NA	Solid lipid encapsulation	[94]
	Cancer	188	TCPSi	APTES	iRGD	SFB	6	NA	NA	[95]
	Cancer	228	THCPSi	Un	Hyaluronic acid	NA	NA	NA	NA	[96]
	Cancer	ca. 400	TOPSi	NA	CPP	PTX, SFB, MTX	PTX, SFB 5, MTX 0.1	NA	Polymer encapsulation	[14b]
	Cancer	ca. 200	THCPSi	1,7-octadiyne−mesitylene	iRGD, Poly(glutamic acid), dextran	NA	NA	NA	NA	[97]
	Cancer	202	THCPSi	Un, Radio labeling, Fluorescence dye labeling	iRGD	SFB	27	SPET/CT, Fluorescence imaging (FI)	NA	[56]
	Cancer	200	THCPSi	APTES	NA	MTX, SFB	SFB 6, MTX 3	NA	Drug conjugation	[98]
	Cancer	260	TOPSi	NA	NA	SFB	6	NA	Polymer encapsulation	[14a]
	Cancer	ca. 80000	THCPSi	APTES	NA	DNA, DOX	DNA 15. DOX 30	NA	Liposome encapsulation	[99]
	Cancer	126	Freshly Etched PSi	NA	NA	DOX	5	Photoluminescence (PL)	Polymer encapsulation	[4l]
	Cancer	260	THCPSi	Un, quercetin	Quercetin	DOX	24	FI	Non-covalent bond stacking (chelation)	[100]
	Cancer	388	THCPSi	Un, cyclodextrin	NA	SFB	18	NA	Polymer conjugation	[101]
	Cancer	252	TOPSi	APTES,	NA	DOX, MTX	DOX 1.2,	NA	Polymer conjugation	[102]

30

			poly(beta-amino ester			MTX 1.8			
Cancer	ca. 200	THCPSi	Un, aptamer, PEI	MTX	SFB	SFB 1, Aptamer ca. 30	NA	Polymer conjugation	[103]
Cancer	193	THCPSi	Un, carbonic anhydrase IX targeting ligand	Carbonic anhydrase IX targeting ligand	DOX	21	FI	Non-covalent bond stacking (hydrogen bond)	[104]
Cancer	190	THCPSi	Un, cysteine, DNA	CPP	SFB, calcein	9.3	FI	Polymer encapsulation, DNA encapsulation	[21d]
Cancer	190	Hydrosilylation (semicarbazide)	MLR2, Rituximab, mAb528	Antibodies	Camptothecin	11	NA	NA	[105]
Cancer	245	Hydrosilylation (allylisocyanate)	Anionic porphyrin	NA	Anionic porphyrin	1.3	NA	Drug conjugation	[106]
Cancer	151	THCPSi	Un, PEI, PMVEMA	PMVEMA	Fluorouracil, celecoxib	Fluorouracil 7.1, celecoxib 6.9	NA	Polymer encapsulation	[13d]
Cancer	257	Hydrosilylation (divinylbenzene)	NA	NA	DOX	40	NA	Non-covalent bond stacking (π-π stacking)	[107]
Cancer	ca. 200	Hydrosilylation (undecylenic acid)	NA	NA	DOX	7	PL	Non-covalent bond stacking (hydrogen bond)	[48b]
Cancer	226	Hydrosilylation ([Ru(5-Fluo-Phen)$_2$(5-E-Phen)](PF$_6$)$_2$)	Isocyanopropyl triethoxysilane	Mannose	Ruthenium(II) complex	1.8	NA	Drug conjugation	[108]
Cancer	36000	Hydrosilylation (undecylenic acid)	Chitosan,	NA	Tamoxifen	33	NA	Polymer conjugation	[109]

31

Cancer	94	TOPSi	APTES	NA	IR820 dye, DOX	IR820 21, DOX 14	NA	Outer-stimuli (photothermal)	[110]
Cancer	422	Silanization (APTES)	FITC	NA	DNA (EF1-Egfp)	1	NA	NA	[45a]
Cancer	ca. 350	TOPSi	APTES, PNIPAm	NA	DOX	24	NA	Outer-stimuli (infrared and radiofrequency electromagnetic heating)	[27]
Cancer	ca. 236	THCPSi	NA	NA	siRNA	ca. 5	NA	Polymer encapsulation	[111]
Anti-bacteria	256	THCPSi	Isocyanato-silane acid, S-nitrosothiol, S-nitrosoglutathione	NA	nitric oxide	NA	NA	Drug conjugation	[47c]
Anti-virus	129	THCPSi	NA	NA	Saliphenylhalamide	2.88	NA	NA	[21e]
Myocardial infarction	182	THCPSi	Un, Radio labeling	Heart homing peptide	NA	NA	SPET/CT	NA	[112]
Diabetes	258	THCPSi	Un	Chitosan	Insulin	ca. 20	NA	Polymer conjugation	[13b]
Wound Healing	ca. 50000	THCPSi	NA	NA	Resveratrol, vancomycin	RSV ca. 15, VCM ca. 3	NA	Polymer encapsulation	[51d]
Wound Healing	161	THCPSi	NA	NA	siRNA	5	NA	Polymer encapsulation	[113]
NA	TOPSi 144, THCPSi 170	TOPSi, THCPSi	NA	NA	Indomethacin, peptide	ca. 15	NA	NA	[13c]
NA	ca. 200	THCPSi	NA	NA	furosemide	15–21	NA	Solid lipid encapsulation	[114]
NA	15000	THCPSi	NA	NA	piroxicam	19	NA	Solid lipid encapsulation	[115]

	Application	Size		Surface 1	Surface 2	Payload	Loading	Imaging	Method	Ref
Quasi-hemispherical/discoidal PSi particles	Cancer	19000	Freshly etched PSi	NA	NA	SPIONs, DOX	4.4	PL	Outer-stimuli (magnetic)	[116]
	Cancer	2600×700	TOPSi	APTES, PEG-PLGA-peptide nanoparticles	NA	Coumarin 6	4	FI	Polymer encapsulation	[117]
	Cancer	600×400	TOPSi	tert-butyl-2 [(allylamino)carbonyl]hydrazine-carboxylate	MLR2 antibody	Camptothecin	11	NA	NA	[16a]
	Cancer	1000×700	TOPSi	APTES	NA	SiRNA loaded in liposome	NA	NA	Liposome loading	[57]
	Cancer	3500	TOPSi	APTES	PMVEMA	SWNTs, QDs	NA	FI	Nanoparticle loading	[4k]
	Cancer	2600×700	TOPSi	APTES	NA	Docetaxel-encapsulated polymeric nanoparticles, siRNA loaded liposomes	114.90 ± 11.76 µg billion^{-1}	NA	Liposome loading, nanoparticle conjugation	[24b]
	Cancer	1000×400	TOPSi	APTES	NA	PTX loaded in PEG-PCL polymer micelles	58	NA	Nanoparticle (PEG-PCL) loading	[25c]
	Cancer	1000×400	TOPSi	APTES, PEI	NA	siRNA	70 µg billion^{-1}	NA	Polymer conjugation	[20]
	Cancer	1000×400	TOPSi	APTES, L-arginine	NA	siRNA	31.4 µg billion^{-1}	NA	Polymer conjugation	[24a]
	Anti-bacteria	93	Freshly etched PSi	NA	Trans-activating protein	Silver nanoparticles	NA	PL	Nanoparticle loading	[118]
	Anti-parasites	5800×500	THCPSi	APTES, rhodamine	NA	Cry5B protein	11	FI	NA	[45b]
	Ocular	15000×2000	TOPSi	NA	NA	Daunorubicin	10.8	NA	Drug conjugation	[119]
	Ocular	ca. 50000	TOPSi	NA	NA	Daunorubicin	5	NA	Nanoparticle (PLGA) encapsulation	[120]
	Ocular	20000×36000×14000	TOPSi	Succinic anhydride	NA	Dexamethasone	7	NA	Drug conjugation	[121]

Application	Size	Type	Surface modification	Targeting ligand	Cargo	Loading	Imaging	Strategy	Ref.
Ocular	52000×36000×21000	TOPSi	Methoxy(dimethyl)octylsilane	NA	Rapamycin, dexamethasone	ca. 8	NA	Drug conjugation, drug absorption	[122]
NA	21000	Freshly etched PSi	Nitrite induced oxidation	NA	Cobinamide, rhodamine B	11	NA	Pore self-sealing	[123]
Central neuron disease	180	TOPSi	Dicalcium orthosilicate	CPP (transportan)	siRNA	20–25	NA	Pore self-sealing	[124]
Central neuron disease	170	TOPSi	3-(ethoxydimethyl)-propylamine silane	Rabies virus glycoprotein	siRNA	7	NA	Nanoparticle (graphene) encapsulation	[125]
Tissue engineering	24500	TOPSi	APTES	NA	BSA	ca. 20 µg billion^{-1}	NA	Polymer encapsulation	[4h]
Tissue engineering	8200	TOPSi	APTES	NA	IL-4, IL-4 loaded PLGA particles	NA	NA	Nanoparticle (PLGA) encapsulation, nanoparticle (PLGA) loading	[126]
Tissue engineering	5000–9000	TOPSi	APTES	NA	Growth factor	ca. 0.1 µg billion^{-1}	NA	Polymer (PLGA) encapsulation	[127]
NA	1600	TOPSi	APTES, E-selectin thioaptamer ligand	E-selectin thioaptamer ligand	QDs, iron oxides, liposomes	NA	FI	Nanoparticle loading	[58a]
Cancer	50	Freshly etched PSi	NA	NA	DOX	80	FI	NA	[21b]
Anti-bacteria	10–40×1000–3000	Freshly etched PSi	NA	NA	Penicillin, streptomycin	NA	NA	NA	[73]
Vascularization	50×5000	Oxidized PSi	APTES	NA	siRNA	NA	NA	NA	[4i]
NA	330–600×400–6300	Oxidized PSi	NA	NA	siRNA	NA	NA	NA	[16b]

PSi needles

34

| NA | 50–600×5000–7000 | Oxidized PSi | NA | NA | BSA, siRNA, QDs | NA | FI | NA | [25e] |

Note: CPP, cell penetrating peptide; FITC, fluorescein isothiocyanate; IL-4, Interleukin 4; mAb528, anti-EGFR antibody; MLR, Anti-p75NTR mouse monoclonal antibody; PCL, poly(ε-caprolactone); PEG, polyethylene glycol; PLGA, poly(lactic-co-glycolic) acid; PMVEMA, poly(methyl vinyl ether-co-maleic acid); PNIPAm, N-isopropylacrylamide based polymers; QDs, quantum dots; SWNTs, single-walled carbon nanotubes; TOPSi, thermally oxidized PSi; Un, Undecylenic acid.

3.1.1. Surface modification of PSi for enhancing drug loading

The loading of molecules into PSi can be carried out via a number of methods, including physical adsorption, covalent bonding, non-covalent bond stacking and drug/particle entrapment.[44,128]

Physical adsorption is the most simple and convenient method relying on the spontaneous adsorption between the payload and the PSi. The surface nature of PSi plays the most critical role in this process. For example, the surface of TCPSi usually tends to be hydrophobic: results suggest that the application of hydrophobic PSi, such as TCPSi and THCPSi, can hugely increase the solubility and dispersity of hydrophobic drugs by altering the crystalline structure of the drug into amorphous state, and further increase their bioavailability.[129] Besides of the hydrophilic-lipophilic property, the surface charge of PSi is also another key factor. Wu *et al.*[45b] loaded anthelmintic pore-forming protein Cry5B in thermally oxidized PSi. The rationale behind the choice of the thermally oxidized PSi is that at pH 3, the protein is highly soluble and bears a net positive charge (isopotential point 5.1), whereas the charge on the oxidized PSi surface is negative. The loading efficiency, determined by measuring the difference in protein concentration (Bicinchoninic acid assay) in the loading solution before and after loading, was 110 ± 10 μg of Cry5B/mg of PSi, or 10% by mass. However, this facile and convenient method generally lacks reproducibility and the relative weak bond between the drug and the particle makes the loading unstable under physiological conditions.[44] In addition, to achieve maximum loading degree, this loading process usually takes place in a saturated drug solution, which may lead to a vast waste of the drugs.

Covalent bonding provides a convenient means to directly conjugate drug molecules on to the surface of PSi. Wang *et al.*[98] successfully conjugated MTX onto the surface of amine terminated PSi (APSTCPSi) with a conjugating/loading degree of ~0.4%, and the construction

of MTX-PSi composite achieved a MTX sustained release up to 96 h. However, it should be noted that the released compound was MTX attached with a fragment 3-aminopropylesilicic acid moiety, suggesting the decomposition of the particles. This method can effectively prolong the drug release time, however one concern is about the change in chemical structure of the released compound.

Instead of constructing drug conjugates, one can also attach a specific biomolecule to capture the drug via non-covalent bond such as chelation bonds or hydrogen bonds. For example, by modifying PSi with iron ions via a dopamine-inspired molecule, the newly developed PSi structure can capture one commonly used anti-cancer drug DOX by chelation bond.[100] The DOX loading capacity of the developed PSi composite was 24 ± 2 wt%, which is higher than the loading capacity of bare PSi (10 ± 1 wt%).[100] This relative delicate method can effectively achieve satisfying loading and release feature of the drug, being even able to respond to acidic condition (pH 6.5). However, these methods are rather related to specific drugs thus lack the pervasiveness of a more general method.

The pores' self-sealing induced drug loading is mainly caused by an alteration of the pore structure, which can be achieved with different procedures. One approach is by oxidation. Upon oxidation of the freshly etched PSi, a volume expansion occurs to accommodate the extra oxygen atoms and therefore the pore structure tends to shrink and collapse, leading to the entrapment of the previously loaded cargo.[123] For example, two model drugs, cobinamide and rhodamine B were loaded into PSi film by this method.[123] Sodium nitrite was added into the drug solution to ensure the oxidation and shrinking of the pore openings. After oxidation, cobinamide and rhodamine B were successfully trapped in the porous matrix. For drug entrapment by oxidation, the drug loading efficiency was increased up to 10-fold and the release rate prolonged by 20-fold. However, one concern is that the oxidation process usually

tends to have a relatively harsh condition and therefore this method is normally applied for constructing multifunctional nanohybrid instead of loading therapeutic molecules. For example, by this method, Dorvee *et al.*[130] synthesized Fe_3O_4@PSi nanohybrid in which iron oxide nanoparticles were effectively encapsulated inside the pores. A multilayered PSi dielectric mirror (rugate filter) was first etched into a single-crystal silicon substrate. A second rugate filter with a different periodicity was etched into the substrate, immediately beneath the first. The bifunctional, freestanding film was placed in water and fractured into micro-sized particles by ultrasonication. The particles were then exposed to a solution of superparamagnetic Fe_3O_4 nanoparticles. The high pH of the magnetite suspension spontaneously induced oxidation of the second PSi layer, presumably trapping the magnetite nanoparticles in an oxide matrix. Another pore-sealing method relies on the reaction between the outer solution and the slowly degraded silicic acid from the PSi, a relatively mild process that can be applied for the entrapment of bio-macromolecules such as RNA.[124] In solutions containing high concentrations of calcium (II) ions, Ca_2SiO_4 was formed where the source of silicate in the shell derived from local dissolution of the PSi matrix. This shell formation occurred primarily at the PSi surface and was self-limiting. After mixing siRNA alone with calcium ion solution, the oligocucleotide became trapped in the porous nanostructure during shell formation. However, in some cases, together with the increased drug loading efficiency, this loading procedure may also lead to some problems such as lack of drug release. For example, previous studies found that one peptide, PYY3-36, can be trapped into the pores of undecylenic-acid-modified thermally hydrocarbonized PSi (UnTHCPSi). The release time of the peptide was prolonged, however, its *in vivo* bioavailability decreased due to limited release.[131] Similar phenomenon was observed when PSi was used as drug carrier for anti-parastic application. The anthelmintic protein Cry5B was incorporated into the PSi particles,

in vivo experiments with hookworm-infected hamsters showed no significant reduction in worm burden with the Cry5B-loaded particles, which was attributed to slow release of the protein from the particles.[45b]

Despite the various methods proposed so far, a more versatile, robust method with high loading degree and controlled release behavior is urgently needed. Among all the methods, increasing the loading degree by manipulating the crystal structure of the loaded drug is emerging as a new paradigm and shows promising results.[132] By alternating the solvent composition, pH value, solvent evaporation or applying microfluidic assisted drug crystallization, one can effectively achieve ultrahigh drug loading.[133] Moreover, in the case of PSi, former studies confirmed that after the loading of drugs, such as indomethacin (IMC) and griseofulvin (GSV), within the pores of PSi, they existed in an amorphous state, which also partly contributes to the improved solubility of the drugs.[129] One can assume that for the drug loaded within the pores of PSi, upon *in situ* crystallization, the irregular morphologies of the pores could be locked due to the newly formed drug crystals, thereby the condensed drug crystalline structures can not only increase the loading degree but also effectively reduce the premature release, yet few studies have been focused on this.

3.1.2. Surface modification of PSi for controlled drug release

Due to the easily accessed pores of PSi, one main challenge for PSi is to achieve a controlled release behavior. Mainly two approaches have been explored to design and equip PSi with controlled release capabilities (**Figure 7**). One solution is the "gating" approach. This involves attaching organic or inorganic materials at the pore openings thus preventing release of the cargo stored in the pores. For example, Kang *et al.*[124] constructed a self-sealing PSi by taking advantage of the dissolved silicate to form a calcium silicate outer layer to block the

pores. For bare PSi, most of the drug (>70%) will be released within 1 h whereas the self-sealing PSi can detain the drug release time up to 5 h. Moreover, the conjugation of polymers, such as β-cyclodextrin on the surface of PSi can effectively control the drug release process.[101] Bare PSi released ~60% and ~80% of the loaded drug (SFN) after 4 h at pH 7.4 and 5.5, respectively. In contrast, upon the surface modification with heptakis(6-amino-6-deoxy)-β-cyclodextrin (HABCD) , the release of SFN from the PSi−HABCD after 4 h was only ~40% at both pH 7.4 and 5.5. A pH-sensitive release behavior was observed by applying a stimuli-responsive polymer, polyethylene glycol-block-poly(L-histidine).[14a] Drug release from this polymer coated PSi in plasma at pH 7.4 was low (<5%), whereas in PBS−fetal bovine serum (FBS) at pH 6.8 and 5.5 a burst release was observed. This pH-dependent behavior of the nanocomposites could be explained by the protonation of the pH-responsive copolymer when exposed to mild acidic media, increasing the repulsive forces among the chains of the polymer to render a less tightly packed structure, and eventually leading to the total disruption of the nanocomposite and release of the drug loaded PSi nanoparticles. Similarly, pH-responsive nanovalve system consisting of an aromatic amino group and a cyclodextrin cap was chosen to be adapted to the PSi nanoparticles. This nanovalve was shown to be tightly closed at the physiological pH of 7.4 and to open autonomously under the acidic conditions (pH <6).[134] The co-encapsulation of gold nanorod and PSi nanoparticles into giant liposome can achieve a photo-thermal release of loaded drug.[135] Mi *et al.*[117] used metalloproteinase-2 (MMP-2) substrates to coat the pores of PSi, further achieving an enzyme sensitive drug release behavior. MMP2 peptide substrate was conjugated to PLGA-PEG nanoparticles, which were further conjugated to the surface of discoidal PSi microparticles. A hydrophobic model drug, coumarin 6, was encapsulated in the polymeric nanoparticles. In the presence of MMP2 enzymes, the polymeric nanoparticles disassociated from the PSi

microparticles. In the absence of MMP2, 40% of coumarin 6 were released from the PSi microparticles after 6 h, as compared to 80% in the presence of MMP2. Outer stimuli such as electromagnetic heating can also be applied to trigger the drug release when PSi is modified with temperature sensitive polymer (N-isopropylacrylamide based polymers (PNIPAm)) at the pores of PSi.[27] However, the application of nanovalves, which is commonly employed in the capping of mesoporous materials such as mesoporous silica, is less investigated in the controlled release from PSi, maybe due to the irregular morphology and the relatively large size (~ 10 nm) of the pores of PSi not in favor of applying small sized uniform nano-gate or even molecular-gate.[100] Moreover, the relative lower functional groups coverage (~30%) on the surface of the PSi sets another obstacle for this method.[85,131] The other approach to equip PSi with controlled release features is to attach drugs to the surface of PSi via stimuli-responsive linkages. For example, the introduction of a polydopamine or dopamine analogues will endow the PSi with the ability to form a ligand-metal ion-drug complex, further achieving a pH-responsive release. One ligand (3-aminopropoxy-linked quercetin) inspired by the structure of dopamine was applied for PSi modification. At pH 7.4, only 14.8 ± 0.9% of the loaded drug (DOX) was released within 4 h, and no clear extra drug was released in the following 20 h. However, the released drug amount was increased at more acidic condition, where 77.3 ± 1.6% of the loaded drug was released at pH 5 within 24 h.[100] Other examples include the formation of a hydrogen bond between the conjugated ligand and the loaded cargo: the pH-induced protonation or de-protonation will disturb the stability of the PSi-drug complex, leading to the release of the drug.[104]

However, the concept "controlled release" is not only about the sustained release or stimuli-responsive release. In clinical application, it is important that different drugs are present in the human body at distinct time points. Typically, this is achieved by a sequential administration

41

of different therapeutic agents. A much easier alternative would be to develop a drug delivery system containing a whole set of medically active compounds which are liberated in an orchestrated and controlled manner. Yet, such a periodically, sequential release of drugs from PSi has been less investigated.
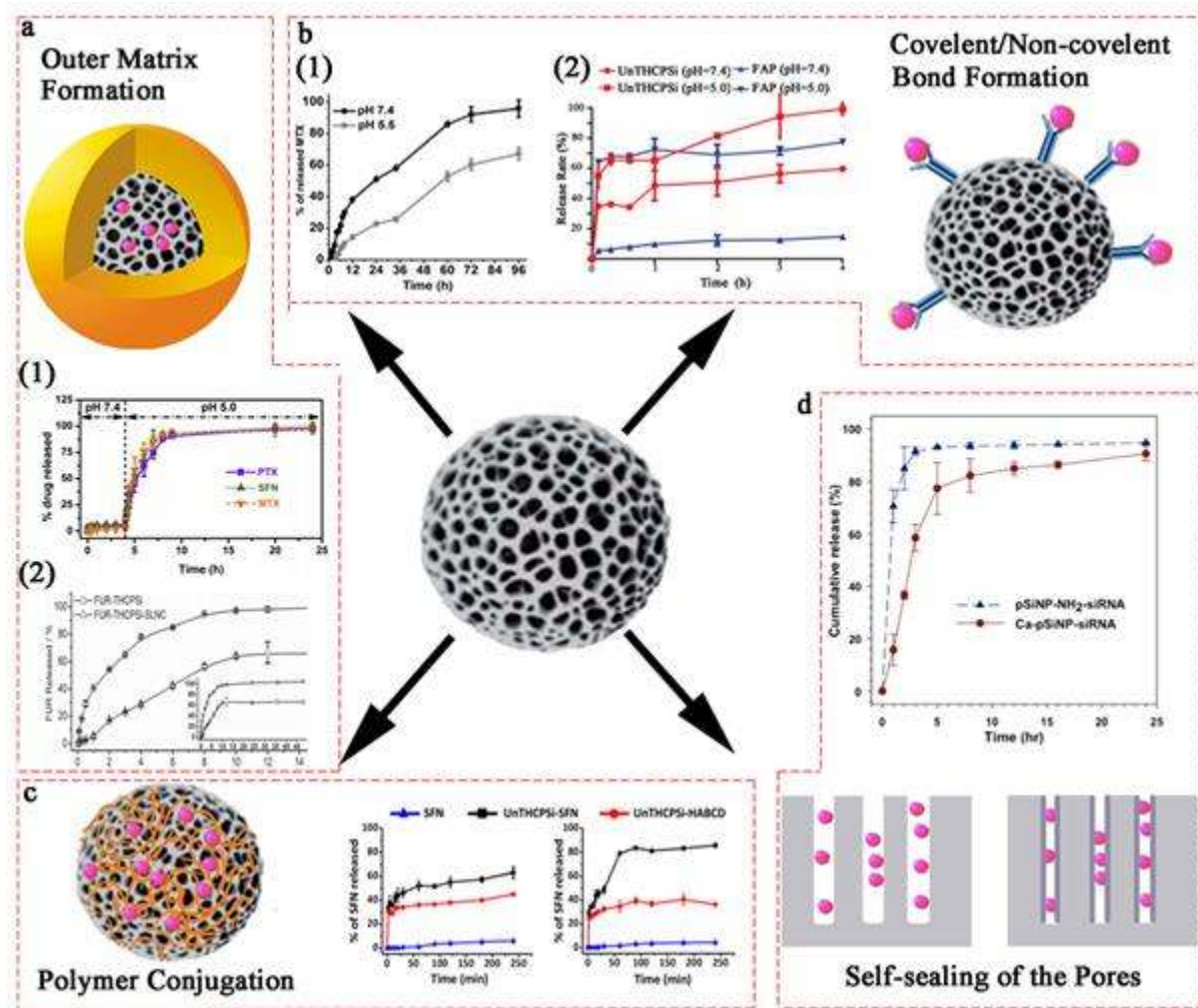

Figure 7. Design and operation of PSi with controlled release behavior. **a1)** pH sensitive polymer or **a2)** Lipid encapsulation of PSi can achieve specific drug release behavior; **b1)** Covalent bonding or **b2)** Non-covalent bonding can sustain the drug release in specific manner; **(c)** Polymer conjugation can also retain the drug release rate; **(d)** The pores' self-sealing can be applied into controlled release. Figures are reproduced with permissions: **a1)** from ref. [14b], Copyright 2015, Elsevier; **a2)** from ref. [94], Copyright 2013, WILEY-VCH; **b1)**

from ref. [98], Copyright 2015, Elsevier; **b2)** from ref. [100], Copyright 2017, WILEY-VCH; **(c)** from ref. [101], Copyright 2015, American Chemical Society; and **(d)** from ref. [124], Copyright 2010, WILEY-VCH.

3.2. Surface modification to enhance targeting ability of PSi

Surface modification of PSi with special ligand will endow the carrier with enhanced adhesion to specific cells, therefore increasing the particle and the drug accumulation at lesion sites.[112,136] Different kinds of targeting ligands are applied for multiple diseases. For example, chitosan modified PSi with mucoadhesive property was applied for the oral administration of insulin.[28,137] Atrial natriuretic peptide (ANP), a heart-homing peptide, was also conjugated to PSi for chronic heart failure reverse. *In vivo* biodistribution of PSi modified with ANP was monitored in Wistar rats. Animals received subcutaneous injection of isoprenaline (5 mg kg^{-1}) 24 h before intravenous administration of radiolabeled peptide modified PSi nanoparticles for establishing the infarcted heart model. Results showed up to 3-fold PSi accumulation within the heart after the peptide modification (**Figure 8a**).[112] Rabies virus glycoprotein (RVG) conjugation of PSi loaded with siRNA was investigated as potent brain targeting drug carrier, and the monitor of the emission from a Dy677 tag attached to the siRNA payload showed that the RVG–PSi construct delivered a substantial quantity of siRNA to the injured site and can reach up to 3-fold more accumulation in damaged brain tissue comparing to healthy brain (**Figure 8b**).[125] A carbonic anhydrase IX (CA IX, 3-(cyclooctylamino)-2,5,6-trifluoro-4-((2-hydroxyethyl)sulfonyl)benzenesulfonamide) targeting ligand-functionalized PSi showed high affinity towards cancer cells under hypoxia condition, which presented potent application into cancer targeting.[104] PSi surface biofunctionalization was developed for tumor associated endothelial cells and in macrophages targeting. Due to the increased expression of Ly6C,

mouse homolog of CD59, in tumor associated endothelial cells and macrophages within the stroma, PSi surface modified with Ly6C antibody can accumulated in tumor associated endothelial cells within 15 min after intravenous injection. At 4 h after administration, 9.8 ± 2.3% of injected dose/g tumor of the Ly6C targeting nanocarriers accumulated in the pancreatic tumors (L3.6pl tumor bearing mice) as compared to 0.5 ± 1.8% with non-targeted nanocarriers (**Figure 8c**).[19b] Various of other antibodies were also tested for tumor targeting.[26b,105] Besides targeting ligand conjugation, strategies employing outer stimuli are also applied for the active targeting.[138] PSi grafted with a temperature responsive polymer (N-isopropylacrylamide), whose critical temperature was tailored to be around 40 °C, leaded to spatiotemporal triggered drug release through infrared and radiofrequency electromagnetic heating. *In vivo* experiments were carried out with lung carcinoma (3LL) tumors inoculated at the left hind paw of male mice of the CBA line. After tumor site specific infrared irradiation, the therapeutic effect, *i.e.*, radiofrequency triggered the release of the cytostatic drug from PSi, could significantly suppress the growth of a carcinoma tumor at local site.[27]

Besides of the conventional targeting methods by connecting targeting moieties on the surface of the nanoparticles, its feasibility and efficiency are sometimes confined by the unintended high uptake by normal tissues/cells, degradation or structure transformation caused by the interaction between ligand and the enzyme or protein in the blood.[139] Furthermore, when they are applied *in vivo*, we usually have to face the variable physiological changes or different requirements, sometimes this may even cause antilogy or paradox. For example, to prolong the circulation time by evading from the MPS system, the most common way is modifying the particle with polyethylene glycol (PEG).[140] However, PEG can hugely hinder the cellular uptake of the particles, therefore may inhibit the release of the drug within the cells.[141] Thereby, we anticipate the well-designed drug delivery system to present different

properties at different stages. To fulfill this idea, nowadays there is a strategy called hierarchical targeting.[142] The designed PSi has the ability to change their properties in response to different environments. Common methods include the changeable size or zeta potential, in-activation and re-activation of the targeting ligand, PEG detachment as well as the morphology switch.[4j,4k,47a] Previously, researchers developed several discoidal PSi microparticles based structure, where several other reagents, such as QDs and carbon nanotubes, are embedded within the pores, further achieving a multi-stage delivery effect.[4j,4k,20,143] Zhang *et al*.[103] fabricated a receptor-mediated surface charge inversion nanoparticle consisted by PSi nanoparticle core and sequentially modified with PEI, MTX, and DNA aptamer AS1411 for enhancing the cell uptake of nucleolin-positive cells. The efficient interaction of AS1411 and the relevant receptor nucleolin caused the disintegration of the negative-charged AS1411 surface. The subsequent surface charge inversion and exposure of the active targeting ligand, MTX, enhanced the cell uptake of the nanoparticles. The newly synthesized nanocomposites with a hydrodynamic diameter around 242 nm were efficiently internalized by nucleolin-positive MDA-MB-231 breast cancer cells, with an efficiency around 5.8 times higher than that of nucleolin-negative cells (NIH 3T3 fibroblasts.

Another convenient way to achieve this hierarchy targeting is layer-by-layer coating. PSi conjugated with targeting ligand can be encapsulated within a protection matrix, when reaching the lesion sites the matrix will degrade and further expose the targeting moiety.[14b] To achieve this aim, a better and a more robust encapsulation method should be further developed, which we will discuss in detail in the following sections.
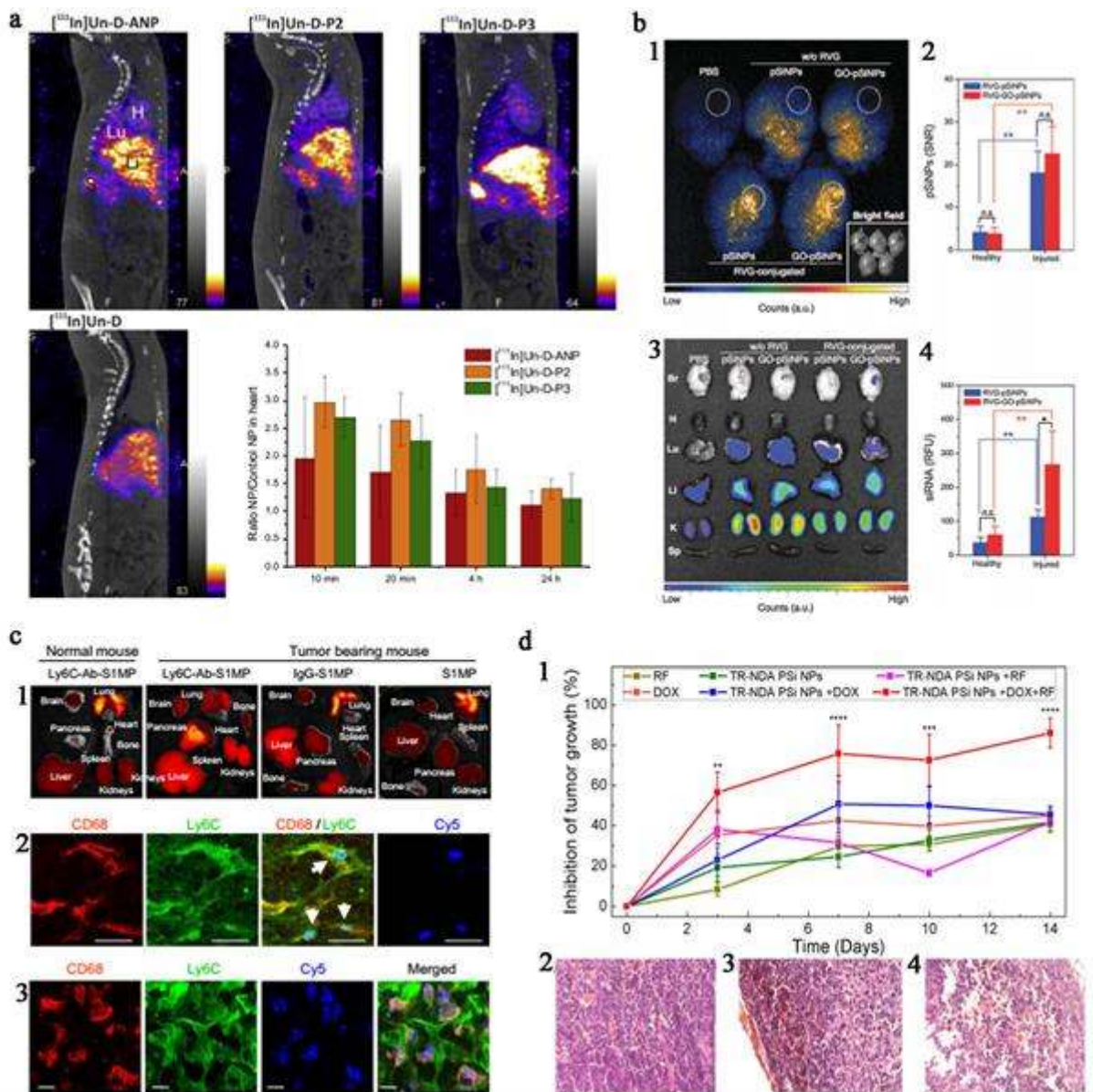
Figure 8. Surface modification of PSi to increase its targeting ability towards corresponding disease. **(a)** Increased heart targeting ability of ANP modified PSi. Representative sagittal SPECT/CT images showing the biodistribution of intravenously administered [111In]NPs at 10 min time point. H denotes for heart, Lu for lung, Li for liver, and S for Spleen. ANP-modified PSi NP-to-control ratio in heart for different peptides at 10 min, 20 min, 4 h, and 24 h time points. **(b)** Luminescence images testing specific targeting of RVG modified PSi to injured mouse brain. **b1)** Time-gated luminescence image of injured mouse brains (lex: 365 nm).

Dashed white circles indicate region of penetrating brain injury. Targeted (''RVG-conjugated'') and nontargeted (''no RVG'') nanoparticles are compared. Inset: Bright field image (in gray scale) under ambient light.Lipid encapsulation of PSi can achieve specific drug release behavior; **b2)** Signal-to-noise ratio (SNR) calculated for luminescent PSi accumulated at healthy (left hemisphere) or injured (right hemisphere) region of the brain tissues. **b3)** Fluorescence image of Dy677-labeled siRNA accumulated in mouse organs obtained from IVIS 200 imaging system (lex: 670 nm, lem: 700 nm). **b4)** Relative fluorescence intensity of Dy677-labeled siRNA at healthy (left hemisphere) or injured (right hemisphere) region of the brain tissues. (**c**) Biodistribution and immunofluorescent analysis of the Ly6c Ab modified PSi intravenously injected into the L3.6pl human tumor bearing or normal mice. **c1)** *Ex vivo* fluorescent imaging (IVIS) of the organs of normal mouse and the tumor bearing mice injected with the nanocarriers conjugated with Ly6C Ab (Ly6C-Ab-S1MP), control IgG (IgG-S1MP) or unconjugated nanocarriers (S1MP). **c2 and c3)** Immunofluorescent analysis of pancreatic tumors in the mouse injected with the nanocarriers conjugated with Ly6C Ab (labeled with Dylight 649 and detected through Cy5 channel). The nanocarriers attached to endothelial cells (CD31) in capillaries which also expressed Ly6C (emitted yellow fluorescence) 15 min after intravenous injection (indicated by white arrows). The nanocarriers were further engulfed by CD68 and Ly6C positive tumor associated macrophages as identified 4 h after the injection. (**d**) *In vivo* assessment of efficiency of RF radiation-based spatiotemporal triggered treatment of the tumor with PSi. **d1)** Inhibition of the tumor growth after injection of 0.05 ml solution of DOX at a concentration of 2 mg/kg (blue), 5 min of the RF irradiation of power 40 W (cyan), 0.05 ml suspension of modified PSi nanoparticles with DOX concentration of 2 mg/kg (magenta) and combined actions of the nanoparticles, DOX and RF irradiation (black). **d2)** The histological image of the tumor before the treatment, the

47

tumor consist of alive cancer cells. **d3)** The histological image after 1 day of the injection of TR-NDA PSi nanoparticles + DOX irradiated with RF, nanoparticles and DOX are penetrating the tumor at the place of the injection. **d4)** The histological image after 3 days of injection shows necrotic parts of the tumor. Figures are reproduced with permissions: **(a)** from ref. [112], Copyright 2016, Elsevier; **(b)** from ref. [125], Copyright 2016, The Royal Society of Chemistry; **(c)** from ref. [19b], Copyright 2013, Elsevier; and **(d)** from ref. [27], Copyright 2016, Elsevier.

3.3. Surface modification to increase physiological stability and biocompatibility of PSi

As mentioned previously, freshly etched PSi with a hydride surface obtains the high reductive ability and can react with multiple biological molecules. Another well-known property of hydride terminated PSi is its photoluminescence, and investigations into the causes and decay of PSi photoluminescence have led to the discovery that this surface is capable of generating singlet oxygen ($^1O_2$) molecules under certain conditions which will further cause cellular toxicity.[78a] Low *et al.*[78b] incubated silicon wafer, freshly etched PSi and thermal oxidized PSi with human lens epithelial cells (SRA 01/04) and found out a dramatic decrease of cell viability when incubating with freshly etched PSi particles, which is caused by the extra ROS generated from the reaction between silicon hydride and the substance within the cell culture medium. However, the observed toxic effect can be completely mitigated by protective surface treatments of PSi microparticles including thermal oxidation, as the surface stabilization may be able to eliminate the remaining excitons trapped in the crystal which are able to transfer electrons to oxygen molecules adsorbed on the surface, converting them into singlet oxygen or other ROS species, therefore the surface modification can vastly increase the biocompatibility of PSi. While several methods applied this feature to achieve

photodynamic anti-cancer therapy, for drug delivery system, a more stable PSi is also needed.[144] However, some of the surface modification, such as thermal carbonization, will end up with the production of hydrophobic PSi, even though this will facilitate the hydrophobic drug loading, it also restrict its dispersity within biological medium.[75] Methods such as secondary modification by PEGylation or dextranylation were proposed to increase its biological stability and MPS stealth ability (**Figure 9a**). For example, studies suggested that TOPSi nanoparticles agglomerated extensively in PBS, and the 0.5 kDa PEGylated PSi nanoparticles also agglomerated, however to a lesser extent than bare PSi due to the presence of PEG, stabilizing the size at ~1.4 μm. In comparison, the 2 kDa PEG-TOPSi nanoparticles dispersion was stable for up to 3 days;[145] dextranylation of THCPSi can also reduce the plasma protein adsorption. Wang *et al.*[97] investigated plasma proteins' association onto the PSi modified with dextran with two different molecular weight (6 kDa and 40 kDa), and the amount of bonded protein was determined by analyzing the opsonized proteins with SDS-PAGE gel electrophoresis and further verified by mass spectrometry. THCPSi-Dex40k showed more negligible protein adsorption than the other modification moieties or the unmodified nanoparticles. Conjugating amphiphilic polymer (PEI-PMVEMA) can also reduce the aggregation of PSi without interfering the hydrophobic drug loading ability. Stability assessment in aqueous medium showed that the particle size (hydrodynamic diameter) and PDI of the bare PSi (THCPSi) increased to over 1 μm and 0.4, respectively, in less than 90 min as a result of aggregation, while polymer-functionalized particles showed no substantial change in both particle size and PDI. Further stability assessment of the nanoparticles for 2 days revealed no change in the size of bare and polymer-conjugated nanoparticles from 2 h to 48 h.[146]

In general, the circulation time of a micro/nano-particle is determined by multiple factors, including size, shape, surface stiffness and protein corona.[18,147] Concerning the influence of the size on the circulation time, a systematic study of the circulation time of unmodified PSi nanoparticles in mice was presented by Park et al.[4]: small PSi nanoparticles (15 nm) were rapidly excreted by the kidneys, with a half-life of 12 min. Particles presenting a size of around 270 nm were taken up by the reticuloendothelial system (RES) in less than 5 min. Finally, particles characterized by an intermediated size (around 150 nm) exhibited a longer circulation time, 27 min, as reported also by other studies: the surface modification with BSA increased the circulation time to 264 min.[148] In the case of THCPSi, the amount of nanoparticles retrieved in the circulation decreased rapidly already after 15 min; the encapsulation of the particles in solid lipid nanoparticles did not enhance the circulation time.[149] Wang et al.[150] investigated the biodistribution of iRGD-modified UnTHCPSi nanoparticles, labelled with ^{111}In; after 65 mins from the injection, only 1.5% of the injected dose was still circulating, while after 27 h this value decreased to less than 0.3%.

As for microparticles, the circulation time and the organ accumulation are size and shape dependent.[151] After 4 h from the injection, the particles were mainly found in liver and spleen, with minimal distribution to lung, heart, and kidneys;[19a] the particles distributed in the whole body during the first min, then accumulated within the RES, and ended up in the liver.[152]

Besides biocompatibility, physiological stability and dispersity, the biodegradability of PSi is another key factor to evaluate its further clinical application. The inherent factors that influencing PSi degradation are also its overall size, porosity, pore size and surface functionalization. For example, the increase of porosity increases the diffusion rate of species in and out the pores, and thus, accelerates the dissolution rate of the silicon network,[54c] the

decreased size of PSi will also accelerate the degradation rate due to the augmented surface/volume ratio.[24a] Freshly etched PSi will undergo fast dissolution, and surface stabilization, such as oxidation and carbonization, will generate a protection layer which can detain the dissolution process of PSi.[153] Alhmoud *et al.*[16a] conducted hydrosilylation reactions with undecylenic acid (Un) and tert-butyl-2 [(allylamino)carbonyl]hydrazine-carboxylate (Sc), respectively, on freshly prepared silicon hydride-terminated particles, and these surface modifications significantly reduced the degradation rate of PSi, as already discussed in Section 2.2.1. In the similar mechanism, secondary surface conjugation or encapsulation such as PEGylation will protect PSi from outer medium, thus tailoring the PSi degradation behavior. The degradation kinetics of PSi modified by PEG with different molecular weight (PEG 245, PEG 333, PEG 509, PEG 686, PEG 862, PEG 1214, PEG 3400, and PEG 5000) were investigated in PBS buffer (pH 7.2) and FBS medium through inductively coupled plasma atomic emission spectroscopy (ICP-AES) method, and the results revealed that the degradation rate decreased with the increased length of the attached PEG chain and the most dramatic effect was observed for PEG 3400 and PEG 5000, which inhibited the degradation of the systems over more than 3 days and in the case of PEG 5000 almost no degradation was seen within the first 48 h (**Figure 9b**).[54d] The rationale for the altered degradation kinetics is the surface modification can change the interaction between the particle and outer medium as discussed previously, as factors such as pH, temperature, salt, amino acid, protein and redox environment of the outer medium can also hugely affect the degradation of PSi,[154] Tzur-Balter *et al.*[155] tested the effect of pH, human serum, ROS and combination thereof on the *in vitro* erosion process of PSi and the results revealed that among which, ROS is the most critical parameter to accelerate the degradation process. The degradation of PSi at different pH (PBS buffer with pH 7.4 and pH 6.5 respectively) did not

dramatically influence the degradation of PSi as the ML_{50} (time needed for 50% of the PSi mass loss) at both pH values were around 7 h, the addition of extra serum decreased the ML_{50} into 6 h, whereas the addition of extra 2 mM of 3-morpholinosydnonimine N-ethylcarbamide (SIN-1), which can be used to generate physiologically relevant levels of peroxynitrite, a highly reactive oxygen species involved in human carcinogenesis, can vastly decrease the ML50 to 3 h. Many studies have shown that the degradation of PSi in physiological media involves the oxidation of the Si scaffold into Si-dioxide, followed by the hydrolysis of the Si–O bonds to release soluble orthosilicic acid species.[8,156] Recent studies also suggested after *in vivo* administration, PSi will be eroded directly through the degradation of the crystalline Si scaffold.[155] More importantly, they found out that PSi undergoes enhanced degradation in diseased environment compared with healthy state, owing to the upregulation of ROS in the lesion vicinity that oxidize the silicon scaffold and catalyze its degradation. As previously shown (**Figure 6**), after the thermal oxidation or carbonization, the surface of PSi is composed by SiC or O_xSiH_y, which is fairly stable, and the ROS accelerated degradation partly suggested that the degradation is related to the decomposition of the surface silicon layer and back-bond oxidation of the Si;[155] however, the degradation and erosion rate among PSi with different surface stabilization method and different surface property is less investigated. Moreover, recent papers suggested that some metal silicate can slowly release orthosilicic acid, followed by the *in situ* formation of SiO_2 compact and inducing the capillary occlusion and tumor starvation, however whether PSi will undertake the same process is also lack of investigation.[157]

Meanwhile, PSi nanoparticles can be effectively uptaken by different kinds of parenchymal cells and MPS systems. The interactions between micro- and nano-systems and the cells or the organisms are mediated by the presence of a hard and a soft protein corona forming on the

surface of particles.[158] In the case of PSi, the presence of the corona influences the uptake of particles by vascular endothelial cells: negatively charged particles coated with the protein corona are taken up in lower amount compared to the same particles in protein-free medium; as for positively charged particles, the incubation with plasma and the formation of the corona turns the surface charge to negative, however, there is no effect on their uptake.[152] Interestingly, the incubation of the same particles together with immune cells leads to a selectively uptake of the negatively charged particles, due to the adsorption of immunoglobulins on the protein corona, leading to their uptake by the gamma immunoglobulin receptors.[159] The proteomic analysis of the protein corona showed that cationic PSi microparticles preferentially adsorb alpha fibrinogen, IgG light chain variable regions and complement component 1, while negatively charged particles preferentially adsorb apolipoproteins A and E; this may partially explain the differences in the biodistribution of cationic and anionic particles, with higher accumulation of negatively charged particles in the liver.[160]

When the surface of PSi particles is modified with other elements (dextran, targeting peptides, hydrophobins), there is a change in the profile of the protein corona. In particular, the protein corona of THCPSi-alkyne particles includes proteins adsorbed along the whole range of molecular weights, except for the complement C3fraction. After surface modification with targeting moieties (iRGD), the protein corona was composed also by the complement C3 fraction. The adsorption of hydrophobin on the surface of THCPSi particles resulted in a change in the protein corona, with the adsorption of both complement C3 fraction and apolipoproteins.[161] On the contrary, after modification of the particles with dextran chains, there was a reduction in the adsorption of proteins with molecular weight higher than 70 kDa, in a fashion dependent on the molecular weight of the dextran.[97] Thus it has the potent to

53

interact with different intracellular organell and different intracellular proteins. Recent studies demonstrated the effect of PSi with different surface properties on human P450 metabolism (CYP) (**Figure 9c**).[162] Three different surface chemistries, including TCPSi, APSTCPSi and alkyne-THCPSi were compared for their effects on the enzyme kinetics of the major CYP isoforms (CYP1A2, CYP2A6, CYP2D6, and CYP3A4) in human liver microsomes *in vitro*, and the enzyme kinetic parameters, K_m and V_{max}, and the intrinsic clearance (CL_{int}) were determined to evaluate their corresponding effects. Results showed statistically significant alterations of most isoenzyme activities in human liver microsomes in the presence of nanoparticles, which may be due to the competitive, noncompetitive and uncompetitive inhibition caused by the particle and other interactions such as nonspecific adsorption of lipids or electrostatic interactions with salts. Among which, and CYP2D6 inhibition was shown to be the most vulnerable enzyme and exhibited a dose-dependent tendency in case of thermally carbonized PSi and thermally hydrocarbonized PSi nanoparticles and attenuated at the concentrations as low as 1 µg ml^{-1}. This is the first study confirmed that even relatively large PSi (in the range of 160–180 nm) may inhibit the CYP enzyme activities *in vitro* and also suggested the potent interaction between intracellular PSi and critical protein within the cells. Former experiments suggested that extra dietary silicon can ameliorate the liver oxidation stress by enhancing the Nrf2 (nuclear factor erythroid 2) pathway.[163] Also there are paper suggesting that orthosilicic acid, the main degradation product of PSi, can stimulates osteoblast differentiation by antagonizing NF-κB activation,[164] considering the inherent nature of PSi that it can be vastly uptaken by various kinds of cells, this triggered the thought to further investigate the potent effect of PSi and its corresponding degradation product on cellular signal pathway. This may provide further fundamental information for further application of PSi into biomedical areas. However, the corresponding studies are less

investigated. Meanwhile, its interaction with immune cells also induces the investigation of

immunoresponsive effect of PSi which we will discussed in detail in the following sections.
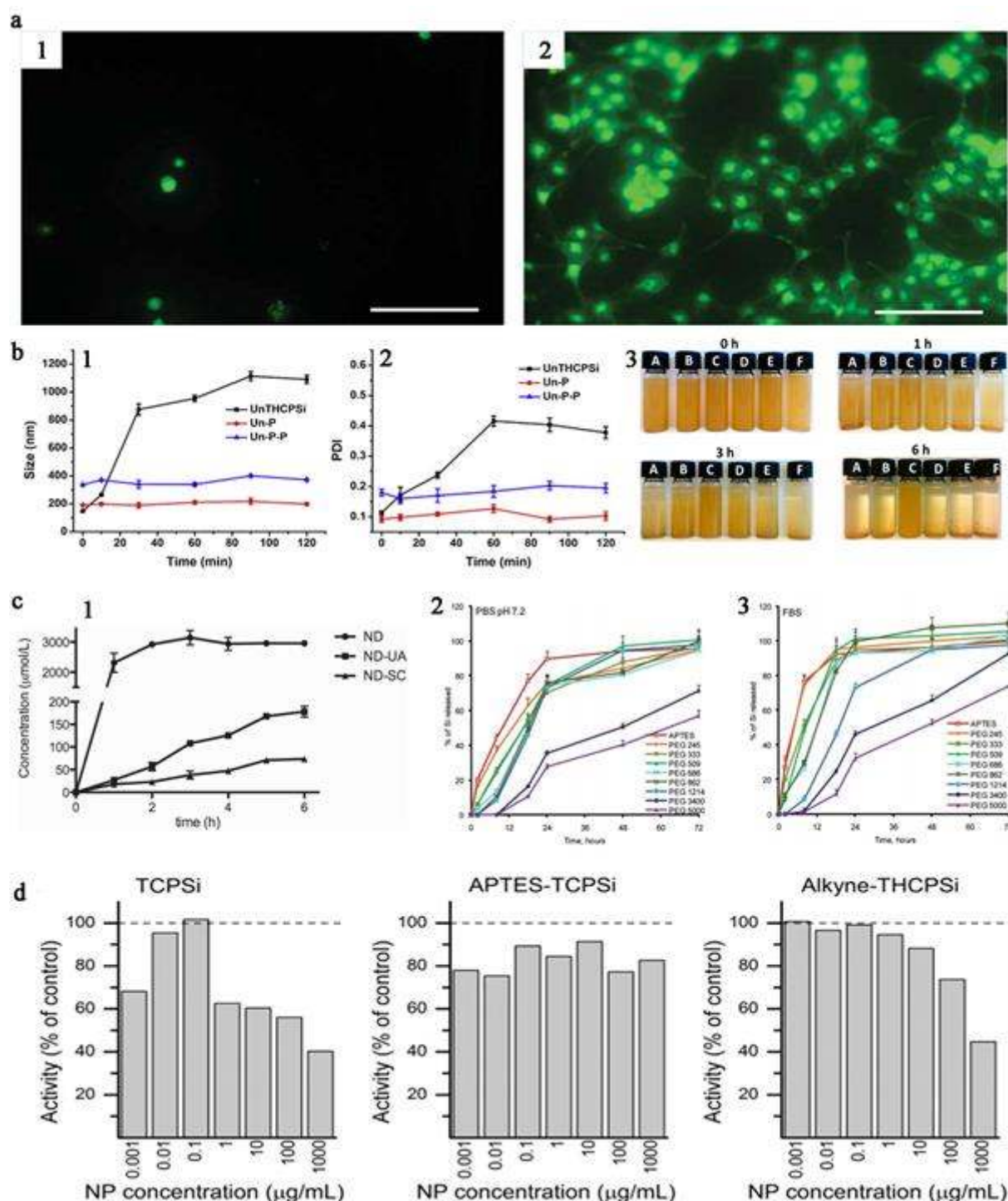

Figure 9. The effect of surface modification on biocompatibility, physiological stability,

degradability and critical protein's activity. **(a)** Human lens epithelial cells on **a1)** a non-

treated PSi membrane and on **a2)** a thermally-oxidized PSi membrane after a 24 h incubation, suggesting the viability loss caused by freshly etched PSi. Cells were stained with DiOC5. **(b)** Increased physiological stability by surface modification. The **b1)** size and **b2)** PDI change of bare PSi or PSi modified with a zwitterionic bi-polymer PEI-PMVEMA after dispersing in aqueous medium for 2 h, demonstrating high stability of the polymer-conjugated nanoparticles over time. **b3)** Photographs of the dispersion stability of the nanoparticles, from A to F: THCPSi-alkyne, THCPSi-Dex6k, THCPSi-Dex40k, THCPSi-PGA, THCPSi-RGDS, and THCPSi-iRGD at time points 0, 1, 3, and 6 h. For each surface functionalization, 100 μg mL^{-1} of the nanoparticles were dispersed in HBSS−HEPES buffer (pH 7.4). **c1)** Degradation of PSi as determined by silicic acid release over 6 h in Tris buffer (pH = 7.2) at room temperature. ND: Non-treated PSi; ND-UA: undecylenic acid modified PSi; ND-SC: tert-butyl-2 [(allylamino)carbonyl]hydrazine-carboxylate modified PSi and degradation kinetics of PEGylated PSi within **c2)** PBS pH 7.2 and **c3)** FBS. **d)** Inhibition of CYP2D6 by TCPSi, APSTCPSi, and Alkyne-THCPSi nanoparticles relative to the control with different nanoparticle concentrations. The control activity (without nanoparticles) is adjusted to 100% (dash line). Figures are reproduced with permissions: **(a)** from ref. [78b], Copyright 2010, WILEY-VCH; **(b1 and b2)** from ref. [146], Copyright 2014, Elsevier; **(b3)** from ref. [97], Copyright 2015, American Chemical Society; **(c1)** from ref. [16a], Copyright 2015, WILEY-VCH; **(c2 and c3)** from ref. [54d], Copyright 2010, WILEY-VCH; and **(d)** from ref. [162], Copyright 2017, Elsevier.

The surface chemistry of PSi influences its colloidal stability. In detail, the colloidal stability of bare PSi, presenting a hydrophobic surface (*e.g.*, THCPSi, UnTHCPSI), is limited both in saline solutions (PBS and HBSS−HEPES) and in human plasma. Particularly, the stability in HBSS−HEPES is time and surface modification-dependent; the more hydrophobic particles

are characterized by lower stability, starting to aggregate and precipitate after 1 h.[97] The surface modification with tumor targeting peptides improves the stability of THCPSi nanoparticles in plasma.[136] Moreover, the modification of the surface with polymers (like PEI), cyclodextrins, or proteins (hydrophobin) greatly enhances the stability both in saline solutions and in human plasma.[101,146,161]

3.4. Surface modification of PSi to facilitate bioimaging

At the intersection between treatment and bioimaging, interest has grown in combining both paradigms into clinically effective formulations, this concept is coined as theranostics.[165] Applying PSi as an imaging agent also draws a lot of attentions recently. Photoluminescence of PSi is surface chemistry related. Completely reversible shifts in the photoluminescence spectra between green luminescence and red luminescence were obtained repetitively.[166] The mechanism for the photoluminescence is silicon oxide growing on the hydrogen-terminated PSi surface, generating significant luminescence attributed to quantum confinement effects and to defects localized at the Si–SiO$_2$ interface.[41] For biomedical usage, photoluminescent PSi provides attractive chemical alternatives to heavy-metal-containing quantum dots, which have been shown to be toxic in biological environments. Based on this, Park *et al*.[41] applied photoluminescent PSi for *in vivo* tumor imaging (**Figure 10a**). The nude mouse bearing an MDA-MB-435 human carcinoma tumor (~0.5 cm, one side of flank) was used and photoluminescent PSi (in 200 μL PBS) were intravenously injected into nude mice at a dose of 20 mg kg^{-1} body mass and the tumor area was imaged under anaesthesia several different times after the administration using the IVIS 200 imaging system equipped with excitation filters including GFP (445-490 nm), DsRed (500-550 nm), and Cy5.5 (615-665 nm) and the emission filter ICG (810-875 nm). After the injection, the PSi with the size of 125.7± 9.7 nm

showed a passive accumulation within the tumor area as revealed in the near-infrared fluorescence image. Moreover, photoluminescent PSi displays a very long radiative lifetime (>10 μs), and this has been harnessed for time-gated imaging. Gated luminescence spectroscopy is the registration of luminescence emission spectra at different decay times from the excitation pulse. This technique can be used to distinguish compounds with different decay time. Particularly in bioimaging application, a fluorescence imaging material with long decay feature can be easily separated from the background signal, which most often consists of short decay fluorescence and scattering which can be achieved by altering the measurement time.[167] In a previous study, photoluminescent PSi was administered through retro-orbital injection of mice bearing 4T1 breast tumors. After 4 h of circulation, the major organs including the tumor were harvested and the fluorescence images of corresponding organ were first acquired by a conventional fluorescence imaging system (IVIS 200, Xenogen), under which the photoluminescent PSi groups only showed slightly more intense signals than PBS-injected control group. However, when applying gated luminescence imaging system, which was mainly composed by excitation source at a repetition rate of 10 Hz and a software (Andor SOLIS) to program delays and timing pulses and to analyze images including signal-to-noise ratio (SNR), a greater fluorescence signal was observed comparing to the background. (**Figure 10b**).[168] However, most of the photoluminescent PSi suffers from the unstable luminescence properties and relatively large emission band. For example, Park *et al.*[41] found out that when photoluminescent PSi is placed in biological solution (phosphate buffered saline (PBS), pH 7.4, 37 °C), the particles lose their luminescence in a short time and dissolve, and also it also lacks a satisfied quantum yields comparing to other heavy-metal quantum dots, all these needs further surface modification to improve the photoluminescent behavior of PSi. Moreover, photoluminescent PSi applied into bioimaging can also be excited by UV-light,

which has the inefficient tissue penetrating ability and potential damage to the tissues. One convenient method to solve this issue is by applying up-conversion nanoparticles. Rare earth elements Er/Yb-doped porous silicon plate has already shown to obtain the potent to effectively act as an up-conversion material due to the vast residence of Er/Yb within the pore structure,[169] yet the investigation for nano-sized up-conversion PSi is less noticed.

Due to the unstable nature of the photoluminescent PSi, sometimes the luminescent signal of the particles is not sufficient post implantation,[155] meanwhile, after the thermal oxidation or carbonization, the photoluminescence of surface stabilized PSi is usually quenched, thus other methods for *in vivo* imaging is required. One common method is by conjugating fluorescence dye on the surface. Janoniene *et al*.[104] applied one fluorescence ligand, 3-(cyclooctylamino)-2,5,6-trifluoro-4-((2-hydroxyethyl)sulfonyl)benzenesulfonamide (VD11-4-2), into the surface modification of PSi. This is a fluorescence compound with maximum emission wavelength at 500 nm while the λ_{ex} of DOX is 490 nm. This gives us the opportunity to assemble a system resulting in the formation of a fluorescence resonance energy transfer (FRET) complex: a donor VD11-4-2 energy transfer to the acceptor DOX, where the fluorescence of VD11-4-2 is quenched as a result of DOX absorbance. Furthermore, this FRET pair is quite stable under various of physiological conditions including temperature (37℃), ionic strength (0.1 M NaCl), and pH (MES buffer at pH 7.4, 5.3, 4.9). Owing to this surface modification and the FRET pair construction, the cellular uptake and drug release process *in vitro* can be effectively monitored. An alternative choice is by radiolabeling. Radiolabeling of the nanocarrier-based therapeutic systems with γ-emitting radionuclides, such as ^{111}In, ^{99m}Tc, ^{123}I, and ^{131}I, can provide a highly sensitive and quantitative evaluation of their *in vivo* biodistribution and imaging. Wang *et al*.[150] chelated ^{111}In on the surface of PSi enabling the monitoring of the *in vivo* biodistribution of the nanocarriers by single photon emission computed tomography

(SPECT) in an ectopic mouse xenograft model of PC3-MM2 cells bearing nude mice. The mice were dosed with ^{111}In-radiolabeled PSi and PSi-iRGD nanoparticles either intravenously or intratumorally and the whole-body SPECT/CT images were acquired at different time points (**Figure 10c1**). In the similar regards, fluorine-18 in the form of [^{18}F]KF/Kryptofix 2.2.2 was conjugated onto PSi via heat treatment, and further applied for imaging the distribution of PSi within digestive tract (**Figure 10c2**).[144]

The formation of nanohybrids by combining PSi together with other imaging agents into one carrier is also one routine to achieve the theranostic platform, and this loading is also largely dependent on the surface modification of PSi. For example, Serda *et al*.[170] successfully loaded SPIONs into thermally oxidized PSi microparticles, and they found out that carboxylated SPIONs were not retained in the porous matrix, while both amine- and chitosan-coated SPIONs were found in abundance, which is mainly caused by the electronic interaction. This SPIONs loaded PSi microparticle can further be used as intracellular trafficking or MRI imaging (**Figure 10d**).[170-171] Also, surface deposition of Au nanoparticles or QDs can be used for special optical imaging, and the loading or deposition is also vastly dependent on the surface modification of PSi.[4k,47a] Tasciotti *et al*.[4k] loaded QDs and SWNTs into the hemi-spherical PSi microparticles with a diameter of 3.2 μm and an average pore size of 30 nm, and further applied this nanocomposites into cellular fluorescence imaging. The results showed that carboxyl QDs, which had a negative surface charge (zeta potential, −32.8 mV), and PEG-FITC-SWNTs (zeta potential, −9.21 mV) could be loaded more efficiently into APTES-modified PSi (zeta potential, +6.52 mV) than into oxidized PSi (zeta potential, −10.1 mV). The deposition of Au nanoparticles onto PSi surface can also improve the photoluminescence feature of PSi via surface plasmon enhancement, and extra surface modification leads to an increase and a blue shift into the photoluminescence which may due to the extra oxidation of

Si–H bonds.[172] However, a nano-sized nanohybrid consisted by PSi and other small nanoparticles are less investigated. We recently used a microfluidic assisted method to encapsulate PSi and Au nanoparticles into a nano-sized polymer matrix through single-step nanoprecipitation, further conducted *in vivo* computed tomography (CT) imaging. This method also provides the possibility to construct different theranostic platform in the future.
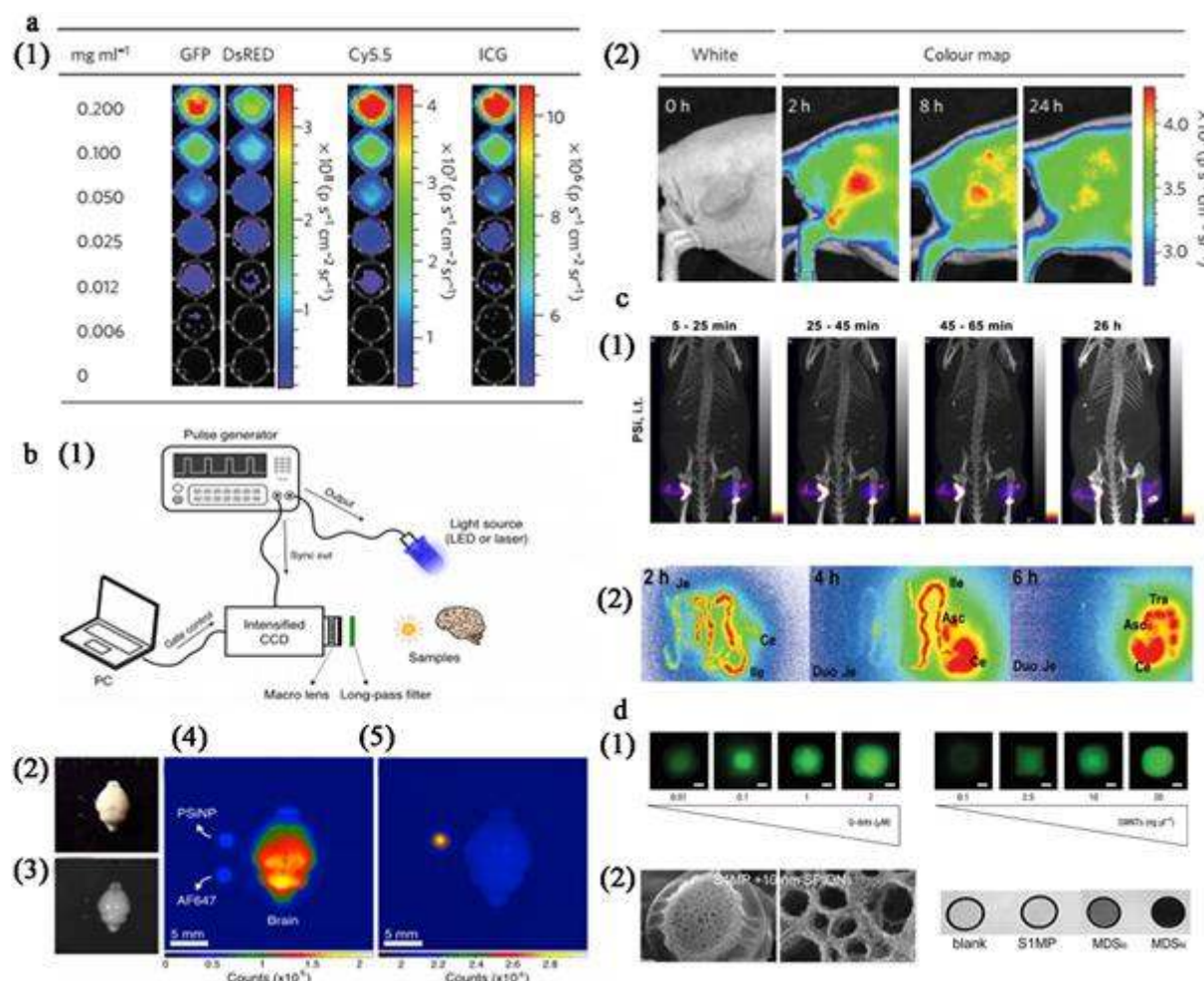

Figure 10. **(a)** Fluorescence images of photoluminescent PSi as a function of concentration using different excitation filters (GFP: 445–490 nm; Discosoma red fluorescent protein (DsRed): 500–550 nm; Cy5.5: 615–665 nm; ICG: 710–760 nm). The emission filter used is ICG (810–875 nm). **(b)** Representative fluorescence images of a mouse bearing an MDA-MB-435 tumor. **b1)** Schematic showing the instrumental setup for gated photoluminescence

imaging of PSi. The iCCD camera and the light source were controlled by an external pulse generator. In the case of laser illumination, the laser fired under control of the laser's internal pulse generator, and the camera was configured to slave to it via TTL trigger. **b2)** Digital color photograph and **b3)** Gray scale image of mouse brain obtained under ambient light. **b4)** CW and **b5)** GLISiNimages of the same brain under UV LED excitation (λ_{ex}= 365 nm, λ_{em}= 460 nm long-pass filter; gate width, 400 μs, 40 accumulations, gate delay for CW = 0 μs, gate delay for GLISiN = 5 μs). Phantom samples corresponding to 150 ng of PSi nanoparticles and 2.5 ng of the molecular dye Alexa Fluor 647 ("AF647") were dropped next to the brain for comparison, as indicated. Note that the signals from the AF647 sample (fluorescence) and the brain tissue (autofluorescence), readily visible at steady state, almost disappear in the GLISiN image, whereas the longer-lived luminescence from PSi nanoparticles is much stronger in the GLISiN image. **(c)** Radio labeled PSi applied into bioimaging **c1)** SPECT/CT fused images of the whole mouse local injected with ^{111}In labeled PSi and **c2)** macroautoradiographs and respective photographs of the GI tracts of rats 2, 4, and 6 h (from left to right) after oral administration of ^{18}F-labeled THCPSi nanoparticles and **(d)**, PSi loaded with **d1)** QDs or SWNTs for fluorescence imaging or **d2)** SPIONs for MRI. Figures are reproduced with permissions: **(a)** from ref. [4l], Copyright 2009, Springer Nature; **(b)** from ref. [168], Copyright 2015, American Chemical Society; **c1)** from ref. [150], Copyright 2015, Elsevier; **c2)** from ref. [144], Copyright 2010, American Chemical Society; **d1)** from ref. [4k], Copyright 2008, Springer Nature; and **d2)** from ref. [25a], Copyright 2010, WILEY-VCH.

4. Emerging technologies for engineering PSi-based composites

As mentioned in Section 3.1, the loading of therapeutics into PSi particles by electrostatic interactions and/or physical adsorption is easily achieved.[7,44] Due to the freely accessible

pores, the payloads can directly interact with the metabolites, ions, and enzymes in body fluids. These interactions can lead to the premature release and even the inactivation of the cargos.[173] To control the release of payloads from PSi, a variety of strategies have been developed. We classify these strategies into two categories: surface chemistry modification and physical encapsulation. The surface chemistry modification has been discussed in Section 3.1. In this section, we will review the PSi-based composites fabricated by physical approaches, including the conventional emulsion method, droplet microfluidics, microfluidic nanoprecipitation, film extrusion and flow reactor. We summarize the physicochemical properties, such as average particle size and release profiles, of the PSi-encapsulated composites in **Table 2**, according to the encapsulation methods.

Table 2. The physicochemical properties of the PSi-encapsulated composites.

Encapsulation techniques	Particle precursors	Drug loading degree	Solvent/non-solvent	Stabilizers	Average size	Estimated t_{50} and t_{100}	Ref.
Conventional emulsion/solvent evaporation	Hemispherical PSi in PLGA	FITC-BSA, −	Dichloromethane/water	2.5% PVA	24 ± 10 μm	In PBS, t_{50} varied from ca. 14 h to ca. 19 days, depending on the relative amount of PLGA	[4h]
	Hemispherical PSi in PLGA	FITC-BSA, −	Dichloromethane/water	2.5% PVA	11 ± 3 μm	In PBS, t_{50} varied from ca. 2 to 17 days	[23b]
	Discoidal PSi in PLGA	FITC-BSA, −	Dichloromethane/water	2.5% PVA	5 ± 0.4, 6 ± 1, 9 ± 3 μm	In PBS, t_{50} varied from ca. 4 to ≥ 10 days	[174]
	Spherical PSi in glycerol monosterate	Furosemide, ca. 15%	Ethanol/water	1% PVA	ca. 200 nm	At pH 7.4, $t_{50} ≈ 1.5$ h, $t_{100} ≈ 10$ h; at pH 5.5, $t_{50} ≈ 4.0$ h, $t_{100} ≈ 12$ h; at pH 1.2, $t_{50} ≈ 7.0$ h, $t_{100} ≥ 14$ h.	[114]
Droplet microfluidics, oil/water	Spherical PSi in HPMCAS mixtures	Atorvastatin and celecoxib, ca. 15% for each	Ethyl acetate/water	2% Poloxamer 407	ca. 129 μm	No drug released at pH 1.2; 40% released at pH 6.0; the rest released at pH 7.4	[175]
	Spherical PSi in HPMCAS	Fluorouracil and celecoxib, ca. 7%	Ethyl acetate/water	2% Poloxamer 407	ca. 30 μm	No drug release at pH < 6.5; the drugs are burst released at pH 7.4	[13d]
	Spherical PSi in HPMCAS	GLP-1, 15% in PSi	Ethyl acetate/water	2% Poloxamer 407	ca. 60 μm	At pH 1.2, no drugs released; at pH 6.8, $t_{50} ≈ 400$ min	[4g]
	Spherical PSi in HPMCAS	Dipeptidyl peptidase 4, −	Ethyl acetate/water	2% Poloxamer 407	ca. 60 μm	At pH 1.2, $t_{50} < 10$ min; at pH 6.8, released in minutes.	[4g]

Droplet microfluidics, water/oil/water	PSi in phospholipid vesicle	Piroxicam, 19%	Water/chloroform and hexane (1:1.18, v/v)/water	10% PVA	*ca.* 114 µm	At pH 6.0, $t_{100} \approx 50$ min; at pH 7.4, $t_{100} \approx 350$ min	[115]
	Spherical PSi, DNA, Gold nanorods in lipid	DOX, 30%; erlotinib, 10%; 17-AAG, 15%	Water/lipid in oil/water	10% PVA	*ca.* 100 µm	t_{50} is ca. 9 h and $t_{100} \geq 24$ h	[99]
Microfluidic nanoprecipitation	AcDX and spherical PSi	SFN, *ca.* 5.0%	Ethanol/water	PVA (2 mg mL^{-1})	*ca.* 350 nm,	At pH 5.0, $t_{50} \approx 3.5$ h and $t_{100} \approx 16$ h	[14b]
	AcDX and spherical PSi	PTX, *ca.* 5.0%	Ethanol/ water	PVA (2 mg mL^{-1})	*ca.* 350 nm,	At pH 5.0, $t_{50} \approx 2.5$ h and $t_{100} \approx 24$ h	[14b]
	AcDX and spherical PSi	MTX, *ca.* 4.5%	Ethanol/ water	PVA (2 mg mL^{-1})	*ca.* 350 nm,	At pH 5.0, $t_{50} \approx 2$ h and $t_{100} \approx 8$ h	[14b]
	PHIS-b-PEG, PLA-b-PEG and spherical PSi	SFN, *ca.* 4.9%	Ethanol and 0.1 M hydrochloric acid/water	Poloxamer 407 solution (2 mg mL^{-1}, pH 12.8)	*ca.* 260 nm	At pH 6.8, and 5.5, t_{50} <10 min and t_{100} <1 h	[14a]
Film extrusion and flow reactor	Spheical PSi nanoparticles and CCM	Horseradish peroxidase, −	Sodium phosphate buffer, pH 7.4	−	*ca.* 243 ± 2 nm	−	[176]
	Spheical PSi@AcDX and CCM	−	Water	−	*ca.* 430 nm	−	[4c]
	Spheical PSi in HPMCAS	Insulin, ca. 13% in chitosan-PSi	Water	−	*ca.* 830 nm	No release at pH 1.2; at pH 6.8, $t_{50} \approx 7$ min and $t_{100} \approx 15$ min	[28]
	Spheical PSi in HPMCAS	DPP4, −	Water	−	*ca.* 830 nm	At pH 6.8 and 1.2, t_{50} < 7 min and $t_{100} \approx 15$ min	[28]

Note: t_{50}, the release duration half-life; t_{100}, duration for release equilibrium; CCM, cancer cell membrane; DPP4, dipeptidyl peptidase 4; HPMCAS, hydroxypropyl methylcellulose acetate succinate; PVA, polyvinyl alcohol.

4.1. Conventional emulsion approach

Since the particle matrix, such as PLGA and solid lipid, is hydrophobic, it is a challenge to encapsulate hydrophilic drugs.[13c] The high drug loading capacity of PSi particles, especially for hydrophilic compounds, can be utilized to regulate the drug loading degree of nanoparticles. Specifically, PSi particles can be encapsulated into the polymer matrix, which is beneficial for drug delivery applications, especially for those hydrophilic therapeutics. Theoretically, the encapsulation of particles loaded with high mass fraction of therapeutics can enhance the loading of drugs that are poorly water soluble in or incompatible with the

polymer or lipid matrix. The encapsulation of PSi particles also shielded their free accessible pores and controlled the drug release from PSi particles.[114,175]

Fan *et al*.[4h] employed the conventional emulsion/solvent evaporation method to encapsulate the quasi-hemispherical PSi microparticles in PLGA microspheres. A model drug, FITC-labeled BSA (FITC-BSA), was loaded into PSi microparticles. The FITC-BSA-loaded PSi microparticles were then encapsulated into the PLGA matrix.[4h,23b,174] The PSi-encapsulated microcomposite, PSi@PLGA, contained multiple PSi particles in each PLGA matrix. Both PLGA and PSi contributed to the sustained release of FITC-BSA. Specifically, the complete release of FITC-BSA form bare PSi particles was ~1 day. In contrast, it took more than 28 days for FITC-BSA to be completely released from PSi@PLGA. PSi@PLGA protected BSA from degradation during the long-term release test. Furthermore, PSi neutralized the acidic degradation by-products of PLGA, minimizing the potential inflammatory responses toward PLGA. In addition to FITC-BSA, the water soluble daunorubicin[120] and the poorly water soluble furosemide[114] were also loaded into PSi-based composites, respectively, for sustained release of payloads.

4.2. Droplet microfluidics

The microfluidic technique has brought unique opportunities toward the full control over the production processes forming droplets with a homogeneous size for controlled drug delivery.[177] Microfluidics also represents an effective technique for PSi particle encapsulation with a particle encapsulation efficiency close to 100% (**Figure 11a**). Due to their homogenous size, the amount of PSi particles and therapeutics in each droplet or particle should be in an exactly similar level. By encapsulating the PSi particles loaded with hydrophilic drugs, such as ranitidine and methotrexate, the loading of hydrophilic drugs by

solid lipid particles greatly enhanced.[94] The co-delivery of atorvastatin and celecoxib with a precisely controlled ratio has been achieved by encapsulating the atorvastatin-loaded PSi microparticles[175] in HPMCAS microparticles using single emulsion droplet microfluidics.

The fluorouracil-loaded PSi nanoparticles encapsulated in HPMCAS polymer matrix achieved the co-delivery of fluorouracil and celecoxib.[13d] Benefiting from the high drug loading to peptides and proteins, the co-delivery of GLP-1 and DPP4 enzyme inhibitor for diabetes therapy by oral administration was achieved.[4g,178] Before the encapsulation by HPMCAS, the GLP-1 was loaded into the PSi nanoparticles, whose surface was sequentially modified with chitosan and CPP. Due to the pH-responsive properties of the HPMCAS polymer, all the payloads released in responsive to the pH condition of the release medium (**Figure 11b**).

With the help of droplet microfluidics, micro- and nano-particles can also be encapsulated in double emulsions. The piroxicam-loaded PSi microparticles were encapsulated into phospholipid vesicles, in which the release of piroxicam was sustained. Specifically, the release half-life for piroxicam increased from ~15 to ~60 min after encapsulating the piroxicam-loaded PSi particles into the phospholipid vesicles.[115] Kong *et al.*[99] developed a giant vesicle by double emulsion droplet microfluidics for co-delivery of multiple drugs and particles. Water soluble doxorubicin, and the poorly water soluble 17-allyl-aminogeldanamycin were directly incorporated into the core and shell of the giant vesicles. The incorporation of erlotinib was achieved by encapsulating the erlotinib-loaded PSi nanoparticles into the giant vesicles. The release of doxorubicin from the giant vesicles was sustained to be similar to that of poorly water soluble erlotinib.

4.3. Microfluidic nanoprecipitation

The carriers prepared by droplet microfluidics are usually in micrometer range. Microfluidic nanoprecipitation is also a versatile approach to form structured nanocomposites by encapsulating nanoparticles.[177a] When polymer precursors experience a change in solvent, they can assemble into nanoparticles. The fluid mixing time in microfluidic devices can be faster than the nucleation time for the nanoparticle precursors. This fast mixing by microfluidic devices enables the formation of smaller nanoparticles with a narrower size distribution than the counterparts prepared by conventional methods. With the help of microfluidic nanoprecipitation (**Figure 11c**), drug-loaded PSi nanoparticles were encapsulated into a pH-responsive AcDX matrix with a number ratio of 1:1 (PSi@AcDX).[14b] With the help of microfluidic nanoprecipitation method, no free PSi particles were observed in the obtained nanosuspension, and the percentage of the PSi-encapsulated nanocomposites was more than 92%. This high PSi-encapsulation efficiency enabled by the microfluidic nanoprecipitation method facilitates the direct use of the obtained nanosuspension without sorting.

As a result of their high loading capacity for MTX, the encapsulation of MTX-loaded PSi nanoparticles enhanced the drug loading degree of MTX from ~0.1% (w/w) to the same level (~5%) of PTX and SFN inside the PSi@AcDX.[14b] The release of all three payloads was controlled by the degradation of the AcDX layer, which occurred at the acidic condition (pH 5.0) (**Figure 11d**). The cell uptake of triple-drug loaded nanocomposites greatly enhanced after the surface functionalization with CPP. Poly(L-histidine)-*b*-PEG (PHIS-*b*-PEG) micelles assembled onto the surface of SFN-loaded PSi (SFN-PSi) nanoparticles to form the nanocomposites (SFN-PSi@PHIS-*b*-PEG).[14a] PHIS-*b*-PEG micelles both temporally sealed the pores of PSi nanoparticles and enhanced their stability in plasma. In the acidic condition,

the pH-responsive PHIS-*b*-PEG micelles disassembled and PSi nanoparticles were uncovered to release SFN.

4.4. Film extrusion

Recently, PSi@AcDX nanocomposites were also engineered for cancer immunotherapy.[4c] Because of the efficient and fast mixing in microfluidic device, the obtained nanocomposites presented narrow size distributions (PDI was ca. 0.17). By film extrusion, the PSi@AcDX nanocomposites were encapsulated into the nanovesicles derived from CCM. The PSi@AcDX encapsulated CCM, PSi@AcDX@CCM, merged the best of the antigenic feature of tumor lysates and the adjuvant property of PSi nanoparticles. All the obtained nanocomposites were highly compatible with two human immortalized cell lines, KG 1 macrophages and B cells with dendritic cells morphology (BDCM). PSi@AcDX@CCM greatly enhanced the secretion of interferon-γ (IFN-γ) for ~ 700% in peripheral blood monocytes (PBMC), without inducing the secretion of IL-4. Therefore, PSi@AcDX@CCM can polarize the newly primed T cells toward a Th1 cell-mediated response.[4c]

The horseradish peroxidase (HRP) enzymes-loaded PSi (HRP-PSi) nanoparticles were directly encapsulated by CCM through film extrusion to form nanoreactors, HRP-PSi@CCM (**Figure 11e–f**).[176] In comparison to free enzymes, the HRP-PSi@CCM nanoreactor showed enhanced substrate affinities (Km, 1.90×10^{-6} *vs.* 0.14×10^{-6} M) and improved reaction rates (V_{max}, 1853×10^{-6} *vs.* 659×10^{-6} M/min), indicating a good catalytic activity for the nanoreactors. Under the stimulated oxidative stress conditions, the HRP-PSi@CCM nanoreactor significantly reduced the intracellular ROS levels and supplemented the subcellular organelles functions.[176] Usually, proteins are sensitive to organic solvents and

heat. The film extrusion approach avoids the use of organic solvents and heating, which can

preserve the functionality of membrane proteins at the greatest extent.

4.5. Flow reactor

The aerosol flow reactor is a simple one-step approach that can be utilized to encapsulate

nanoparticles within polymer matrix, forming the nano-in-nano vectors. As shown in **Figure 11g**, the nanoparticle precursors are atomized into small droplets by a Collison-type jet

atomizer. Benefiting from the small diameter and relatively high surface area, the formed

droplets can be dried in laminar flow reactor at a relatively low temperature, such as 80 °C.

With the help of an aerosol flow reactor, GLP-1-loaded PSi nanoparticles together with DPP4

inhibitor were encapsulated into a pH-responsive HPMCAS nanomatrix (**Figure 11g**).[28] The

surface functionalization by chitosan enhanced the mucoadhesiveness of PSi nanoparticles, as

well as their interaction with cells for ~50 times. The outer HPMCAS matrix successfully

protected the encapsulated GLP-1 from degradation in harsh stomach environment. The

obtained nanocomposites improved the intestinal permeability of GLP-1 from less than 1×10^{-8}

to ~6×10^{-8} cm s^{-1}. This high GLP-1 permeability can be ascribed to the permeability

enhancement effect of chitosan and the reduced degradation of GLP-1 by DPP4 inhibitor. In a

non-obese type 2 diabetes rat model, the oral administration of GLP-1 and DPP4 inhibitor co-

loaded nanocomposites resulted in around 32% decrease in blood glucose levels and

approximately 6-fold increase in pancreatic insulin content, as compared to the aqueous

solution of GLP-1 and DPP4 inhibitor.[179] The obtained nanocomposites were successfully

used for advanced oral type 2 diabetes mellitus therapy. Although the obtained droplets were

dried at 80 °C, this relatively low temperature may still harm the stability and activity of the encapsulated therapeutics, especially the proteins and peptides.
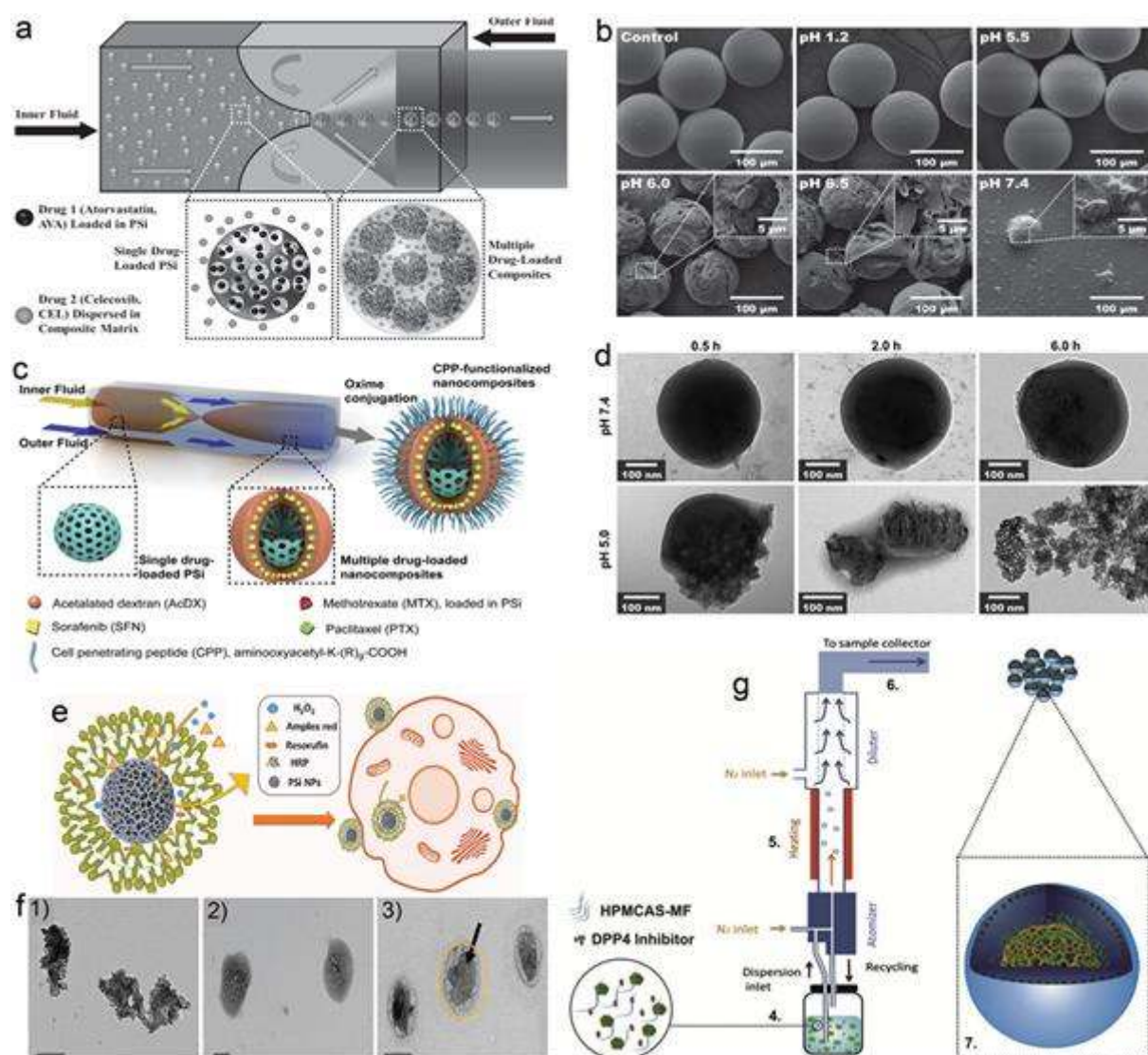

Figure 11. Encapsulation of PSi particles. **(a)** Schematic of the droplet microfluidic approach to prepare the pH-responsive multidrug loaded PSi@HPMCAS microcomposites. **(b)** Dissolution of PSi@HPMCAS at different pH conditions. **(c)** Schematic of the process to synthesize multidrug loaded PSi@AcDX. **(d)** Degradation of PSi@AcDX at different pH-conditions as a function of time. **(e)** Schematic of a biomimetic nanoreactor composed of HRP enzyme loaded in PSi nanoparticles and surface decorated with CCM. **(f)** TEM images of **f1)** PSi nanoparticles, **f2)** cell membrane vesicles, and **f3)** PSi@CCM nanoreactors. Scale bars are

200 nm. **(g)** Schematic of the flow reactor for the preparation of PSi@HPMCAS co-loaded with GLP-1 and DDP4 inhibitors. Figures are reproduced with permissions: **(a–b)** from ref. [175], Copyright 2014, WILEY-VCH; **(c–d)** from ref. [14b], Copyright 2015, Elsevier; **(e–f)** from ref. [176], Copyright 2017, WILEY-VCH; and **(g)** from ref.[28], Copyright 2015, Elsevier.

5. PSi for cancer immunotherapy

As discussed in the previous sections, PSi has proven to be an excellent material for the loading and delivery of therapeutics. Recently, the materials science field has moved towards the evaluation of the immunogenic properties of the materials.[180] The immunogenicity of silicon platforms has been investigated by Ainslie *et al.*:[181] this surface induced the secretion of proinflammatory cytokines by PBMC. Moreover, PSi micro- and nano-particles, characterized by different surfaces, show different immunogenic profiles on cells of the immune system.[31,54a,182]

Immunotherapy is nowadays one of elective treatments for cancer.[183] Cancer immunotherapy aims to fight the proliferation of the tumor cells by employing elements of the immune system.[184] Passive immunotherapy leans on the administration of cytokines, monoclonal antibodies (used in targeted therapies against cells overexpressing a marker), or T-cells (tumor infiltrating, adoptive and chimeric antigen receptor (CAR)).[185] Monoclonal antibodies have a long tradition in the clinics as targeted therapies. They mainly act according to four mechanisms: ability to induce the formation of the complement, leading to cell lysis; signaling to the cells of the immune system; antibody dependent cell cytotoxicity (ADCC), due to the binding to the Fc receptor on immune cells (like natural killer cells); targeting of drug and drug-loaded nanoparticles to the cancer cells.[186]

71

In an opposite fashion, active cancer immunotherapy enrolls the patient's own immune system by administration of checkpoint inhibitors (monoclonal antibodies targeted to the immunological synapse or to the connections between T cells and cancer cells), or by cancer vaccines.[30,185] A vaccine presents disease-relevant peptides to antigen presenting cells (APCs), like dendritic cells (DCs), to stimulate an immune response against the diseases.[187] The APC will process the peptide, presenting an epitope on the major histocompatibility complexes I and II (MHC I/II) to prime, respectively, CD8$^+$ or CD4$^+$ T -cells.[184,188] Nanoparticles have a potential application as vaccines vehicles and adjuvants: they are in the same size range of virus and bacteria; they can directly delivery the antigens to the DCs population in the lymph nodes; moreover, they can serve as depot formulation for the antigen, achieving a prolonged release; their surface can be functionalized with adjuvant molecules, mimicking a pathogen and finally, the delivery of adjuvants through nanoparticles increases the cross presentation of antigens on MHC I with the priming of CD8$^+$ T -cells, of great significance in cancer immunotherapy.[189]

5.1. PSi particles as vaccine adjuvants

Micro- and nano-particles own intrinsic adjuvant properties based on their physicochemical characteristics: size, surface charge, elasticity, shape, hydrophilicity/hydrophobicity of the particles, hydroxyl content of the surface, and functionalization of the surface.[180b,188]

As for PSi microparticles, the intrinsic adjuvant effect of the particles is achieved by induction of an interferon I response and activation of the inflammasome used by the innate immune system in presence of a viral infection.[4b] Furthermore, PSi microparticles localize within the early endosomes and move to the endoplasmatic reticulum, avoiding the late endosomes and recycling endosomes, thereby delivering the antigens intracellularly, as shown in **Figure 12a**.

The incubation of discoidal PSi microparticles further loaded with immunogenic liposomes encapsulating an antigen against human epidermal growth factor receptor 2 (HER-2) resulted in an increased activation of DCs both *in vitro* and *in vivo*. The pulsing of DCs with particles loaded with a model antigen, chicken ovalbumin (OVA), promoted the maturation of the DCs together with a successful presentation of the antigen, inducing the proliferation of B3Z OVA specific T cells and the secretion of interleukin 2. As for the *in vivo* evaluation, the intravenous administration of the antigen-loaded particles partially controlled the tumor growth; however, a prolonged control over the development of the tumor, with an enhance activation of the immune system, was achieved after administration of DCs pulsed with the antigen-loaded particles, as presented in **Figure 12b1**. Furthermore, the vaccine formulation demonstrated also a prophylactic effect in transgenic mice models, retarding the development of the tumor lesions (**Figure 12b2**).[4b]
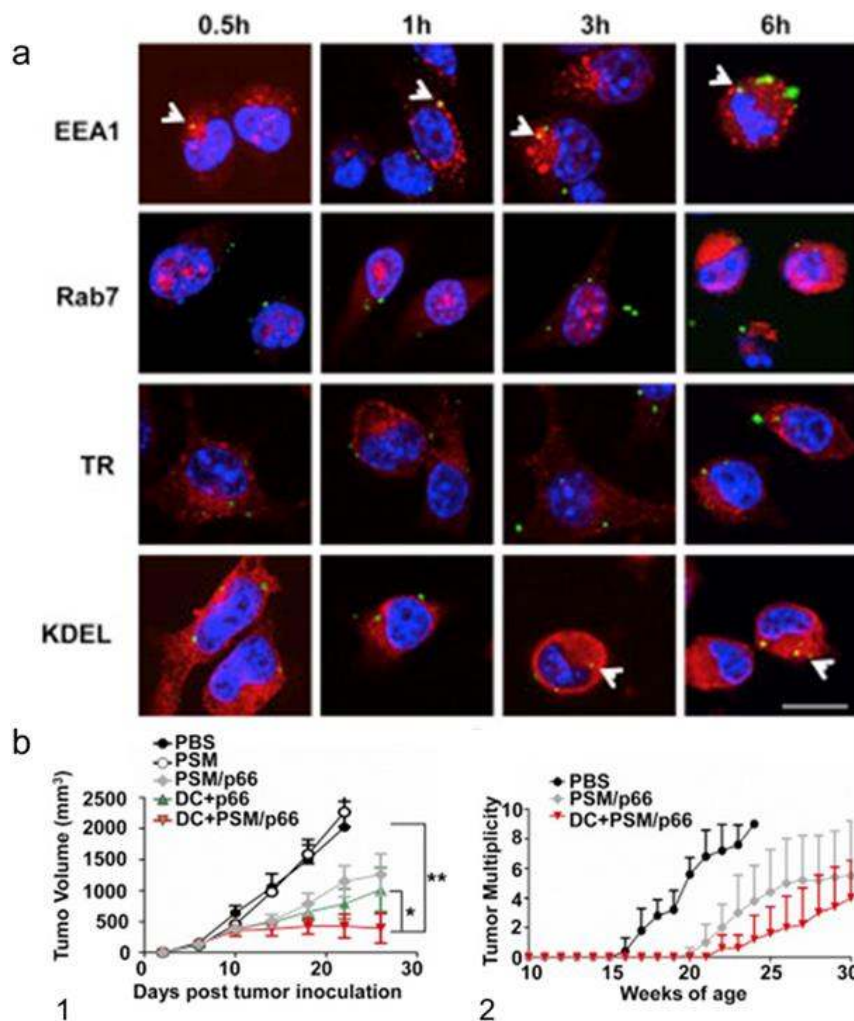
Figure 12. **(a)** Internalization dynamics of antigen-loaded PSi microparticles into DCs at different time points. The particles were loaded with FITC-labeled ovalbumin (FITC-OVA), while the different subcellular organelles were stained specifically: early endosome antigen 1 (EEA1) for early endosomes, Rab7 for late endosomes, transferrin receptor (TR) for recycling endosomes, endoplasmic reticulum protein retention receptor 1 (KDEL) for the endoplasmic reticulum). Scale bar, 25 μm. **b1)** Inhibition of the tumor growth in a TUBO murine breast cancer model after intravenous administration of antigen-loaded PSi microparticles (PSM/p66) or DCs primed by antigen loaded PSi particles (DC+PSM/p66); **b2)** Tumor nodules developed by Balb-neuT mice injected intravenously with the treatments. Modified and reprinted with permission from ref. [4b], Copyright 2015, Cell Press.

The surface of these microparticles can also be modified with adjuvants: Meraz *et al.*[190] adsorbed lipopolysaccharide (LPS) or monophosphoryl lipid A (MPLA) on PSi microparticles evaluating first the effect of the particles on the immune system, as shown in **Figure 13**, followed by the assessment of the efficacy of a combinatorial therapy based on adjuvant-modified microparticles administered with DOX-loaded liposomes.[190] The microparticles alone (presenting a positively charged surface, APTES), despite promoting the secretion of the pro-inflammatory cytokine interleukin-1β (IL-1β) due to activation of the inflammasome, did not induce the maturation of murine bone marrow-derived dendritic cells (BMDC).[182] On the contrary, the administration of the LPS/MPLA-modified particles alone or in combination with DOX resulted in maturation of DCs, migration of DCs pulsed with the particles to the lymph nodes, enhanced control over the tumor development in a murine model of breast cancer after intravenous administration, and in a modification of the tumor microenvironment, with the increase in the number of CD8$^+$ T-cells.[182,190]

The effect of the different surface chemistry of PSi nanoparticles on the immunogenicity of the particles was investigated by Shahbazi *et al.*:[31] the incubation of human monocyte-derived DCs with the particles, at the cytocompatible concentration of 25 µg mL^{-1}, lead to the identification of two highly immunostimulant surface modifications, THCPSi and TOPSi, while the other nanoparticles (TCPSi, APTES functionalized THCPSi (APSTCPSi) and UnTHCPSi) did not induce the expression of costimulatory signals (CD80,83,86, human leukocyte antigen - antigen D related (HLA-DR)), as shown in **Figure 13a1–2**.[31] UnTHCPSi and APSTCPSi particles, after further modification respectively with PEI or with PMVEMA showed an intermediate profile of immunoactivation. Moreover, the incubation with THCPSi and TOPSi particles induced a Th1-biased immune response, with the secretion of

Interleukin-12 (IL-12) and IFN-γ, and the priming of CD8$^+$ T-cells, particularly after incubation with TOPSi, as shown in **Figure 13a3–4**. The immunogenicity of THCPSi particles can be explained based on their hydrophobicity, as reported also in other studies,[191] as well as the lack of immunostimulation for particles rich in OH and NH groups.[192] TOPSi particles however present hydroxyl groups on the surface and are hydrophilic, yet they are still highly immunostimulant. According to Shahbazi *et al.*,[31,193] this effect is due to the immunogenicity of the ortho-silicic acid released by the fast degradation of TOPSi particles in physiological conditions.
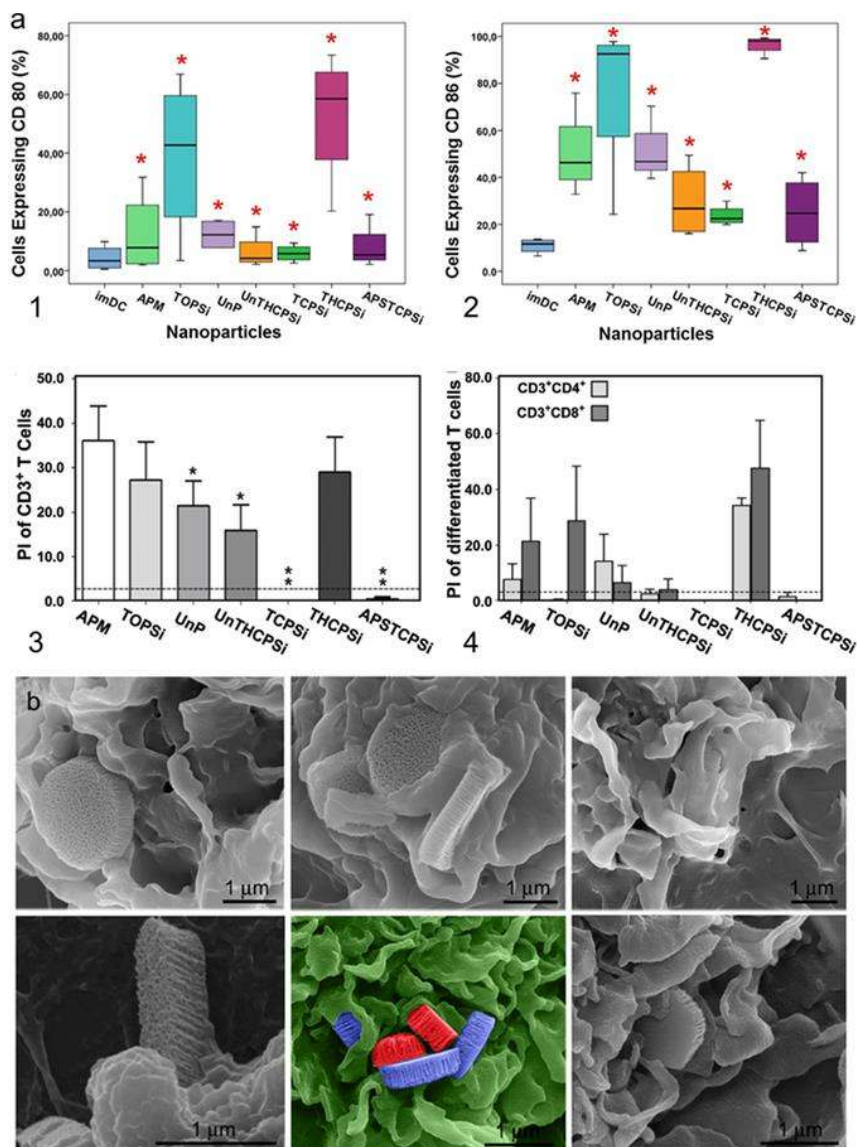
Figure 13. (a) Percentage of human monocyte derived DCs expressing the costimulatory signals **a1)** CD80 and **a2)** CD86 after incubation with PSi nanoparticles with different surfaces at the concentration of 25 µg mL^{-1}, **a3)** Proliferation of T-cells after incubation with the different PSi nanoparticles at the concentration of 25 µg mL^{-1} for 6 days; **a4)** Proliferation of the subpopulations CD^{4+} and CD^{8+} cells after incubation with the PSi nanoparticles for 6 days. Modified and reprinted with permission from ref. [31], Copyright 2014, Elsevier, and from ref. [190], Copyright 2014, Public Library of Science.

Recently, a combination of TOPSi particles with a biocompatible polymer with known adjuvant properties (AcDX) and an innovative source of antigens, membrane derived from cancer cells, was described by Fontana *et al.*.[4c] PSi particles were first encapsulated within a polymeric matrix by nanoprecipitation in microfluidics, followed by the film extrusion together with the cell membrane derived from cancer cells, as shown in **Figure 14**. The incubation of the multistage system, at the concentration of 100 µg mL^{-1}, with PBMC induced the maturation of antigen presenting cells (shown by the increase in the presentation of both CD80 and 86) and in the secretion of IFN-γ; moreover the co-culture of PBMC, previously activated with the systems, with cancer cells with homologous membrane resulted into the inhibition of the cancer cells' proliferation.[4c]
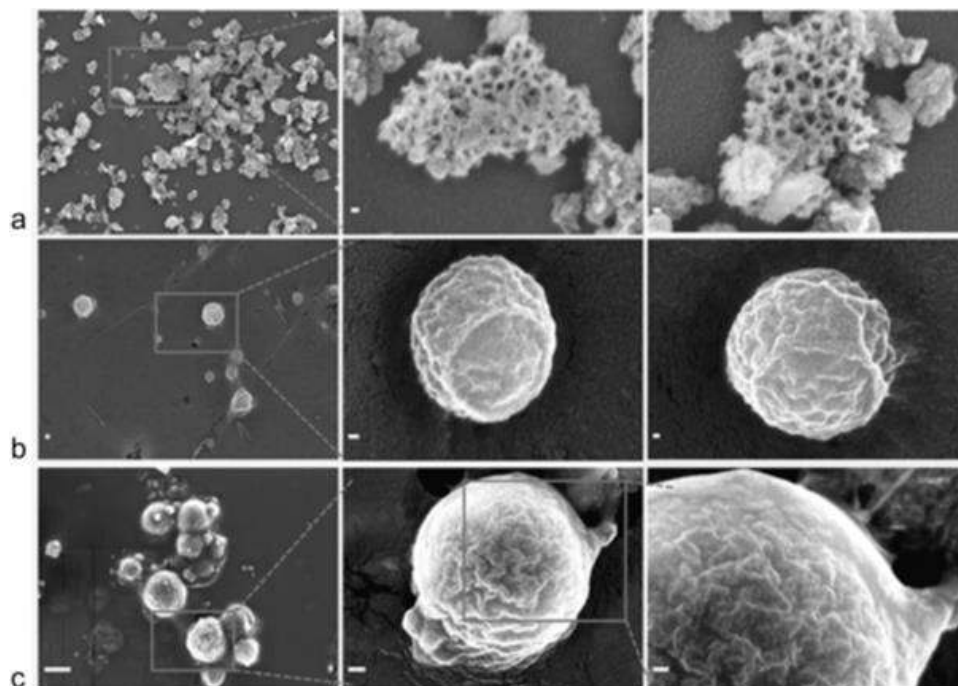
Figure 14. SEM images of **(a)** TOPSi; **(b)** TOPSi@AcDX; **(c)** TOPSi@AcDX@CCM nanovaccines. Scale bars: (a) and (b) 100 nm left, 20 nm center and right; (c) 200 nm left, 50 nm center, and 20 nm right. Modified and reproduced with permission from ref. [4c], Copyright 2016, WILEY-VCH.

5.2. Loading of PSi with chemotherapeutics and functionalization with antibodies for combined chemoimmunotherapy

PSi nanoparticles are versatile platforms that allow the simultaneous loading of a chemotherapeutic drug and the functionalization of the surface with monoclonal antibodies, useful both for the targeting of the nanoparticles to the cancer cells and to stimulate complement activation, ADCC and immune response against the cancer cell.[32,186b]

PSi nanoparticles show potential applications in the delivery of monoclonal antibodies for immunotherapy: Gu *et al.*[4a] first loaded avidin in the pores of the particles, followed by biotinylated-anti CD40 antibodies to stimulate the activation of antigen presenting cells, as shown in **Figure 15a**. The stimulation of B cells was entirely due to the antibody delivered

rather than any intrinsic adjuvant effect of the particles; moreover the administration of antibody-loaded particles induced higher immunostimulation compared to the soluble antibody (**Figure 15a2**).[4a]

Secret *et al.*[105] employed PSi nanoparticles for the delivery of camptothecin. Three different monoclonal antibodies, proposed for the targeting of three different tumors (neuroblastoma, glioblastoma, and B-cell lymphoma) were covalently bound on the surface of the nanoparticles. The antibodies were bound to the surface of the particles via a semicarbazide chemistry, to preferentially orient the antibody molecule, as shown in **Figure 15b1**. However, the authors only evaluated the targeting functionality of the antibody *in vitro* and did not investigate the possible immunological applications (**Figure 15b2**). Moreover, antibody-functionalized PSi nanoparticles have been co-loaded with camptothecin and gold nanoclusters for targeted combined chemothermotherapy in B cells as a proof-of-concept.[194] UnTHCPSi particles have been loaded with the kinase inhibitor SFN, while an antibody against the epithelial cell adhesion molecule (CD326) was covalently attached on the surface by 1-ethyl-3-[3-dimethylaminopropyl]carbodiimide hydrochloride (EDC) / N-hydroxysuccinimide (NHS) chemistry.[32] The loaded chemotherapeutic resulted in the inhibition of the proliferation of two immortalized breast cancer cell lines, while the presence of the monoclonal antibody induced ADCC and secretion of IL-12 by the effector immune cells, only in the cell line expressing the target marker on the cell membrane, as presented in **Figure 15c1–4**.
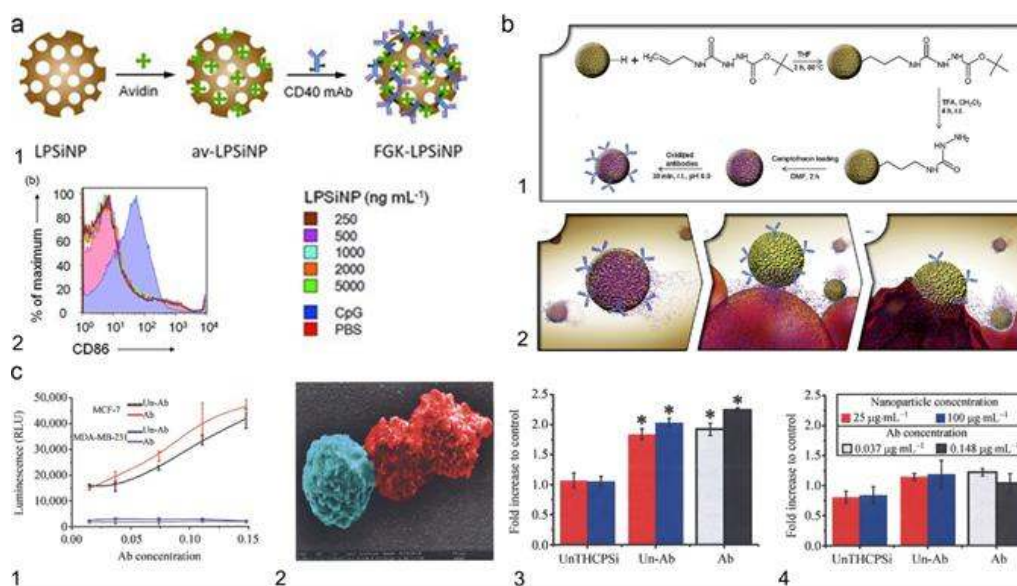
Figure 15. a1) Schematic of the method to load anti-CD40 antibody into PSi nanoparticles; **a2**) Enhancement in the presentation of CD86 by B cells after incubation with the antibody-loaded particles at different concentrations for 42 h. Modified and reprinted with permission from ref. [4a], Copyright 2012, WILEY-VCH. **b1)** Schematic of the semicarbazide reaction to functionalize the surface of PSi nanoparticles with monoclonal antibodies; **b2)** Proposed mode of action of the formulation. Reprinted with permission from ref. [105], Copyright 2013, WILEY-VCH. **c1)** ADCC effect of the developed formulation onto two different breast cancer cell lines, MCF-7 and MDA-MB-231; **c2)** False color SEM image of the association between immune cell (blue) and cancer cell (red) after incubation with the system; **c3)** and **c4)** Production of IL-12 in MCF-7 and MDA-MB-231 after incubation with the chemoimmunotherapeutic platform for 24 h. Modified and reprinted with permission from ref. [32], Copyright 2015, Springer.

6. Conclusions and outlook

Here, we have presented a comprehensive overview of recent advances in the area of PSi for biomedical applications with focus both on drug delivery and cancer immunotherapy. PSi

with their controllable geometry, tunable nanoporous structure and versatile surface properties

has unique advantages that may allow clinically applicable formulations for disease therapy.

From the point view of fabrication, novel approaches have been developed to fabricate spherical PSi particles. Comminution of PSi films derived from "top-down" approach by microfluidization shows a great potential for mass production of spherical PSi particles. Bottom-up strategy using silicon tetrachloride for synthesizing spherical PSi particles reduces the mass loss of silicon and avoids the use of harsh etchants such as hydrofluoric acid. The combination of electrochemical etching and silicon microfabrication technique contributes to the precise fabrication of quasi-hemispherical/discoidal PSi particles and PSi needles. Quasi-hemispherical/discoidal PSi particles are applied as the matrix to construct MSVs which show great potential to sequentially overcome the multiple biological barriers that particles encountering from the intravenous administration site to the disease site, while PSi needles can deliver therapeutics intracellularly and induce localized therapeutic effects. Meanwhile, new fabrication methods of PSi focusing on bottom-up approach should be further explored. Most of currently proposed alternative methods, such as magnesiothermic reduction, halide reduction and silica template reduction, generally tend to involve harsh reaction conditions and the newly formed PSi is usually micro-sized. An alternative method, especially using relatively mild reaction conditions, to produce nano-sized PSi is highly desired.

From the point view of surface chemistry, the inherent drawbacks of freshly etched PSi can be solved by various primary surface modification and secondary surface modification methods, and the choice of surface modification method for PSi can be adjusted according to its specific application. PSi after surface modification is able to achieve controlled release behavior such as sustained release, pH triggered release, and thermal-sensitive release as well as photodynamic release. The conjugation of targeting moieties can alter cellular interactions,

81

and thus can be tailored for different disease. Furthermore, surface modification of PSi plays the most critical role in its photoluminescence. Comparing to other photoluminescence agents, such as QDs, photoluminescent PSi shows a much better biocompatibility due to the endogenous element silicon, and the photoluminescence properties can be further adjusted by surface modification. Different surface properties of PSi can not only affect its drug loading and release behavior, targeting ability and imaging ability, most importantly it may also impact its biofate. Given the breadth of currently arising opportunities and concerns associated with PSi in living systems, it is of great importance to deeply understand the complex processes that govern its cellular uptake and intracellular behavior, as well as *in vivo* fate, which are largely dependent on the surface properties of PSi. Especially considering the great importance of orthosilicic acid, which is the main degradation product of PSi, within the biological pathways, further investigation about nano-toxicology of PSi with different surface properties holds its great value.

In addition to chemical modification, another strategy to control the release of payloads from PSi particles is by physical encapsulation them in polymeric and solid lipid particles. For polymeric and solid lipid particles, their drug loading capacity can be enhanced by encapsulating the PSi particles with high mass fraction of therapeutics. The PSi particles-encapsulated composites merge the high drug loading of PSi particles and controlled drug release of conventional solid particles. Toward the physical approaches, the PSi-based composites could be fabricated by the conventional emulsion method, droplet microfluidics, microfluidic nanoprecipitation, film extrusion and flow reactor. In comparison to the conventional emulsion method, microfluidic technique provides the precisely and full control over the production processes to form microparticles and nanoparticles with a homogeneous size for controlled drug delivery. For conventional emulsion method, droplet microfluidics

and microfluidic nanoprecipitation, the use of organic solvents is inevitable. This might affect the stability and activity of the therapeutics loaded in PSi particles, especially for the sensitive proteins and peptides. Benefiting from their high drug loading capacity, PSi particles have been embedded inside the polymeric and solid lipid particles to enhance their drug loading capacity. However, the organic solvent used to dissolve the particle precursors and to disperse the drug-loaded PSi particles is possible to extract the payloads from PSi particles. The leakage of payloads from PSi particles during the preparation process weakens the loading degree enhancement ability of PSi particles for polymeric and solid lipid particles.

Proteins and peptides are sensitive to enzymes in the body fluids, therefore, the encapsulation of proteins and peptides-loaded PSi particles will protect the payloads from degradation. However, organic solvents may inactive the proteins and peptides. The organic solvent free approaches, such as film extrusion and flow reactor, are favorable for encapsulating the proteins and peptides loaded PSi particles. Proteins and peptides can be adsorbed onto the surface of PSi particles through the physicochemical interactions. Due to the relatively strong interactions with PSi, the release of proteins and peptides is in a relatively slow manner in the aqueous medium. This slow release minimizes the loss of proteins and peptides during the preparation process. The relatively high temperature (80 °C) has been used to dry the formed small droplets in the flow reactor. The flow reactor method is restricted to the payloads that are stable to the set drying temperature. For film extrusion, PSi particles are stopped by the film easily, which may hamper the coating efficiency. The optimization of the suspension medium is critical to perform the film extrusion for PSi particles. All the physical encapsulation methods have their own limitations, we need to carefully select the most appropriate method to perform the PSi particle encapsulation. In general, the selection of

encapsulation method depends on the solubility and stability of payloads, the loading degree of payloads in PSi particles and the surface properties of PSi particles.

The field of immunotherapy with nanoparticulate carriers is in continuous evolution. The applications of such systems in cancer immunotherapy have been widely investigated.[30,180] PSi has shown promising applications as a platform for chemoimmunotherapy and as material displaying intrinsic adjuvant properties useful in cancer immunotherapy.[4c,31-32,182,190] Innovative applications of nanoparticles are currently being researched for the treatment of autoimmune diseases, both as carrier for immunomodulatory drugs like rapamycin, and as platform for nanovaccines able to induce an immunotolerant response. [195] Based on the research about the material's interactions with the immune system,[31,195e] we envisioned potential future applications of PSi particles also in the treatment of autoimmune diseases.

In conclusion, the promising research results of some PSi structures encourage further exploration of PSi for biomedical applications, particularly in drug delivery and cancer immunotherapy. Nevertheless, the clinical application of PSi is still in its infancy as there remain significant barriers to the clinical applications of PSi. These barriers include understanding the performance of PSi under specific disease pathology, while taking into consideration the effects of the geometry, surface chemistry and modification, and physical encapsulation of PSi. Such mechanistic understanding is crucial for determining and predicting the *in vivo* fate of PSi-based materials when applied for both drug delivery and cancer immunotherapy. Although encouraging *in vitro*, *in vivo* and human safety data are available for some PSi structures, the biocompatibility, biodistribution and biodegradability of PSi-based materials *in vivo* still need to be further comprehensively investigated, especially for nano-sized composite PSi after surface modification. It is anticipated that the combination of multidiscipline, including materials, chemistry, engineering, pharmaceutical science,

biology and medicine, can make exciting breakthroughs in the near future and accelerate the clinical translation of PSi.

Received: ((will be filled in by the editorial staff))

Revised: ((will be filled in by the editorial staff))

Published online: ((will be filled in by the editorial staff))

[1]   A. Uhlir, *Bell System Technical Journal* **1956**, 35, 333.

[2]   L. T. Canham, *Appl Phys Lett* **1990**, 57, 1046.

[3]   L. T. Canham, *Advanced Materials* **1995**, 7, 1033.

[4]   a) L. Gu, L. E. Ruff, Z. Qin, M. Corr, S. M. Hedrick, M. J. Sailor, *Advanced Materials* **2012**, 24, 3981; b) X. Xia, J. Mai, R. Xu, Jorge Enrique T. Perez, Maria L. Guevara, Q. Shen, C. Mu, H.-Y. Tung, David B. Corry, Scott E. Evans, X. Liu, M. Ferrari, Z. Zhang, Xian C. Li, R.-f. Wang, H. Shen, *Cell Reports* **2015**, 11, 957; c) F. Fontana, M. A. Shahbazi, D. Liu, H. Zhang, E. Makila, J. Salonen, J. T. Hirvonen, H. A. Santos, *Adv Mater* **2017**, 29; d) M.-A. Shahbazi, M. Hamidi, E. M. Makila, H. Zhang, P. V. Almeida, M. Kaasalainen, J. J. Salonen, J. T. Hirvonen, H. A. Santos, *Biomaterials* **2013**, 34, 7776;

e) D. Fan, G. R. Akkaraju, E. F. Couch, L. T. Canham, J. L. Coffer, *Nanoscale* **2011**, 3, 354; f) M. Yuryev, M. P. A. Ferreira, V. Balasubramanian, A. M. R. Correia, E. M. Mäkilä, V. Jokinen, L. Andriichuk, M. Kemell, J. J. Salonen, J. T. Hirvonen, H. A. Santos, C. Rivera, *Nanomedicine* **2016**; g) F. Araujo, N. Shrestha, M. A. Shahbazi, D. Liu, B. Herranz-Blanco, E. M. Mäkilä, J. J. Salonen, J. T. Hirvonen, P. L. Granja, B. Sarmento, H. A. Santos, *ACS Nano* **2015**, 9, 8291; h) D. Fan, E. De Rosa, M. B. Murphy, Y. Peng, C. A. Smid, C. Chiappini, X. Liu, P. Simmons, B. K. Weiner, M. Ferrari, E. Tasciotti, *Advanced Functional Materials* **2012**, 22, 282; i) C. Chiappini, E. De Rosa, J. O. Martinez, X. Liu, J. Steele, M. M. Stevens, E. Tasciotti, *Nat Mater* **2015**, 14, 532; j) R. Xu, G. Zhang, J. Mai, X. Deng, V. Segura-Ibarra, S. Wu, J. Shen, H. Liu, Z. Hu, L. Chen, Y. Huang, E. Koay, Y. Huang, J. Liu, J. E. Ensor, E. Blanco, X. Liu, M. Ferrari, H. Shen, *Nat Biotech* **2016**, advance online publication; k) E. Tasciotti, X. Liu, R. Bhavane, K. Plant, A. D. Leonard, B. K. Price, M. M.-C. Cheng, P. Decuzzi, J. M. Tour, F. Robertson, M. Ferrari, *Nat Nano* **2008**, 3, 151; l) J.-H. Park, L. Gu, G. von Maltzahn, E. Ruoslahti, S. N. Bhatia, M. J. Sailor, *Nat Mater* **2009**, 8, 331; m) J. S. Ananta, B. Godin, R. Sethi, L. Moriggi, X. Liu, R. E. Serda, R. Krishnamurthy, R. Muthupillai, R. D. Bolskar, L. Helm, M. Ferrari, L. J. Wilson, P. Decuzzi, *Nat Nano* **2010**, 5, 815.

[5]   a) A. Magasinski, P. Dixon, B. Hertzberg, A. Kvit, J. Ayala, G. Yushin, *Nat Mater* **2010**, 9, 353; b) H. Kim, B. Han, J. Choo, J. Cho, *Angewandte Chemie International Edition* **2008**, 47, 10151; c) A. T. Tesfaye, R. Gonzalez, J. L. Coffer, T. Djenizian, *ACS Applied Materials & Interfaces* **2015**, 7, 20495.

[6]   a) H. Bahruji, M. Bowker, P. R. Davies, *International Journal of Hydrogen Energy* **2009**, 34, 8504; b) F. Erogbogbo, T. Lin, P. M. Tucciarone, K. M. LaJoie, L. Lai, G. D. Patki, P. N. Prasad, M. T. Swihart, *Nano Letters* **2013**, 13, 451.

[7] J. Salonen, A. M. Kaukonen, J. Hirvonen, V. P. Lehto, *J. Pharm. Sci.* **2008**, 97, 632.

[8] S. H. C. Anderson, H. Elliott, D. J. Wallis, L. T. Canham, J. J. Powell, *Phys. Status Solidi* **2003**, 197, 331.

[9] a) R. Herino, G. Bomchil, K. Barla, C. Bertrand, J. L. Ginoux, *Journal of The Electrochemical Society* **1987**, 134, 1994; b) C. Chiappini, E. Tasciotti, J. R. Fakhoury, D. Fine, L. Pullan, Y.-C. Wang, L. Fu, X. Liu, M. Ferrari, *ChemPhysChem* **2010**, 11, 1029; c) B. Godin, C. Chiappini, S. Srinivasan, J. F. Alexander, K. Yokoi, M. Ferrari, P. Decuzzi, X. Liu, *Advanced Functional Materials* **2012**, 22, 4225.

[10] a) J. Riikonen, A. Correia, M. Kovalainen, S. Näkki, M. Lehtonen, J. Leppänen, J. Rantanen, W. Xu, F. Araújo, J. Hirvonen, K. Järvinen, H. A. Santos, V.-P. Lehto, *Biomaterials* **2015**, 52, 44; b) L. M. Bimbo, M. Sarparanta, E. Makila, T. Laaksonen, P. Laaksonen, J. Salonen, M. B. Linder, J. Hirvonen, A. J. Airaksinen, H. A. Santos, *Nanoscale* **2012**, 4, 3184.

[11] a) K. L. Jarvis, T. J. Barnes, C. A. Prestidge, *Advances in Colloid and Interface Science* **2012**, 175, 25; b) F. Dai, J. Zai, R. Yi, M. L. Gordin, H. Sohn, S. Chen, D. Wang, *Nature Communications* **2014**, 5, 3605.

[12] a) H. A. Santos, J. Riikonen, J. Salonen, E. Makila, T. Heikkila, T. Laaksonen, L. Peltonen, V.-P. Lehto, J. Hirvonen, *Acta Biomaterialia* **2010**, 6, 2721; b) H. A. Santos, J. Riikonen, T. Heikkila, J. Salonen, L. Peltonen, E. Makila, T. Laaksonen, N. Kumar, D. Murzin, V. P. Lehto, J. Hirvonen, *European Journal of Pharmaceutical Sciences* **2008**, 34, S36.

[13] a) N. Shrestha, M.-A. Shahbazi, F. Araujo, H. Zhang, E. M. Makila, J. Kauppila, B. Sarmento, J. J. Salonen, J. T. Hirvonen, H. A. Santos, *Biomaterials* **2014**, 35, 7172; b) N. Shrestha, F. Araújo, M.-A. Shahbazi, E. Mäkilä, M. J. Gomes, B. Herranz-Blanco, R.

Lindgren, S. Granroth, E. Kukk, J. Salonen, J. Hirvonen, B. Sarmento, H. A. Santos, *Advanced Functional Materials* **2016**, 26, 3405; c) D. Liu, L. M. Bimbo, E. M. Mäkilä, F. Villanova, M. Kaasalainen, B. Herranz-Blanco, C. M. Caramella, V. P. Lehto, J. Salonen, K. H. Herzig, J. T. Hirvonen, H. A. Santos, *Journal of Controlled Release* **2013**, 170, 268; d) H. Zhang, D. Liu, M. A. Shahbazi, E. M. Mäkilä, B. Herranz-Blanco, J. Salonen, J. T. Hirvonen, H. A. Santos, *Advanced Materials* **2014**, 26, 4497.

[14] a) B. Herranz-Blanco, D. Liu, E. Mäkilä, M.-A. Shahbazi, E. Ginestar, H. Zhang, V. Aseyev, V. Balasubramanian, J. Salonen, J. Hirvonen, H. A. Santos, *Advanced Functional Materials* **2015**, 25, 1488; b) D. Liu, H. Zhang, E. Mäkilä, J. Fan, B. Herranzblanco, C. F. Wang, R. Rosa, A. J. Ribeiro, J. Salonen, J. Hirvonen, *Biomaterials* **2015**, 39, 249.

[15] D. S. Roberts, D. Estrada, N. Yagi, E. J. Anglin, N. A. Chan, M. J. Sailor, *Part Part Syst Char* **2017**, 34.

[16] a) H. Alhmoud, B. Delalat, R. Elnathan, A. Cifuentes-Rius, A. Chaix, M.-L. Rogers, J.-O. Durand, N. H. Voelcker, *Advanced Functional Materials* **2015**, 25, 1137; b) R. Elnathan, B. Delalat, D. Brodoceanu, H. Alhmoud, F. J. Harding, K. Buehler, A. Nelson, L. Isa, T. Kraus, N. H. Voelcker, *Advanced Functional Materials* **2015**, 25, 7215.

[17] B. Pelaz, C. Alexiou, R. A. Alvarez-Puebla, F. Alves, A. M. Andrews, S. Ashraf, L. P. Balogh, L. Ballerini, A. Bestetti, C. Brendel, S. Bosi, M. Carril, W. C. W. Chan, C. Chen, X. Chen, X. Chen, Z. Cheng, D. Cui, J. Du, C. Dullin, A. Escudero, N. Feliu, M. Gao, M. George, Y. Gogotsi, A. Grünweller, Z. Gu, N. J. Halas, N. Hampp, R. K. Hartmann, M. C. Hersam, P. Hunziker, J. Jian, X. Jiang, P. Jungebluth, P. Kadhiresan, K. Kataoka, A. Khademhosseini, J. Kopeček, N. A. Kotov, H. F. Krug, D. S. Lee, C.-M. Lehr, K. W. Leong, X.-J. Liang, M. Ling Lim, L. M. Liz-Marzán, X. Ma, P. Macchiarini, H. Meng, H.

Möhwald, P. Mulvaney, A. E. Nel, S. Nie, P. Nordlander, T. Okano, J. Oliveira, T. H. Park, R. M. Penner, M. Prato, V. Puntes, V. M. Rotello, A. Samarakoon, R. E. Schaak, Y. Shen, S. Sjöqvist, A. G. Skirtach, M. G. Soliman, M. M. Stevens, H.-W. Sung, B. Z. Tang, R. Tietze, B. N. Udugama, J. S. VanEpps, T. Weil, P. S. Weiss, I. Willner, Y. Wu, L. Yang, Z. Yue, Q. Zhang, Q. Zhang, X.-E. Zhang, Y. Zhao, X. Zhou, W. J. Parak, *ACS Nano* **2017**, 11, 2313.

[18] E. Blanco, H. Shen, M. Ferrari, *Nat Biotech* **2015**, 33, 941.

[19] a) T. Tanaka, L. S. Mangala, P. E. Vivas-Mejia, R. Nieves-Alicea, A. P. Mann, E. Mora, H. D. Han, M. M. K. Shahzad, X. Liu, R. Bhavane, J. Gu, J. R. Fakhoury, C. Chiappini, C. Lu, K. Matsuo, B. Godin, R. L. Stone, A. M. Nick, G. Lopez-Berestein, A. K. Sood, M. Ferrari, *Cancer Research* **2010**, 70, 3687; b) K. Yokoi, B. Godin, C. J. Oborn, J. F. Alexander, X. Liu, I. J. Fidler, M. Ferrari, *Cancer Letters* **2013**, 334, 319; c) P. V. Almeida, M.-A. Shahbazi, A. Correia, E. Mäkilä, M. Kemell, J. Salonen, J. Hirvonen, H. A. Santos, *Nanomedicine* **2017**.

[20] M. Zhang, R. Xu, X. Xia, Y. Yang, J. Gu, G. Qin, X. Liu, M. Ferrari, H. Shen, *Biomaterials* **2014**, 35, 423.

[21] a) I. K. Yazdi, M. B. Murphy, C. Loo, X. Liu, M. Ferrari, B. K. Weiner, E. Tasciotti, *Journal of Tissue Engineering* **2014**, 5, 2041731414536573; b) F. Peng, Y. Su, X. Wei, Y. Lu, Y. Zhou, Y. Zhong, S.-T. Lee, Y. He, *Angewandte Chemie International Edition* **2013**, 52, 1457; c) S. Müller, A. Cavallaro, K. Vasilev, N. H. Voelcker, H. Schönherr, *Macromolecular Chemistry and Physics* **2016**, 217, 2243; d) M.-A. Shahbazi, P. V. Almeida, A. Correia, B. Herranz-Blanco, N. Shrestha, E. Mäkilä, J. Salonen, J. Hirvonen, H. A. Santos, *Journal of Controlled Release* **2017**, 249, 111; e) L. M. Bimbo, O. V. Denisova, E. Makila, M. Kaasalainen, J. K. De Brabander, J. Hirvonen, J. Salonen, L.

Kakkola, D. Kainov, H. A. Santos, *ACS Nano* **2013**, 7, 6884; f) L. M. Bimbo, E. Makila,

T. Laaksonen, V.-P. Lehto, J. Salonen, J. Hirvonen, H. A. Santos, *Biomaterials* **2011**, 32,

2625; g) L. M. Bimbo, E. Mäkilä, J. Raula, T. Laaksonen, P. Laaksonen, K. Strommer, E.

I. Kauppinen, J. Salonen, M. B. Linder, J. Hirvonen, H. A. Santos, *Biomaterials* **2011**,

32, 9089; h) P. Kinnari, E. Makila, T. Heikkila, J. Salonen, J. Hirvonen, H. A. Santos,

International Journal of Pharmaceutics **2011**, 414, 148.

[22] F. Araujo, N. Shrestha, M.-A. Shahbazi, P. Fonte, E. M. Makila, J. J. Salonen, J. T.

Hirvonen, P. L. Granja, H. A. Santos, B. Sarmento, *Biomaterials* **2014**, 35, 9199.

[23] a) B. Scott, J. Shen, S. Nizzero, K. Boom, S. Persano, Y. Mi, X. Liu, Y. Zhao, E. Blanco,

H. Shen, M. Ferrari, J. Wolfram, *Pharmacological Research* **2016**, 111, 413; b) S.

Minardi, M. Sandri, J. O. Martinez, I. K. Yazdi, X. Liu, M. Ferrari, B. K. Weiner, A.

Tampieri, E. Tasciotti, *Small* **2014**, 10, 3943; c) S. J. P. McInnes, C. T. Turner, S. A. Al-

Bataineh, M. J. I. Airaghi Leccardi, Y. Irani, K. A. Williams, A. J. Cowin, N. H.

Voelcker, *Journal of Materials Chemistry B* **2015**, 3, 4123.

[24] a) J. Shen, R. Xu, J. Mai, H.-C. Kim, X. Guo, G. Qin, Y. Yang, J. Wolfram, C. Mu, X.

Xia, J. Gu, X. Liu, Z.-W. Mao, M. Ferrari, H. Shen, *ACS Nano* **2013**, 7, 9867; b) Y. Mi,

C. Mu, J. Wolfram, Z. Deng, T. Y. Hu, X. Liu, E. Blanco, H. Shen, M. Ferrari, *Advanced

Healthcare Materials* **2016**, 5, 936; c) J. Shen, X. Wu, Y. Lee, J. Wolfram, Z. Yang, Z.-

W. Mao, M. Ferrari, H. Shen, *JoVE (Journal of Visualized Experiments)* **2015**, e52075.

[25] a) A. Gizzatov, J. Key, S. Aryal, J. Ananta, A. Cervadoro, A. L. Palange, M. Fasano, C.

Stigliano, M. Zhong, D. Di Mascolo, A. Guven, E. Chiavazzo, P. Asinari, X. Liu, M.

Ferrari, L. J. Wilson, P. Decuzzi, *Advanced Functional Materials* **2014**, 24, 4584; b) R.

E. Serda, A. MacK, M. Pulikkathara, A. M. Zaske, C. Chiappini, J. R. Fakhoury, D.

Webb, B. Godin, J. L. Conyers, X. W. Liu, J. A. Bankson, M. Ferrari, *Small* **2010**, 6,

1329; c) E. Blanco, T. Sangai, A. Hsiao, S. Ferrati, L. Bai, X. Liu, F. Meric-Bernstam, M. Ferrari, *Cancer Letters* **2013**, 334, 245; d) T. Tanei, F. Leonard, X. Liu, J. F. Alexander, Y. Saito, M. Ferrari, B. Godin, K. Yokoi, *Cancer Research* **2016**, 76, 429; e) C. Chiappini, J. O. Martinez, E. De Rosa, C. S. Almeida, E. Tasciotti, M. M. Stevens, *ACS Nano* **2015**, 9, 5500.

[26] a) A. P. Mann, P. Scodeller, S. Hussain, J. Joo, E. Kwon, G. B. Braun, T. Mölder, Z.-G. She, V. R. Kotamraju, B. Ranscht, S. Krajewski, T. Teesalu, S. Bhatia, M. J. Sailor, E. Ruoslahti, *Nature Communications* **2016**, 7, 11980; b) J. O. Martinez, M. Evangelopoulos, V. Karun, E. Shegog, J. A. Wang, C. Boada, X. Liu, M. Ferrari, E. Tasciotti, *Biomaterials* **2014**, 35, 9824.

[27] K. Tamarov, W. Xu, L. Osminkina, S. Zinovyev, P. Soininen, A. Kudryavtsev, M. Gongalsky, A. Gaydarova, A. Närvänen, V. Timoshenko, V.-P. Lehto, *Journal of Controlled Release* **2016**, 241, 220.

[28] N. Shrestha, M. A. Shahbazi, F. Araújo, E. Mäkilä, J. Raula, E. I. Kauppinen, J. Salonen, B. Sarmento, J. Hirvonen, H. A. Santos, *Biomaterials* **2015**, 68, 9.

[29] a) J. Couzin-Frankel, *Science* **2013**, 342, 1432; b) F. S. Hodi , S. J. O'Day , D. F. McDermott , R. W. Weber , J. A. Sosman , J. B. Haanen , R. Gonzalez , C. Robert , D. Schadendorf , J. C. Hassel , W. Akerley , A. J. M. van den Eertwegh , J. Lutzky , P. Lorigan , J. M. Vaubel , G. P. Linette , D. Hogg , C. H. Ottensmeier , C. Lebbé , C. Peschel , I. Quirt , J. I. Clark , J. D. Wolchok , J. S. Weber , J. Tian , M. J. Yellin , G. M. Nichol , A. Hoos , W. J. Urba *New England Journal of Medicine* **2010**, 363, 711; c) S. A. Grupp, M. Kalos, D. Barrett, R. Aplenc, D. L. Porter, S. R. Rheingold, D. T. Teachey, A. Chew, B. Hauck, J. F. Wright, M. C. Milone, B. L. Levine, C. H. June, *New England*

Journal of Medicine **2013**, 368, 1509; d) E. I. Buchbinder, F. S. Hodi, *Nat Rev Clin Oncol* **2016**, 13, 77.

[30] C. Wang, Y. Ye, Q. Hu, A. Bellotti, Z. Gu, *Adv Mater* **2017**.

[31] M. A. Shahbazi, T. D. Fernandez, E. M. Makila, X. Le Guevel, C. Mayorga, M. H. Kaasalainen, J. J. Salonen, J. T. Hirvonen, H. A. Santos, *Biomaterials* **2014**, 35, 9224.

[32] M.-A. Shahbazi, N. Shrestha, E. Mäkilä, F. Araújo, A. Correia, T. Ramos, B. Sarmento, J. Salonen, J. Hirvonen, H. A. Santos, *Nano Research* **2015**, 8, 1505.

[33] a) T. Sun, Y. S. Zhang, B. Pang, D. C. Hyun, M. Yang, Y. Xia, *Angewandte Chemie International Edition* **2014**, 53, 12320; b) V. Castagnola, J. Cookman, J. M. de Araujo, E. Polo, Q. Cai, C. P. Silveira, Z. Krpetic, Y. Yan, L. Boselli, K. A. Dawson, *Nanoscale Horizons* **2017**, 2, 187; c) L. Talamini, M. B. Violatto, Q. Cai, M. P. Monopoli, K. Kantner, Ž. Krpetić, A. Perez-Potti, J. Cookman, D. Garry, C. P. Silveira, L. Boselli, B. Pelaz, T. Serchi, S. Cambier, A. C. Gutleb, N. Feliu, Y. Yan, M. Salmona, W. J. Parak, K. A. Dawson, P. Bigini, *ACS Nano* **2017**, 11, 5519.

[34] a) R. A. Bley, S. M. Kauzlarich, J. E. Davis, H. W. H. Lee, *Chemistry of Materials* **1996**, 8, 1881; b) J. L. Heinrich, C. L. Curtis, G. M. Credo, M. J. Sailor, K. L. Kavanagh, *Science* **1992**, 255, 66; c) Z. Qin, J. Joo, L. Gu, M. J. Sailor, *Part Part Syst Char* **2014**, 31, 252.

[35] a) C. Lam, Y. F. Zhang, Y. H. Tang, C. S. Lee, I. Bello, S. T. Lee, *J Cryst Growth* **2000**, 220, 466; b) J. Salonen, L. Laitinen, A. M. Kaukonen, J. Tuura, M. Bjorkqvist, T. Heikkila, K. Vaha-Heikkila, J. Hirvonen, V. P. Lehto, *Journal of Controlled Release* **2005**, 108, 362.

[36] H. A. Santos, *Porous silicon for biomedical applications*, 2014.

[37] L. Russo, F. Colangelo, R. Cioffi, I. Rea, L. D. Stefano, *Materials* **2011**, 4, 1023.

[38] M. J. Sailor, *Porous Silicon in Practice: Preparation, Characterization and Applications*, 2012.

[39] K. L. Jarvis, T. J. Barnes, C. A. Prestidge, *Langmuir* **2008**, 24, 14222.

[40] N. Stevulova, T. Suzuki, M. Senna, M. Balintova, V. Sepelak, K. Tkacova, *Solid State Ionics* **1997**, 101, 681.

[41] L. P. Verdoni, M. J. Fink, B. S. Mitchell, *Chem Eng J* **2011**, 172, 591.

[42] A. C. Silva, E. Gonzalez-Mira, M. L. Garcia, M. A. Egea, J. Fonseca, R. Silva, D. Santos, E. B. Souto, D. Ferreira, *Colloid Surface B* **2011**, 86, 158.

[43] J.-M. Lim, A. Swami, L. M. Gilson, S. Chopra, S. Choi, J. Wu, R. Langer, R. Karnik, O. C. Farokhzad, *ACS Nano* **2014**, 8, 6056.

[44] E. J. Anglin, L. Cheng, W. R. Freeman, M. J. Sailor, *Adv. Drug Delivery Rev.* **2008**, 60, 1266.

[45] a) N. Wareing, K. Szymanski, G. R. Akkaraju, A. Loni, L. T. Canham, R. Gonzalez-Rodriguez, J. L. Coffer, *Small* **2017**, 13, 1602739; b) C.-C. Wu, Y. Hu, M. Miller, R. V. Aroian, M. J. Sailor, *ACS Nano* **2015**, 9, 6158.

[46] a) A. S.-W. Goh, A. Y.-F. Chung, R. H.-G. Lo, T.-N. Lau, S. W.-K. Yu, M. Chng, S. Satchithanantham, S. L.-E. Loong, D. C.-E. Ng, B.-C. Lim, *International Journal of Radiation Oncology* Biology* Physics* **2007**, 67, 786; b) P. Ross, J. Meenan, M. O'Doherty, J. Calara, D. Palmer, S. Heatley, P. Chow, "Novel delivery via endoscopic ultrasound of a 32 P brachytherapy device in addition to gemcitabine in advanced pancreatic cancer", presented at *ASCO Gastronintest. Cancer Symp*, 2008.

[47] a) A. Venuta, J. Wolfram, H. Shen, M. Ferrari, *Journal of Materials Chemistry B* **2017**, 5, 207; b) J. M. Kinsella, S. Ananda, J. S. Andrew, J. F. Grondek, M.-P. Chien, M. Scadeng, N. C. Gianneschi, E. Ruoslahti, M. J. Sailor, *Advanced Materials* **2011**, 23, H248; c) M.

Hasanzadeh Kafshgari, B. Delalat, F. J. Harding, A. Cavallaro, E. Makila, J. Salonen, K. Vasilev, N. H. Voelcker, *Journal of Materials Chemistry B* **2016**, 4, 2051.

[48] a) B. Xia, B. Wang, J. Shi, Y. Zhang, Q. Zhang, Z. Chen, J. Li, *Acta Biomaterialia* **2017**, 51, 197; b) T. Yong, J. Hu, X. Zhang, F. Li, H. Yang, L. Gan, X. Yang, *ACS Applied Materials & Interfaces* **2016**, 8, 27611; c) Y. Wan, S. Apostolou, R. Dronov, B. Kuss, N. H. Voelcker, *Nanomedicine* **2014**, 9, 2309.

[49] A. B. Foraker, R. J. Walczak, M. H. Cohen, T. A. Boiarski, C. F. Grove, P. W. Swaan, *Pharmaceutical Research* **2003**, 20, 110.

[50] a) M. A. Tolli, M. P. A. Ferreira, S. M. Kinnunen, J. Rysa, E. M. Makila, Z. Szabo, R. E. Serpi, P. J. Ohukainen, M. J. Valimaki, A. M. R. Correia, J. J. Salonen, J. T. Hirvonen, H. J. Ruskoaho, H. A. Santos, *Biomaterials* **2014**, 35, 8394; b) G. U. Ruiz-Esparza, V. Segura-Ibarra, A. M. Cordero-Reyes, K. A. Youker, R. E. Serda, A. S. Cruz-Solbes, J. Amione-Guerra, K. Yokoi, D. K. Kirui, F. E. Cara, J. Paez-Mayorga, J. H. Flores-Arredondo, C. E. Guerrero-Beltrán, G. Garcia-Rivas, M. Ferrari, E. Blanco, G. Torre-Amione, *European Journal of Heart Failure* **2016**, 18, 169.

[51] a) F. Fontana, M. Mori, F. Riva, E. Mäkilä, D. Liu, J. Salonen, G. Nicoletti, J. Hirvonen, C. Caramella, H. A. Santos, *ACS Applied Materials & Interfaces* **2015**; b) C. T. Turner, S. J. P. McInnes, E. Melville, A. J. Cowin, N. H. Voelcker, *Advanced Healthcare Materials* **2017**, 6, 1600707; c) R. B. Vasani, E. J. Szili, G. Rajeev, N. H. Voelcker, *Chemistry – An Asian Journal* **2017**, n/a; d) M. Mori, P. V. Almeida, M. Cola, G. Anselmi, E. Makila, A. Correia, J. Salonen, J. Hirvonen, C. Caramella, H. A. Santos, *European Journal of Pharmaceutics and Biopharmaceutics* **2014**, 88, 635.

[52] a) P. Decuzzi, R. Pasqualini, W. Arap, M. Ferrari, *Pharmaceutical Research* **2008**, 26, 235; b) G. Adriani, M. D. de Tullio, M. Ferrari, F. Hussain, G. Pascazio, X. Liu, P.

Decuzzi, *Biomaterials* **2012**, 33, 5504; c) A. L. van de Ven, P. Kim, O. H. Haley, J. R. Fakhoury, G. Adriani, J. Schmulen, P. Moloney, F. Hussain, M. Ferrari, X. Liu, S.-H. Yun, P. Decuzzi, *Journal of Controlled Release* **2012**, 158, 148; d) R. D'Apolito, G. Tomaiuolo, F. Taraballi, S. Minardi, D. Kirui, X. Liu, A. Cevenini, R. Palomba, M. Ferrari, F. Salvatore, E. Tasciotti, S. Guido, *Journal of Controlled Release* **2015**, 217, 263.

[53] a) J. O. Martinez, A. Parodi, X. Liu, M. G. Kolonin, M. Ferrari, E. Tasciotti, *Small* **2013**, 9, 1696; b) J. O. Martinez, C. Boada, I. K. Yazdi, M. Evangelopoulos, B. S. Brown, X. Liu, M. Ferrari, E. Tasciotti, *Small* **2013**, 9, 1722; c) T. Tanaka, B. Godin, R. Bhavane, R. Nieves-Alicea, J. Gu, X. Liu, C. Chiappini, J. R. Fakhoury, S. Amra, A. Ewing, Q. Li, I. J. Fidler, M. Ferrari, *International Journal of Pharmaceutics* **2010**, 402, 190.

[54] a) B. Godin, J. Gu, R. E. Serda, S. Ferrati, X. Liu, C. Chiappini, T. Tanaka, P. Decuzzi, M. Ferrari, *Controlled release newsletter / Controlled Release Society* **2008**, 25, 9; b) J. O. Martinez, M. Evangelopoulos, C. Chiappini, X. Liu, M. Ferrari, E. Tasciotti, *Journal of Biomedical Materials Research Part A* **2014**, 102, 3540; c) J. O. Martinez, C. Chiappini, A. Ziemys, A. M. Faust, M. Kojic, X. Liu, M. Ferrari, E. Tasciotti, *Biomaterials* **2013**, 34, 8469; d) B. Godin, J. Gu, R. E. Serda, R. Bhavane, E. Tasciotti, C. Chiappini, X. Liu, T. Tanaka, P. Decuzzi, M. Ferrari, *Journal of Biomedical Materials Research Part A* **2010**, 94A, 1236; e) E. Tasciotti, B. Godin, J. O. Martinez, C. Chiappini, R. Bhavane, X. Liu, M. Ferrari, *Molecular Imaging* **2011**, 10, 56.

[55] O. M. Jonathan, E. Michael, B. Rohan, A. Stefania, S. Francesco, L. Xuewu, F. Mauro, T. Ennio, *Current Drug Targets* **2015**, 16, 1582.

[56] Z. Deng, Y. Li, J. Fan, G. Wang, Y. Li, Y. Zhang, G. Cai, H. Shen, M. Ferrari, T. Y. Hu, *Scientific Reports* **2015**, 5.

[57] R. Xu, Y. Huang, J. Mai, G. Zhang, X. Guo, X. Xia, E. J. Koay, G. Qin, D. R. Erm, Q. Li, X. Liu, M. Ferrari, H. Shen, *Small* **2013**, 9, 1799.

[58] a) A. P. Mann, T. Tanaka, A. Somasunderam, X. Liu, D. G. Gorenstein, M. Ferrari, *Advanced Materials* **2011**, 23, H278; b) H. Shen, C. Rodriguez-Aguayo, R. Xu, V. Gonzalez-Villasana, J. Mai, Y. Huang, G. Zhang, X. Guo, L. Bai, G. Qin, X. Deng, Q. Li, D. R. Erm, B. Aslan, X. Liu, J. Sakamoto, A. Chavez-Reyes, H. D. Han, A. K. Sood, M. Ferrari, G. Lopez-Berestein, *Clinical Cancer Research* **2013**, 19, 1806.

[59] M. P. Scavo, E. Gentile, J. Wolfram, J. Gu, M. Barone, M. Evangelopoulos, J. O. Martinez, X. Liu, C. Celia, E. Tasciotti, E. Vilar, H. Shen, *Colloids and Surfaces B: Biointerfaces* **2015**, 136, 694.

[60] J. Mai, Y. Huang, C. Mu, G. Zhang, R. Xu, X. Guo, X. Xia, D. E. Volk, G. L. Lokesh, V. Thiviyanathan, D. G. Gorenstein, X. Liu, M. Ferrari, H. Shen, *Journal of Controlled Release* **2014**, 187, 22.

[61] B. Godin, E. Tasciotti, X. Liu, R. E. Serda, M. Ferrari, *Accounts of Chemical Research* **2011**, 44, 979.

[62] W. Li, Z. Jan, Y. Ding, Y. Liu, C. Janko, M. Pischetsrieder, C. Alexiou, A. R. Boccaccini, *Scientific Reports* **2016**, 6, 23140.

[63] M. S. Gerstel, V. A. Place, *US Patent US3964482 A*, 1976.

[64] S. Hashmi, P. Ling, G. Hashmi, M. Reed, R. Gaugler, W. Trimmer, *BioTechniques* **1995**, 19, 766.

[65] S. Henry, D. V. McAllister, M. G. Allen, M. R. Prausnitz, *Journal of Pharmaceutical Sciences* **1998**, 87, 922.

[66] a) G. Ma, C. Wu, *Journal of Controlled Release* **2017**, 251, 11; b) R. Elnathan, M. Kwiat, F. Patolsky, N. H. Voelcker, *Nano Today* **2014**, 9, 172; c) K. van der Maaden, R. Luttge,

P. J. Vos, J. Bouwstra, G. Kersten, I. Ploemen, *Drug Delivery and Translational Research* **2015**, 5, 397.

[67] a) S. W. Han, C. Nakamura, I. Obataya, N. Nakamura, J. Miyake, *Biosensors and Bioelectronics* **2005**, 20, 2120; b) W. Kim, J. K. Ng, M. E. Kunitake, B. R. Conklin, P. Yang, *Journal of the American Chemical Society* **2007**, 129, 7228; c) A. K. Shalek, J. T. Robinson, E. S. Karp, J. S. Lee, D.-R. Ahn, M.-H. Yoon, A. Sutton, M. Jorgolli, R. S. Gertner, T. S. Gujral, G. MacBeath, E. G. Yang, H. Park, *Proceedings of the National Academy of Sciences* **2010**, 107, 1870.

[68] a) S. Rajaraman, H. T. Henderson, *Sensors and Actuators B: Chemical* **2005**, 105, 443; b) K. B. Vinayakumar, G. M. Hegde, M. M. Nayak, N. S. Dinesh, K. Rajanna, *Microelectronic Engineering* **2014**, 128, 12.

[69] a) J. Jing, E. H. T. Francis, M. Jianmin, I. Ciprian, *Journal of Micromechanics and Microengineering* **2006**, 16, 958; b) F. Gentile, M. L. Coluccio, R. P. Zaccaria, M. Francardi, G. Cojoc, G. Perozziello, R. Raimondo, P. Candeloro, E. Di Fabrizio, *Nanoscale* **2014**, 6, 8208; c) C. Chiappini, X. Liu, J. R. Fakhoury, M. Ferrari, *Advanced Functional Materials* **2010**, 20, 2231.

[70] B. Chen, J. Wei, F. E. H. Tay, Y. T. Wong, C. Iliescu, *Microsystem Technologies* **2008**, 14, 1015.

[71] C. Iliescu, B. Chen, J. Wei, Z. Yue, in *2009 International Semiconductor Conference*, Vol. 1, Sinaia; Romania 2009, 203.

[72] a) M. G. Allen, M. R. Prausnitz, D. V. McAllister, F. P. M. Cros, *US6334856 B1*, 2002; b) L. T. Canham, *US6770480 B1*, 2004; c) R. Lüttge, S. N. Bystrova, B. J. G. Van, M. Domanski, P. W. H. Loeters, R. G. H. Lammertink, A. J. A. Winnubst, *US 8603384 B2*, 2009; d) D. Scholten, M. Stumber, F. Laermer, A. Feyh, 2015.

[73] K. S. Brammer, C. Choi, S. Oh, C. J. Cobb, L. S. Connelly, M. Loya, S. D. Kong, S. Jin, *Nano Letters* **2009**, 9, 3570.

[74] a) C. Chiappini, P. Campagnolo, C. S. Almeida, N. Abbassi-Ghadi, L. W. Chow, G. B. Hanna, M. M. Stevens, *Advanced Materials* **2015**, 27, 5147; b) H. Z. Alhmoud, T. M. Guinan, R. Elnathan, H. Kobus, N. H. Voelcker, *Analyst* **2014**, 139, 5999.

[75] L. Vaccari, D. Canton, N. Zaffaroni, R. Villa, M. Tormen, E. D. Fabrizio, *Microelectron. Eng.* **2006**, 83, 1598.

[76] Q. Shabir, K. Webb, D. K. Nadarassan, A. Loni, L. T. Canham, M. Terracciano, L. De Stefano, I. Rea, *Silicon* **2017**, 1.

[77] S. M. Haidary, E. P. Córcoles, N. K. Ali, *Journal of Nanomaterials* **2012**, 2012.

[78] a) D. Kovalev, E. Gross, J. Diener, V. Y. Timoshenko, M. Fujii, *Appl. Phys. Lett.* **2004**, 85, 3590; b) S. P. Low, K. A. Williams, L. T. Canham, N. H. Voelcker, *Journal of Biomedical Materials Research Part A* **2010**, 93A, 1124.

[79] a) A. E. Pap, K. Kordás, G. Tóth, J. Levoska, A. Uusimäki, J. Vähäkangas, S. Leppävuori, T. F. George, *Appl. Phys. Lett.* **2005**, 86, 1; b) K. H. Wu, C. W. Li, J. H. Liu, *Microelectron. Eng.* **2015**, 148, 70; c) G. Aggarwal, P. Mishra, B. Joshi, Harsh, S. S. Islam, *J. Porous Mater.* **2014**, 21, 23; d) Andrea Edit Pap, Krisztián Kordás, Thomas F. George, S. Leppävuori, *J. Phys. Chem. B* **2004**, 108, 12744.

[80] D. T. Cao, L. T. Q. Ngan, C. T. Anh, *Surf. Interface Anal.* **2013**, 45, 762.

[81] J. F. Wang, J. S. Chen, Z. F. Zhou, *Eur. J. Inorg. Chem.* **2015**, 2015, 1330.

[82] A. Loni, L. Batchelor, E. Caffull, L. Canham, *ECS J. Solid State Sci. Technol.* **2015**, 4, P149.

[83] J. E. Bateman, R. D. Eagling, B. R. Horrocks, A. Houlton, D. R. Worrall, *Chem. Commun.* **1997**, 23, 2275.

[84] J. Salonen, M. Björkqvist, E. Laine, L. Niinistö, *Appl. Surf. Sci.* **2004**, 225, 389.

[85] E. Mäkilä, L. M. Bimbo, M. Kaasalainen, B. Herranz, A. J. Airaksinen, M. Heinonen, E. Kukk, J. Hirvonen, H. A. Santos, J. Salonen, *Langmuir* **2012**, 28, 14045.

[86] V. A. Makara, N. I. Klyui, A. G. Rozhin, V. G. Litovchenko, Y. P. Piryatinskii, O. B. Korneta, *Phys. Status Solidi* **2003**, 197, 355.

[87] M. Björkqvist, J. Salonen, E. Laine, *Appl. Surf. Sci.* **2004**, 222, 269.

[88] B. M. Kostishko, Y. S. Nagornov, S. Y. Salomatin, S. R. Atazhanov, *Tech. Phys. Lett.* **2004**, 30, 88.

[89] J. M. Buriak, M. P. Stewart, M. J. Allen, *Mrs Proc.* **1998**, 536, 173.

[90] a) R. Boukherroub, J. Wojtyk, D. D. Wayner, D. J. Lockwood, *J. Electrochem. Soc.* **2002**, 149, H59; b) J. C. Small, H. M. Dam, J. L. Siegel, A. J. Crepinsek, T. A. Neal, A. A. Althoff, N. S. Line, L. A. P. Jr, *Polyhedron* **2016**, 114, 225; c) D. Dattilo, L. Armelao, G. Fois, G. Mistura, M. Maggini, *Langmuir* **2007**, 23, 12945; d) S. A. Alekseev, †, V. Lysenko, a. V. N. Zaitsev, D. Barbier‡, *J. Phys. Chem. C* **2007**, 111, 15217; e) Jillian M. Buriak, †, Michael P. Stewart, Todd W. Geders, Matthew J. Allen, Hee Cheul Choi, Jay Smith, Daniel Raftery, † and, Leigh T. Canham, *J. Am. Chem. Soc.* **2015**, 121, 11491.

[91] a) J. Rytkönen, R. Miettinen, M. Kaasalainen, V. P. Lehto, J. Salonen, A. Närvänen, *J. Nanomater.* **2012**, 2012, 4873; b) J. M. B. And, M. J. Allen, *J. Am. Chem. Soc.* **2012**, 120, 1339; c) A. Petit, M. Delmotte, A. Loupy, J. N. Chazalviel, F. Ozanam, R. Boukherroub, *J. Phys. Chem. C* **2008**, 112, 16622.

[92] M. J. Sweetman, C. J. Shearer, J. G. Shapter, N. H. Voelcker, *Langmuir* **2011**, 27, 9497.

[93] a) T. Kumeria, M. I. Sjp, S. Maher, A. Santos, *Expert Opin. Drug Delivery* **2017**, 11, 1; b) P. A. Kulyavtsev, R. P. Spencer, *Pharm. Pat. Anal.* **2017**, 6, 77; c) H. Shen, J. You, G.

Zhang, A. Ziemys, Q. Li, L. Bai, X. Deng, D. R. Erm, X. Liu, C. Li, M. Ferrari, *Adv. Healthcare Mater.* **2012**, 1, 84.

[94] D. Liu, B. Herranz-Blanco, E. M. Mäkilä, L. R. Arriaga, S. Mirza, D. A. Weitz, N. Sandler, J. Salonen, J. T. Hirvonen, H. A. Santos, *ACS Applied Materials & Interfaces* **2013**, 5, 12127.

[95] C. F. Wang, E. M. Mäkilä, M. H. Kaasalainen, D. Liu, M. P. Sarparanta, A. J. Airaksinen, J. J. Salonen, J. T. Hirvonen, H. A. Santos, *Biomaterials* **2014**, 35, 1257.

[96] P. V. Almeida, M. A. Shahbazi, E. Mäkilä, M. Kaasalainen, J. Salonen, J. Hirvonen, H. A. Santos, *Nanoscale* **2014**, 6, 10377.

[97] C.-F. Wang, E. M. Mäkilä, C. Bonduelle, J. Rytkönen, J. Raula, S. Almeida, A. Närvänen, J. J. Salonen, S. Lecommandoux, J. T. Hirvonen, H. A. Santos, *ACS Applied Materials & Interfaces* **2015**, 7, 2006.

[98] C. F. Wang, E. M. Mäkilä, M. H. Kaasalainen, M. V. Hagström, J. J. Salonen, J. T. Hirvonen, H. A. Santos, *Acta Biomaterialia* **2015**.

[99] F. Kong, X. Zhang, H. B. Zhang, X. M. Qu, D. Chen, M. Servos, E. Makila, J. Salonen, H. A. Santos, M. T. Hai, D. A. Weitz, *Advanced Functional Materials* **2015**, 25, 3330.

[100] Z. Liu, V. Balasubramanian, C. Bhat, M. Vahermo, E. Mäkilä, M. Kemell, F. Fontana, A. Janoniene, V. Petrikaite, J. Salonen, *Adv. Healthcare Mater.* **2016**, 6, 1601009.

[101] A. Correia, M. A. Shahbazi, E. M. Mäkilä, S. Almeida, J. J. Salonen, J. T. Hirvonen, H. A. Santos, *ACS Appl. Mater. Interfaces* **2015**, 7, 23197.

[102] W. Xu, R. Thapa, D. Liu, T. Nissinen, S. Granroth, A. Närvänen, M. Suvanto, H. A. Santos, V.-P. Lehto, *Molecular Pharmaceutics* **2015**.

[103] F. Zhang, A. Correia, E. Mäkilä, W. Li, J. Salonen, J. J. Hirvonen, H. Zhang, H. l. A. Santos, *ACS Appl. Mater. Interfaces* **2017**, 9, 10034.

[104] A. Janoniene, Z. Liu, L. Baranauskiene, E. Mäkilä, M. Ming, J. Salonen, J. Hirvonen, H. Zhang, V. Petrikaite, H. A. Santos, *ACS Appl. Mater. Interfaces* **2017**.

[105] E. Secret, K. Smith, V. Dubljevic, E. Moore, P. Macardle, B. Delalat, M.-L. Rogers, T. G. Johns, J.-O. Durand, F. Cunin, N. H. Voelcker, *Advanced Healthcare Materials* **2013**, 2, 718.

[106] E. Secret, M. Maynadier, A. Gallud, M. Gary-Bobo, A. Chaix, E. Belamie, P. Maillard, M. J. Sailor, M. Garcia, J.-O. Durand, F. Cunin, *Chemical Communications* **2013**, 49, 4202.

[107] B. Xia, B. Wang, W. Zhang, J. Shi, *RSC Advances* **2015**, 5, 44660.

[108] N. Z. Knezevic, V. Stojanovic, A. Chaix, E. Bouffard, K. E. Cheikh, A. Morere, M. Maynadier, G. Lemercier, M. Garcia, M. Gary-Bobo, J.-O. Durand, F. Cunin, *Journal of Materials Chemistry B* **2016**, 4, 1337.

[109] S. M. Haidary, A. B. Mohammed, E. P. Córcoles, N. K. Ali, M. R. Ahmad, *Microelectronic Engineering* **2016**, 161, 1.

[110] B. Xia, B. Wang, Z. Chen, Q. Zhang, J. Shi, *Advanced Materials Interfaces* **2016**, 3, n/a.

[111] M. Hasanzadeh Kafshgari, M. Alnakhli, B. Delalat, S. Apostolou, F. J. Harding, E. Makila, J. J. Salonen, B. J. Kuss, N. H. Voelcker, *Biomaterials Science* **2015**, 3, 1555.

[112] M. P. Ferreira, S. Ranjan, A. M. Correia, E. M. Mäkilä, S. M. Kinnunen, H. Zhang, M. A. Shahbazi, P. V. Almeida, J. J. Salonen, H. J. Ruskoaho, *Biomaterials* **2016**, 94, 93.

[113] C. T. Turner, M. Hasanzadeh Kafshgari, E. Melville, B. Delalat, F. Harding, E. Mäkilä, J. J. Salonen, A. J. Cowin, N. H. Voelcker, *ACS Biomaterials Science & Engineering* **2016**, 2, 2339.

[114] D. Liu, E. M. Mäkilä, H. Zhang, B. Herranz, M. Kaasalainen, P. Kinnari, J. Salonen, J. T. Hirvonen, H. A. Santos, *Advanced Functional Materials* **2013**, 23, 1893.

[115] B. Herranz-Blanco, L. R. Arriaga, E. Makila, A. Correia, N. Shrestha, S. Mirza, D. A. Weitz, J. Salonen, J. Hirvonen, H. A. Santos, *Lab on a Chip* **2014**, 14, 1083.

[116] L. Gu, J.-H. Park, K. H. Duong, E. Ruoslahti, M. J. Sailor, *Small* **2010**, 6, 2546.

[117] Y. Mi, J. Wolfram, C. Mu, X. Liu, E. Blanco, H. Shen, M. Ferrari, *Pharmacological Research* **2016**, 113, Part A, 92.

[118] T. Kim, G. B. Braun, Z.-g. She, S. Hussain, E. Ruoslahti, M. J. Sailor, *ACS Applied Materials & Interfaces* **2016**, 8, 30449.

[119] a) E. C. Wu, J. S. Andrew, A. Buyanin, J. M. Kinsella, M. J. Sailor, *Chemical Communications* **2011**, 47, 5699; b) H. Hou, K. Huffman, S. Rios, W. R. Freeman, M. J. Sailor, L. Cheng, *Investigative Ophthalmology & Visual Science* **2015**, 56, 2755.

[120] K. Nan, F. Ma, H. Hou, W. R. Freeman, M. J. Sailor, L. Cheng, *Acta Biomaterialia* **2014**, 10, 3505.

[121] H. Hou, C. Wang, K. Nan, W. R. Freeman, M. J. Sailor, L. Cheng, *Investigative Ophthalmology & Visual Science* **2016**, 57, 557.

[122] H. Hou, A. Nieto, A. Belghith, K. Nan, Y. Li, W. R. Freeman, M. J. Sailor, L. Cheng, *Acta Biomaterialia* **2015**, 24, 309.

[123] N. L. Fry, G. R. Boss, M. J. Sailor, *Chemistry of Materials* **2014**, 26, 2758.

[124] J. Kang, J. Joo, E. J. Kwon, M. Skalak, S. Hussain, Z.-G. She, E. Ruoslahti, S. N. Bhatia, M. J. Sailor, *Advanced Materials* **2016**, 28, 7962.

[125] J. Joo, E. J. Kwon, J. Kang, M. Skalak, E. J. Anglin, A. P. Mann, E. Ruoslahti, S. N. Bhatia, M. J. Sailor, *Nanoscale Horiz.* **2016**, 1.

[126] S. Minardi, B. Corradetti, F. Taraballi, J. H. Byun, F. Cabrera, X. Liu, M. Ferrari, B. K. Weiner, E. Tasciotti, *Annals of Biomedical Engineering* **2016**, 44, 2008.

[127] S. Minardi, L. Pandolfi, F. Taraballi, X. Wang, E. De Rosa, Z. D. Mills, X. Liu, M. Ferrari, E. Tasciotti, *ACS Applied Materials & Interfaces* **2017**, 9, 14566.

[128] a) A. Tamayo, M. A. Mazo, R. Ruiz-Caro, A. Martín-Illana, L. M. Bedoya, M. D. Veiga-Ochoa, J. Rubio, *Chem. Eng. J.* **2015**, 280, 165; b) N. H. Maniya, S. R. Patel, Z. V. P. Murthy, *Superlattices Microstruct.* **2015**, 85, 34; c) E. M. Mäkilä, H. Kivelä, N. Shrestha, A. Correia, M. Kaasalainen, E. Kukk, J. Hirvonen, H. A. Santos, J. J. Salonen, *Langmuir* **2016**; d) M. Wang, P. S. Hartman, A. Loni, L. T. Canham, N. Bodiford, J. L. Coffer, *Langmuir* **2015**, 31, 6179.

[129] E. Mäkilä, M. P. Ferreira, H. Kivelä, S. M. Niemi, A. Correia, M. A. Shahbazi, J. Kauppila, J. Hirvonen, H. A. Santos, J. Salonen, *Langmuir* **2014**, 30, 2196.

[130] J. R. Dorvee, A. M. Derfus, S. N. Bhatia, M. J. Sailor, *Nat. Mater.* **2004**, 3, 896.

[131] M. Kovalainen, J. Mönkäre, E. Mäkilä, J. Salonen, V. P. Lehto, K. H. Herzig, K. Järvinen, *Pharm. Res.* **2012**, 29, 837.

[132] a) Y. Hou, J. Shao, Q. Fu, J. Li, J. Sun, Z. He, *Int. J. Pharm.* **2016**, 516, 372; b) L. Z, X. S, G. W, H. H, C. M, W. Y, H. B, D. W, Z. H, W. X, *Nanoscale* **2016**, 8, 18782; c) M. Evangelopoulos, A. Parodi, J. O. Martinez, I. K. Yazdi, A. Cevenini, A. L. van de Ven, N. Quattrocchi, C. Boada, N. Taghipour, C. Corbo, B. S. Brown, S. Scaria, X. Liu, M. Ferrari, E. Tasciotti, *Biomaterials* **2016**, 82, 168; d) Y. Zhou, J. Du, L. Wang, Y. Wang, *J. Nanosci. Nanotechnol.* **2017**.

[133] a) D. Liu, H. Zhang, S. Cito, J. Fan, E. Mäkilä, J. Salonen, J. Hirvonen, T. M. Sikanen, D. A. Weitz, H. A. Santos, *Nano Lett.* **2017**, 17, 606; b) D. Liu, C. R. Bernuz, J. Fan, W.

Li, A. Correia, J. Hirvonen, H. A. Santos, *Advanced Functional Materials* **2017**, 27, 1604508.

[134] M. Xue, X. Zhong, Z. Shaposhnik, Y. Qu, F. Tamanoi, X. Duan, J. I. Zink, *Journal of the American Chemical Society* **2011**, 133, 8798.

[135] F. Kong, H. Zhang, X. Qu, X. Zhang, D. Chen, R. Ding, E. Mäkilä, J. Salonen, H. A. Santos, M. Hai, *Adv. Mater.* **2016**, 28, 10195.

[136] P. J. Kinnari, M. L. K. Hyvonen, E. M. Makila, M. H. Kaasalainen, A. Rivinoja, J. J. Salonen, J. T. Hirvonen, P. M. Laakkonen, H. A. Santos, *Biomaterials* **2013**, 34, 9134.

[137] N. Shrestha, F. Araújo, M. A. Shahbazi, E. Mäkilä, M. J. Gomes, B. Herranz‐Blanco, R. Lindgren, S. Granroth, E. Kukk, J. Salonen, *Adv. Funct. Mater.* **2016**, 26, 3405.

[138] a) S. Pace, R. B. Vasani, F. Cunin, N. H. Voelcker, *New J. Chem.* **2013**, 37, 228; b) E. Segal, A. Perelman L., F. Cunin, F. Di Renzo, M. Devoisselle J., Y. Y. Li, J. Sailor M., *Adv. Funct. Mater.* **2010**, 17, 1153.

[139] R. Bazak, M. Houri, S. El Achy, S. Kamel, T. Refaat, *Journal of Cancer Research and Clinical Oncology* **2015**, 141, 769.

[140] D. P. Lankveld, R. G. Rayavarapu, P. Krystek, A. G. Oomen, H. W. Verharen, T. G. van Leeuwen, W. H. De Jong, S. Manohar, *Nanomedicine* **2011**, 6, 339.

[141] a) S. Wang, L. Zhang, C. Dong, L. Su, H. Wang, J. Chang, *Chem. Commun.* **2015**, 51, 406; b) Y. Barenholz, *J. Controlled Release* **2012**, 160, 117.

[142] S. Wang, P. Huang, X. Chen, *Adv. Mater.* **2016**, 28, 7340.

[143] Z. Yuan, S. Srinivasab, J. F. Alexander, X. Liu, W. Arap, R. Pasqualini, M. Ferrari, S. K. Libutti, B. G. Vilentchouk, Vol. 76, AACR, 2016.

[144] L. M. Bimbo, M. Sarparanta, H. A. Santos, A. J. Airaksinen, E. Mäkilä, T. Laaksonen, L. Peltonen, V. P. Lehto, J. Hirvonen, J. Salonen, *ACS Nano* **2010**, 4, 3023.

[145] S. Näkki, J. Rytkönen, T. Nissinen, C. Florea, J. Riikonen, P. Ek, H. Zhang, H. A. Santos, A. Närvänen, W. Xu, V. P. Lehto, *Acta Biomaterialia* **2015**, 13, 207.

[146] M. A. Shahbazi, P. V. Almeida, E. M. Mäkilä, M. H. Kaasalainen, J. J. Salonen, J. T. Hirvonen, H. A. Santos, *Biomaterials* **2014**, 35, 7488.

[147] G. Caracciolo, O. C. Farokhzad, M. Mahmoudi, *Trends in Biotechnology* **2016**, 35, 257.

[148] B. Xia, W. Zhang, J. Shi, S.-j. Xiao, *ACS Applied Materials & Interfaces* **2013**, 5, 11718.

[149] A. M. Kallinen, M. P. Sarparanta, D. Liu, E. M. Makila, J. J. Salonen, J. T. Hirvonen, H. A. Santos, A. J. Airaksinen, *Molecular Pharmaceutics* **2014**, 11, 2876.

[150] C. F. Wang, M. P. Sarparanta, E. M. Mäkilä, M. L. Hyvönen, P. M. Laakkonen, J. J. Salonen, J. T. Hirvonen, A. J. Airaksinen, H. A. Santos, *Biomaterials* **2015**, 48, 108.

[151] P. Decuzzi, B. Godin, T. Tanaka, S. Y. Lee, C. Chiappini, X. Liu, M. Ferrari, *Journal of Controlled Release* **2010**, 141, 320.

[152] C. Chiappini, E. Tasciotti, R. E. Serda, L. Brousseau, X. Liu, M. Ferrari, *physica status solidi (c)* **2011**, 8, 1826.

[153] F. De Angelis, A. Pujia, C. Falcone, E. Iaccino, C. Palmieri, C. Liberale, F. Mecarini, P. Candeloro, L. Luberto, A. de Laurentiis, G. Das, G. Scala, E. Di Fabrizio, *Nanoscale* **2010**, 2, 2230.

[154] J. G. Croissant, Y. Fatieiev, N. M. Khashab, *Advanced Materials* **2017**, 29, n/a.

[155] A. Tzur-Balter, Z. Shatsberg, M. Beckerman, E. Segal, N. Artzi, *Nature Communications* **2015**, 6, 6208.

[156] a) E. C. Wu, J. S. Andrew, L. Cheng, W. R. Freeman, L. Pearson, M. J. Sailor, *Biomaterials* **2011**, 32, 1957; b) E. C. Wu, J.-H. Park, J. Park, E. Segal, F. Cunin, M. J. Sailor, *ACS Nano* **2008**, 2, 2401.

[157] Z. Chen, D. Ni, Y. Liu, H. Yao, W. Bu, J. Shi, *Nat. Nanotechnol.* **2017**, 12, 378.

[158] a) M. P. Monopoli, C. Aberg, A. Salvati, K. A. Dawson, *Nat Nano* **2012**, 7, 779; b) A. Lesniak, A. Salvati, M. J. Santos-Martinez, M. W. Radomski, K. A. Dawson, C. Åberg, *Journal of the American Chemical Society* **2013**, 135, 1438; c) M. C. Lo Giudice, L. M. Herda, E. Polo, K. A. Dawson, *Nature Communications* **2016**, 7, 13475.

[159] R. E. Serda, J. Gu, R. C. Bhavane, X. Liu, C. Chiappini, P. Decuzzi, M. Ferrari, *Biomaterials* **2009**, 30, 2440.

[160] R. E. Serda, E. Blanco, A. Mack, S. J. Stafford, S. Amra, Q. Li, A. van de Ven, T. Tanaka, V. P. Torchilin, J. E. Wiktorowicz, *Molecular imaging* **2011**, 10, 7290.2011.00008.

[161] M. Sarparanta, L. M. Bimbo, J. Rytkonen, E. Makila, T. J. Laaksonen, P. Laaksonen, M. Nyman, J. Salonen, M. B. Linder, J. Hirvonen, H. A. Santos, A. J. Airaksinen, *Molecular Pharmaceutics* **2012**, 9, 654.

[162] E. Ollikainen, D. Liu, A. Kallio, E. Mäkilä, H. Zhang, J. Salonen, H. A. Santos, T. Sikanen, *Eur. J. Pharm. Sci.* **2017**, 104, 124.

[163] J. A. Santos-Lopez, A. Garcimartin, P. Merino, M. E. Lopez-Oliva, S. Bastida, J. Benedi, F. J. Sanchez-Muniz, *PLoS One* **2016**, 11, e0147469.

[164] X. Zhou, F. M. Moussa, S. Mankoci, P. Ustriyana, N. Zhang, S. Abdelmagid, J. Molenda, W. L. Murphy, F. F. Safadi, N. Sahai, *Acta Biomaterialia* **2016**, 39, 192.

[165] K. Pant, O. Sedláček, R. A. Nadar, M. Hrubý, H. Stephan, *Advanced Healthcare Materials* **2017**, 6, n/a.

[166] P. M. Fauchet, E. Ettedgui, A. Raisanen, L. J. Brillson, F. Seiferth, S. K. Kurinec, Y. Gao, C. P. L. Tsybeskov, *Mrs Proc.* **1993**, 298.

[167] I. M. Alaoui, in *Imaging for Detection and Identification*, (Ed: J. Byrnes), Springer Netherlands, Dordrecht 2007, 243.

[168] J. Joo, X. Liu, V. R. Kotamraju, E. Ruoslahti, Y. Nam, M. J. Sailor, *ACS Nano* **2015**, 9, 6233.

[169] L. Luo, X. X. Zhang, K. F. Li, K. W. Cheah, J. X. Shi, W. K. Wong, M. L. Gong, *Adv. Mater.* **2004**, 16, 1664.

[170] R. E. Serda, A. Mack, A. V. D. Ven, S. Ferrati, J. Kenneth Dunner, B. Godin, C. Chiappini, M. Landry, B. Lou, X. Liu, *Small* **2010**, 6, 2691.

[171] C. M. Lundquist, C. Loo, I. M. Meraz, J. D. Cerda, X. Liu, R. E. Serda, *Med. Sci.* **2014**, 2, 51.

[172] M. B. D. L. Mora, J. Bornacelli, R. Nava, R. Zanella, J. A. Reyes-Esqueda, *J. Lumin.* **2014**, 146, 247.

[173] J. Liu, X. Jiang, C. Ashley, C. J. Brinker, *Journal of the American Chemical Society* **2009**, 131, 7567.

[174] S. Minardi, L. Pandolfi, F. Taraballi, E. De Rosa, I. K. Yazdi, X. Liu, M. Ferrari, E. Tasciotti, *ACS Applied Materials and Interfaces* **2015**, 7, 16364.

[175] D. Liu, H. Zhang, B. Herranz-Blanco, E. M. Mäkilä, V. P. Lehto, J. Salonen, J. T. Hirvonen, H. A. Santos, *Small* **2014**, 10, 2029.

[176] V. Balasubramanian, A. Correia, H. Zhang, F. Fontana, E. Makila, J. Salonen, J. Hirvonen, H. A. Santos, *Adv Mater* **2017**, 29, 1605375.

[177] a) D. Liu, H. Zhang, F. Fontana, J. T. Hirvonen, H. A. Santos, *Lab Chip* **2017**, 17, 1856; b) W. Li, D. Liu, H. Zhang, A. Correia, E. M. Mäkilä, J. Salonen, J. T. Hirvonen, H. A. Santos, *Acta Biomaterialia* **2017**, 48, 238.

[178] F. Araujo, N. Shrestha, M. J. Gomes, B. Herranz-Blanco, D. Liu, J. T. Hirvonen, P. L. Granja, H. A. Santos, B. Sarmento, *Nanoscale* **2016**, 8, 10706.

[179] N. Shrestha, F. Araújo, M. A. Shahbazi, E. Mäkilä, M. J. Gomes, M. Airavaara, E. I. Kauppinen, J. Raula, J. Salonen, J. Hirvonen, B. Sarmento, H. A. Santos, *Journal of Controlled Release* **2016**, 232, 113.

[180] a) A. S. Cheung, D. J. Mooney, *Nano Today* **2015**, 10, 511; b) D. J. Irvine, M. C. Hanson, K. Rakhra, T. Tokatlian, *Chem Rev* **2015**, 115, 11109.

[181] K. M. Ainslie, S. L. Tao, K. C. Popat, T. A. Desai, *ACS Nano* **2008**, 2, 1076.

[182] I. M. Meraz, B. Melendez, J. Gu, S. T. Wong, X. Liu, H. A. Andersson, R. E. Serda, *Mol Pharm* **2012**, 9, 2049.

[183] W. Dai, X. Wang, G. Song, T. Liu, B. He, H. Zhang, X. Wang, Q. Zhang, *Adv Drug Deliv Rev* **2017**.

[184] F. Fontana, D. Liu, J. Hirvonen, H. A. Santos, *Wiley Interdiscip Rev Nanomed Nanobiotechnol* **2017**, 9.

[185] L. Wayteck, K. Breckpot, J. Demeester, S. C. De Smedt, K. Raemdonck, *Cancer Lett* **2014**, 352, 113.

[186] a) G. J. Weiner, *Nat Rev Cancer* **2015**, 15, 361; b) L. M. Weiner, R. Surana, S. Wang, *Nat Rev Immunol* **2010**, 10, 317.

[187] a) S. H. van der Burg, R. Arens, F. Ossendorp, T. van Hall, C. J. Melief, *Nat Rev Cancer* **2016**, 16, 219; b) K. Shao, S. Singha, X. Clemente-Casares, S. Tsai, Y. Yang, P. Santamaria, *ACS Nano* **2015**, 9, 16.

[188] R. H. Fang, L. Zhang, *Annu Rev Chem Biomol Eng* **2016**, 7, 305.

[189] D. M. Smith, J. K. Simon, J. R. Baker, Jr., *Nat Rev Immunol* **2013**, 13, 592.

[190] I. M. Meraz, C. H. Hearnden, X. Liu, M. Yang, L. Williams, D. J. Savage, J. Gu, J. R. Rhudy, K. Yokoi, E. C. Lavelle, R. E. Serda, *PLoS One* **2014**, 9, e94703.

[191] a) F. Shima, T. Akagi, M. Akashi, *Bioconjugate Chemistry* **2015**, 26, 890; b) Y. Kakizawa, J. S. Lee, B. Bell, T. M. Fahmy, *Acta Biomaterialia* **2017**, 57, 136.

[192] a) D. F. Moyano, M. Goldsmith, D. J. Solfiell, D. Landesman-Milo, O. R. Miranda, D. Peer, V. M. Rotello, *J Am Chem Soc* **2012**, 134, 3965; b) Y. Yang, M. Jambhrunkar, P. L. Abbaraju, M. Yu, M. Zhang, C. Yu, *Adv Healthc Mater* **2017**.

[193] L. M. Jurkic, I. Cepanec, S. K. Pavelic, K. Pavelic, *Nutr Metab (Lond)* **2013**, 10, 2.

[194] A. Cifuentes-Rius, A. Ivask, E. Sporleder, I. Kaur, Y. Assan, S. Rao, D. Warther, C. A. Prestidge, J.-O. Durand, N. H. Voelcker, *Small* **2017**, 1701201.

[195] a) P. Serra, P. Santamaria, *Clin Immunol* **2015**, 160, 3; b) D. R. Getts, L. D. Shea, S. D. Miller, N. J. King, *Trends Immunol* **2015**, 36, 419; c) M. Gharagozloo, S. Majewski, M. Foldvari, *Nanomedicine* **2015**, 11, 1003; d) L. Northrup, M. A. Christopher, B. P. Sullivan, C. Berkland, *Adv Drug Deliv Rev* **2016**, 98, 86; e) S. Stead, S. McInnes, P. T. Coates, N. Voelcker, *Cytotherapy* **2017**, 19, S48.

Porous silicon (PSi) has attracted increasing attention for biomedical applications. With controllable geometry, tunable nanoporous structure, large pore volume, high specific surface area and versatile surface chemistry, PSi exhibits superior performance as a versatile drug carrier. In this review, the recent progresses of PSi in drug delivery and cancer immunotherapy are reviewed and discussed.

Keyword porous silicon, drug delivery, nanomedicine, immunotherapy, surface modification

Wei Li, Zehua Liu, Flavia Fontana, Yaping Ding, Dongfei Liu, Jouni T. Hirvonen and Hélder A. Santos

Title Tailoring porous silicon for biomedical applications: from drug delivery to cancer immunotherapy
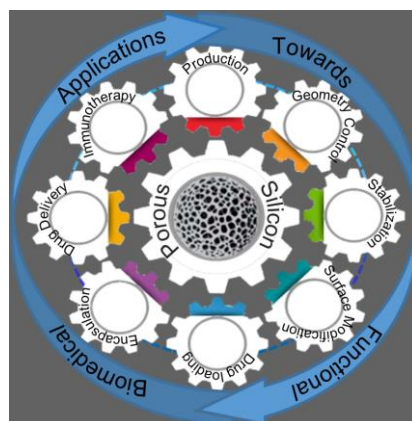
Dr. **Wei Li** is a postdoctoral researcher in Prof. Santos' group at the Faculty of Pharmacy, University of Helsinki. He received his bachelor (2008) and master (2011) degrees in materials science and engineering from Xi'an Jiaotong University. Then he studied biomaterials under the supervision of Prof. Aldo R. Boccaccini at University of Erlangen-Nuremberg and obtained his PhD degree in 2015. His research interests are related to drug delivery, biomaterials and tissue engineering.
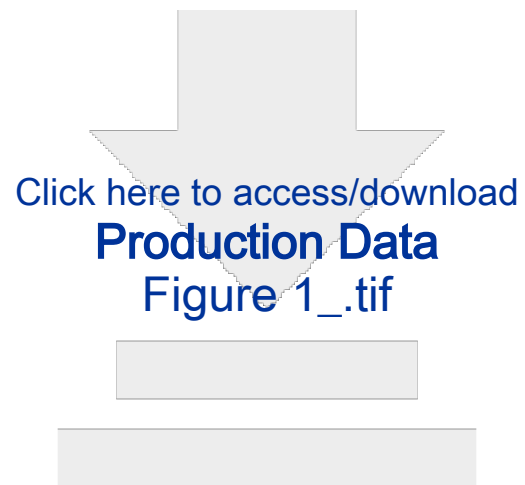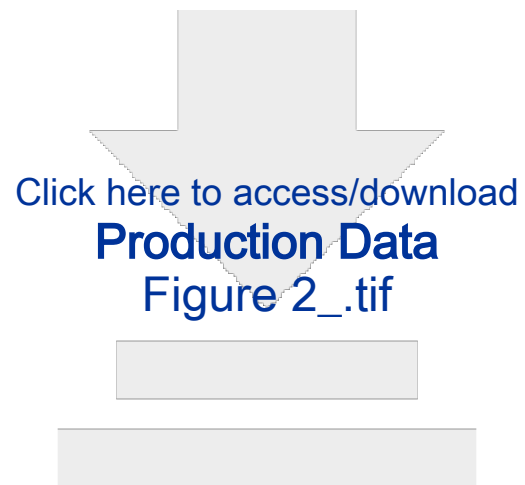

Prof. Jouni Hirvonen is the Dean at the Faculty of Pharmacy, University of Helsinki (Finland). He is the PI of more than 25 externally funded research projects (National Technology Agency TEKES, The Academy of Finland, EU Framework Programmes, national and international foundations, national and international drug industry). In 2007, Prof. Hirvonen received the CRS/Eurand Grand Prize Award based on novel approaches for oral

drug delivery applications. He acts as a pharmaceutics expert in the national and international drug regulation development: Fimea and European Pharmacopoeia (EDQM). He is Executive Committee member in the European Association of Faculties of Pharmacy. His scientific expertise are in the field of controlled drug delivery and pharmaceutical nanotechnology.

Prof. Hélder A. Santos obtained his Doctoral of Science in Technology (Chem. Eng.) in 2007 from the Helsinki University of Technology, Finland. Currently, he heads the Research Unit Pharmaceutical Nanotechnology and Chemical Microsystems Research Unit, and the Preclinical Drug Formulation and Analysis Group at the Faculty of Pharmacy, University of Helsinki, Finland. In 2010, he received the Talent Prize in Science awarded by the Portuguese Government, and in 2013 and 2014, he received the Young Researcher Award and was distinguished by the exceptional scientific productivity, respectively, by the Faculty of Pharmacy (University of Helsinki). In 2016, he was awarded the Academy of Finland Award for Social Impact**.** He is the Editor and Editorial Board Member of several peer-reviewed international journals. His scientific expertise are in the development of nanoparticles/nanomedicines for biomedical and healthcare applications, particularly porous silicon nanomaterials for simultaneous controlled drug delivery, diagnostic and treatment of cancer, diabetes, and cardiovascular diseases, and further translation of these nanotechnologies into the clinic.

Figure 1

Click here to access/download
Production Data
Figure 1_.tif

Figure 2

Click here to access/download
Production Data
Figure 2_.tif

Figure 3

Click here to access/download
Production Data
Figure 3_.tif

Figure 4

Click here to access/download
Production Data
Figure 4_.tif

Figure 5

Click here to access/download
Production Data
Figure 5_.tif

Figure 6

Click here to access/download
Production Data
Figure 6_.tif

Figure 7

Click here to access/download
Production Data
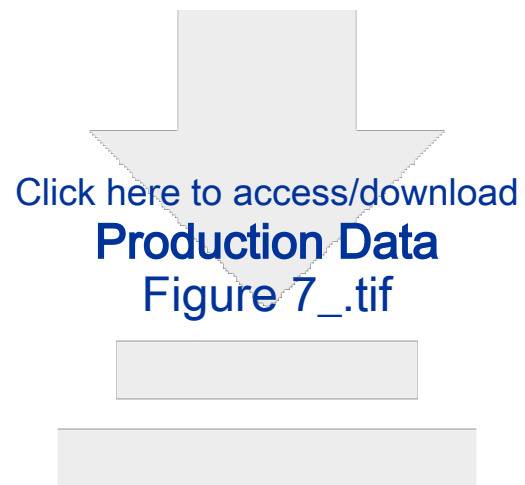Figure 7_.tif

Figure 8

Click here to access/download
Production Data
Figure 8_.tif

Figure 9

Click here to access/download
Production Data
Figure 9_.tif

Figure 10

Click here to access/download
Production Data
Figure 10_.tif

Figure 11

Click here to access/download
Production Data
Figure 11_.tif

Figure 12

Click here to access/download
Production Data
Figure 12_.tif

Figure 13

Click here to access/download
Production Data
Figure 13_.tif

Figure 14

Click here to access/download
Production Data
Figure 14_.tif

Figure 15

Click here to access/download
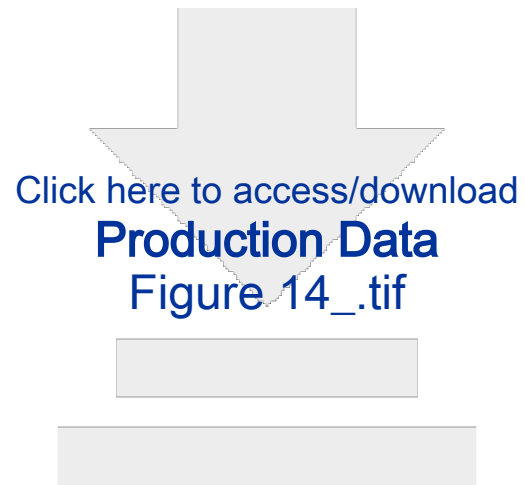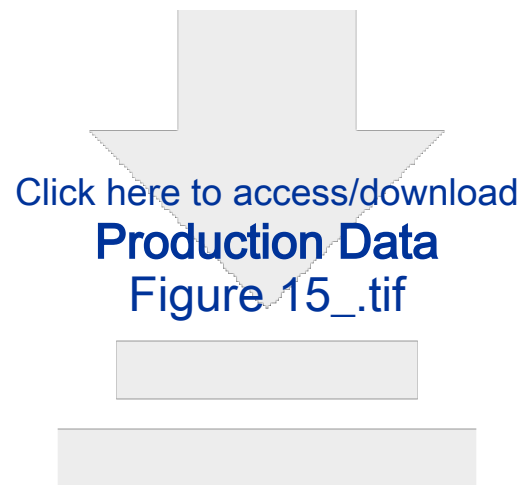**Production Data**
Figure 15_.tif

Graphical Abstract

Click here to access/download
Production Data
Table of Contents.tif